

MECA0023-1 - ADVANCED SOLID MECHANICS

Professeur: J.-P. PONTHOT

Assistant: G. WAUTELET

- Numerical Project -

Hollow Thick-walled Sphere subjected to an Internal Pressure

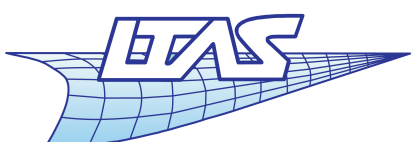
Group 14

Quentin Borlon

Louis Francotte

François Rigo

University of Liege
Faculty of applied sciences
Academic year 2015-2016



Contents

1	Introduction	1
2	Part 1 : Study of elasto-plastic behavior with linear hardening	3
2.1	Introduction	3
2.1.1	No hardening model	3
2.1.2	Isotropic linear hardening	9
2.1.3	Kinematic linear hardening	12
2.1.4	Mixed linear hardening	15
3	Part 2: Study of elasto-plastic behavior with non-linear hardening	19
3.1	Non-linear kinematic hardening	19
3.2	Non-linear kinematic hardening combined with linear isotropic hardening	26
3.3	Non-linear kinematic hardening combined with a non-linear isotropic hardening	29
3.4	Non linear kinematic hardening in the case of a simple tension test	32
3.5	Dissipation energy	34
4	Part 3: Study of elasto-viscoplastic behavior	36
4.1	Sawtooth loading	38
4.1.1	Linear isotropic hardening	38
4.1.2	Mixed hardening	41
4.2	Sawtooth loading with plateaus of 1 [s]	42
4.2.1	Linear isotropic hardening	42
4.2.2	Mixed hardening	44
4.3	One cycle of sawtooth loading followed by constant $\frac{u_{max}}{2}$: "relaxation"	45
4.3.1	Variation of stress components ($\eta = 10^4$ [MPa.s], linear isotropic hardening)	45
4.3.2	Asymptotic value of $\bar{\sigma}^{VM}$ without hardening ($\eta = 10^4$ [MPa.s])	47
4.3.3	Asymptotic value of $\bar{\sigma}^{VM}$ with linear isotropic hardening and extrapolation for mixed hardening ($\eta = 10^4$ [MPa.s])	48
4.4	Internal (hydrostatic) pressure	51
4.5	Signum distance ($\eta = 10^4$ [MPa.s], linear isotropic hardening)	53
4.5.1	Sawtooth loading	53
4.5.2	One loading followed by constant u_{max}	55
5	Part 4: Sensitive study of numerical parameters	57
5.1	Analytical solution	57
5.1.1	Introduction	57
5.1.2	Boundary conditions	57
5.1.3	Equilibrium equation	59
5.1.4	Kinematic equations	59
5.1.5	Constitutive equations	59
5.1.6	Elastic solution $0 \leq u < u_y^0$	59
5.1.7	Elasto-plastic solution $u > u_y^0$	62
5.2	Influence of the loading speed	64
5.3	Influence of spatial discretisation	65
5.3.1	Introduction	65
5.3.2	Number of radial divisions	65
5.3.3	Number of circumferential divisions	67
5.3.4	Radial distribution of the elements	67
5.3.5	Comparison of stresses at outer surface	68

5.4	Influence of temporal discretisation	71
5.4.1	Introduction	71
5.4.2	General discretisation and discretisation of Metafor	71
5.4.3	Elasto-plasticity without hardening	72
5.4.4	Elasto-plasticity with linear isotropic hardening	72
5.4.5	Elasto-viscoplasticity with mixed hardening and $\eta = 10^4$ [MPa.s]	73
5.5	Remarks on radial return algorithm	75
5.6	Validation of the numerical simulation based on the TPE	78
6	Conclusion	80
A	Example of <code>file.py</code> to modify parameters of dictionary	83
B	Values exported from Metafor	83

List of Figures

1	Sectional view of the hollow sphere under pressure	1
2	Simplification and conventions of notations	1
3	Radial displacement u [mm] of the inner surface for 2 cycles	1
4	Stress-strain and Haigh Westergaard's space evolution for no hardening model	3
5	Evolution of the von Mises' equivalent stress with respect to time.No hardening.	4
6	Comparison between analytical and numerical solution for $\bar{\sigma}_{VM}$ in the elastic domain.	5
7	Evolution of $\bar{\varepsilon}_p$ with respect to time for no hardening model.	5
8	Evolution of the reaction pressure with respect to time for no hardening model.	6
9	Evolution of the reaction pressure with respect to displacement for no hardening model.	6
10	Evolution of $\bar{\varepsilon}_p$ with respect to p for no hardening model.	7
11	Evolution of the residual stresses in the thick walled sphere for no hardening model.	8
12	Evolution of stress tensor components with respect to time for no hardening model.	8
13	Evolution of the plastic energy dissipation with respect to time for no hardening model.	9
14	Stress-strain and Haigh Westergaard's space evolution for isotropic linear hardening model.	9
15	Evolution of the von Mises' equivalent stress with respect to time.Isotropic linear hardening.	10
16	Evolution of $\bar{\varepsilon}_p$ with respect to time for no isotropic linear hardening.	11
17	Evolution of the reaction pressure with respect to time for isotropic linear hardening model.	11
18	Evolution of the reaction pressure with respect to displacement for isotropic linear hardening model.	12
19	Evolution of the residual stresses in the thick walled sphere for isotropic linear hardening model.	12
20	Evolution of the plastic energy dissipation with respect to time for isotropic linear hardening model.	13
21	Stress-strain and Haigh Westergaard's spa e evolution for kinematic linear hardening model.	13
22	Evolution of the equivalent stress with respect to time for kinematic linear hardening.	14
23	Evolution of $\bar{\varepsilon}_p$ with respect to time for kinematic linear hardening model.	14
24	Evolution of the equivalent back-stress with respect to time for kinematic linear hardening model.	15
25	Stress-strain and Haigh Westergaard's space evolution for mixed hardening model.	16
26	Evolution of the equivalent stress with respect to time for mixed linear hardening.	16
27	Evolution of the equivalent back-stress with respect to time for mixed linear hardening.	17
28	Evolution of $\bar{\varepsilon}_p$ with respect to time for mixed linear hardening model.	17
29	Evolution of the time derivative of the equivalent plastic strain during a loading unloading cycle with a non linear kinematic hardening material.	21
30	Evolution of the equivalent backstress with respect to time with different values for η_k . Non linear kinematic hardening.	21
31	Evolution of the equivalent stress with respect to time with different values for η_k . Non linear kinematic hardening.	22
32	Evolution of the equivalent strain with respect to time with different values for η_k . Non linear kinematic hardening.	22
33	Evolution of the pressure with respect to time with different values for η_k . Non linear kinematic hardening.	23
34	Influence of the maximum displacement on the equivalent backstress for a non-linear kinematic hardening.	24

35	Influence of the maximum displacement on the equivalent stress for a non-linear kinematic hardening.	24
36	Influence of the maximum displacement on the equivalent plastic strain for a non-linear kinematic hardening.	25
37	Evolution of the yield stress with respect to the equivalent plastic strain in a non-linear kinematic and linear isotropic hardening assumption.	27
38	Evolution of the equivalent backstress in case of non-linear kinematic linear isotropic hardening.	27
39	Evolution of the equivalent plastic strain in case of non-linear kinematic linear isotropic hardening.	28
40	Evolution of the current yield stress in case of non-linear kinematic linear isotropic hardening.	28
41	Evolution of the Von Mises equivalent stress in case of non-linear kinematic linear isotropic hardening.	29
42	Evolution of the equivalent stress in case of non-linear kinematic linear isotropic hardening.	29
43	Evolution of the yield stress with respect to the equivalent plastic strain	30
44	Evolution of the equivalent backstress with the number of achieved cycles. Non linear mixed hardening.	31
45	Evolution of the equivalent stress with the number of achieved cycles. Non linear mixed hardening.	31
46	Evolution of the yield stress with the number of achieved cycles. Non linear mixed hardening.	32
47	Evolution of the derivative of the yield stress with respect to the equivalent plastic strain.	32
48	Evolution of the equivalent plastic strain with time in case of a non linear mixed hardening.	33
49	Evolution of the equivalent stress in the plastic phases. Tensile test.	33
50	Plastic dissipation linear kinematic model.	34
51	Plastic dissipation non-linear kinematic model.	34
52	Influence of strain rate on the shape of $\sigma - \bar{\varepsilon}$ curve (1D case in viscoplasticity), comparison with plasticity	36
53	Equivalent model for elasto-viscoplasticity	36
54	Evolution of $\sqrt{\frac{2}{3}}\lambda$ for several m as a function of $\frac{d}{\eta}$	37
55	Temporal variation of the Von Mises equivalent stress $\bar{\sigma}^{V^M}$ [MPa] at inner surface for several viscosity parameters η [MPa.s] with linear isotropic hardening for 2 cycles of loading/unloading in sawtooth	39
56	Temporal variation of the equivalent viscoplastic strain $\bar{\varepsilon}^{vp}$ [-] at inner surface (extrapolated at the inner left node P1 on curve C4) for several 1 parameters η [MPa.s] with linear isotropic hardening for 2 cycles of loading/unloading in sawtooth	40
57	Temporal variation of the pressure $-\sigma_{XX}$ [MPa] at inner surface (extrapolated at the inner left node P1 on curve C4) for several 1 parameters η [MPa.s] with linear isotropic hardening for 2 cycles of loading/unloading in sawtooth	40
58	Mixed hardening, in which the yield surface expands and translates with plastic deformation, and the corresponding uniaxial stress-strain curve in case of strain imposed resulting in cyclic plasticity (in 3D plane stress state) [3]	41
59	Temporal variation of ... at inner surface (extrapolated at node P1 on curve C4) for several 1 parameters η [MPa.s] with mixed hardening for 2 cycles of loading/unloading in sawtooth	42

60	Temporal variation of the Von Mises equivalent stress $\bar{\sigma}^{VM}$ [MPa] at inner surface for several viscosity parameters η [MPa.s] with linear isotropic hardening for 2 cycles of loading/unloading in sawtooth with plateaus of 1 [s] for $u_{max}, 0, -u_{max}$	42
61	Variation of ... at inner surface (extrapolated at the inner left node P1 on curve C4) for several viscosity parameters η [MPa.s] with linear isotropic hardening for 2 cycles of loading/unloading in sawtooth with plateaus of 1 [s] for $u_{max}, 0, -u_{max}$	43
62	Variation of ... at inner surface (extrapolated at the inner left node P1 on curve C4) for several viscosity parameters η [MPa.s] with mixed hardening for 2 cycles of loading/unloading in sawtooth with plateaus of 1 [s] for $u_{max}, 0, -u_{max}$	44
63	Relaxation phenomenon ($\sigma(t)$) and ε constant	45
64	Metafor axis system and spherical axis system	45
65	Temporal variation of ... at inner surface (extrapolated at the inner left node P1 on curve C4) for $\eta = 10^4$ [MPa.s] with linear hardening for one cycle of sawtooth loading followed by constant $\frac{u_{max}}{2}$	46
66	Temporal variation of ... at outer surface (extrapolated at the inner left node P2 on curve C2) for $\eta = 10^4$ [MPa.s] with linear hardening for one cycle of sawtooth loading followed by constant $\frac{u_{max}}{2}$	46
67	Temporal variation of the equivalent Von Mises stress $\bar{\sigma}_{VM}$ [MPa] at inner surface (extrapolated at the inner left node P1 on curve C4) for several viscosity parameters η [MPa.s] with no hardening for 1 cycles of loading until u_{max} during 12 [s], displacement [mm] is in red	48
68	Temporal variation of ... at inner surface (extrapolated at the inner left node P1 on curve C4) for $\eta = 10^4$ [MPa.s] with linear isotropic, mixed and no hardening for 1 cycles of loading until u_{max} during 8 [s], displacement [mm] is in red	50
69	Temporal variation of ... at inner surface (extrapolated at the inner left node P1 on curve C4) for several η [MPa.s] 1 cycle of loading until u_{max} during 8 [s]	52
70	Temporal variation of the hydrostatic pressure $\bar{\sigma}_{VM}$ [MPa] at inner surface (extrapolated at the inner left node P1 on curve C4) for $\eta = 10^4$ [MPa.s] with linear isotropic and mixed hardening for 1 cycles of loading until u_{max} during 2 [s], displacement [mm] is in red, comparison with "almost elastic" case $\eta = 10^8$ [MPa.s]	53
71	Schematic representation of the signum distance d	54
72	Temporal variation of the signum distance δ [MPa] at inner surface for several loading time [s] with linear isotropic hardening for cycles of loading/unloading in sawtooth for $\eta = 10^4$ [MPa.s]	54
73	Temporal variation of the signum distance δ [MPa] at inner surface for several loading time [s] with linear isotropic hardening for cycles of loading/unloading in sawtooth depending on η [MPa.s]	55
74	Temporal variation of the signum distance δ [MPa] at inner surface for several loading time [s] with linear isotropic hardening for one loading followed by constant u_{max} for $\eta = 10^4$ [MPa.s]	56
75	Variation of the maximal signum distance δ_{max} [MPa] at inner surface for several loading time [s] with linear isotropic hardening for one loading followed by constant u_{max}	56
76	Spherical coordinates [4]	57
77	Distribution of components r, θ, ϕ of tensors σ, ε and distribution of axial displacement along the sphere (from R_1 to R_2); this is done for a maximal displacement $u(R_1) = 0.1$ [mm] to be in elasticity ; $E = 70000$ [MPa], $\nu = 0.33$ [-], $R_1 = 75$ [mm], $R_2 = 350$ [mm]	61

78	Temporal variation of components r, θ, ϕ of tensors σ, ε and distribution of axial displacement for a sawtooth loading/unloading cycle (at inner surface R_1); this is done for a maximal displacement $u_{max} = 0.1$ [mm] (at $u_r(R_1)$) to be in elasticity ; $E = 70000$ [MPa], $\nu = 0.33$ [-], $R_1 = 75$ [mm], $R_2 = 350$ [mm]	62
79	Evolution of plastic and elastic zones from inner surface	62
80	Influence of the loading speed with on the time integration scheme.	65
81	Influence of the loading speed with on the time integration scheme.	65
82	Evolution of $\bar{\varsigma}_{VM}$ at the peak with different Nr.	66
83	Evolution of the realtive error on $\bar{\varsigma}_{VM}$ at the peak with different Nr.	66
84	Evolution of $\bar{\varsigma}_{VM}$ at the peak with different No.	67
85	Evolution of $\bar{\varsigma}_{VM}$ at the peak with different distribution ratios.	67
86	Influence of the mesh on the equivalent Von Mises stress [MPa] at outer surface for elasto-viscoplasticity with $\eta = 10^4$ [MPa.s] without hardening for 3 cycles in sawtooth with 1 [s] loading	69
87	Influence of the mesh on the XX stress [MPa] at outer surface for elasto-viscoplasticity with $\eta = 10^4$ [MPa.s] without hardening for 3 cycles in sawtooth with 1 [s] for each loading	69
88	Influence of the mesh on the YY stress [MPa] at outer surface for elasto-viscoplasticity with $\eta = 10^4$ [MPa.s] without hardening for 3 cycles in sawtooth with 1 [s] for each loading	69
89	Influence of the mesh on the equivalent Von Mises stress [MPa] at inner surface for elasto-viscoplasticity with $\eta = 10^4$ [MPa.s] without hardening for 3 cycles in sawtooth with 1 [s] for each loading	70
90	Influence of time step Δt [s] on the consideration of displacement u	71
91	Influence of the time step [s] on the equivalent Von Mises stress [MPa] at inner surface for elasto-plasticity without hardening for 2 cycles in sawtooth with 1 [s] for each loading	73
92	Influence of the time step [s] on the equivalent Von Mises stress [MPa] at inner surface for elasto-plasticity with linear isotropic hardening for 2 cycles in sawtooth with 1 [s] for each loading	73
93	Influence of the time step [s] on the equivalent Von Mises stress [MPa] at inner surface for elasto-viscoplasticity with linear isotropic hardening for 2 cycles in sawtooth with 1 [s] for each loading	74
94	Influence of the mesh and the time step [s] on the equivalent plastic strain [-] at inner surface for elasto-plasticity with linear mixed hardening for 3 cycles in sawtooth with 1 [s] for each loading	75
95	Illustration of return mapping algorithm with different values of θ	76
96	Equilibrium of reactions in the sphere	77
97	3D view of the sphere computed in Metafor , equivalent Von Mises stresses [MPa] .	77
98	Influence of the mesh and the time step [s] on the reaction pressure [MPa] at inner surface for elasto-plasticity with linear mixed hardening for 3 cycles in sawtooth with 1 [s] for each loading	78

List of Tables

1	Geometry and loading [mm]	2
2	Material data	2
3	Evolution of real CPU time [s] with the time step Δt [s] for Fig. 93	74
4	Final value of $\bar{\varepsilon}(t)$ [-] depending on the mesh and the number of cycle, $\Delta t = 0.01$ [s], at inner surface for elasto-plasticity with linear mixed hardening for cycles in sawtooth with 1 [s] for each loading	75
5	Final value of $\bar{\varepsilon}(t)$ [-] depending on the time step Δt [s] and the number of cycle, mesh: $N_r = 54, N_o = 8, d = \frac{R_2}{R_1}$, at inner surface for elasto-plasticity with linear mixed hardening for cycles in sawtooth with 1 [s] for each loading	76
6	Final value of $p(t) = -\bar{\sigma}_{XX}(t)$ [MPa] depending on the mesh and the number of cycle, $\Delta t = 0.01$ [s], at inner surface for elasto-plasticity with linear mixed hardening for cycles in sawtooth with 1 [s] for each loading	78
7	Final value of $p(t) = -\bar{\sigma}_{XX}(t)$ [MPa] depending on the time step Δt [s] and the number of cycle, mesh: $N_r = 54, N_o = 8, d = \frac{R_2}{R_1}$, at inner surface for elasto-plasticity with linear mixed hardening for cycles in sawtooth with 1 [s] for each loading	78

1 Introduction

To illustrate concepts seen during theoretical lectures of *Advanced solid mechanics*, we will study a practical problem well known: a thick hollow sphere submitted to internal pressure p . The problem is illustrated on Fig. 1.

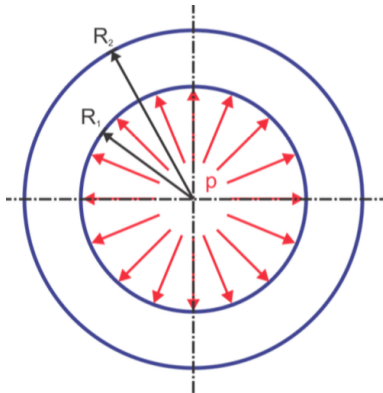


Figure 1 – Sectional view of the hollow sphere under pressure

This pressure will be produced by a displacement-controlled excitation. Fig. 1 is a section, we can bring the 3D sphere to a 2D circle because of the symmetry of the problem, called *axisymmetric*. We will take profit of this symmetry to simplify the circle and consider only one quarter of the circle (Fig. 2). We must thus add *boundary conditions* on curves C_1 and C_3 : roller supports which allows radial translation but not the perpendicular translation.

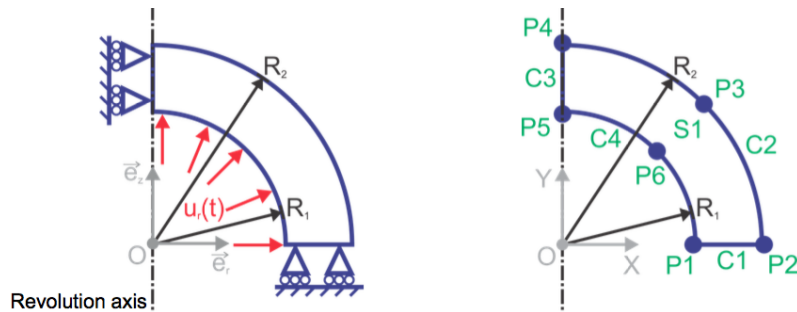


Figure 2 – Simplification and conventions of notations

This will be a displacement with cycles of loading/unloading between maximal displacement u_{max} . To begin, there will be 2 cycles as shown on Fig. 3 but more cycles will be needed to observe certain behaviors. Note that at times $t = 1\text{s}$ and $t = 3\text{s}$, elastic phases occur : beginning of the unloading phases (from u_{max} back to 0).

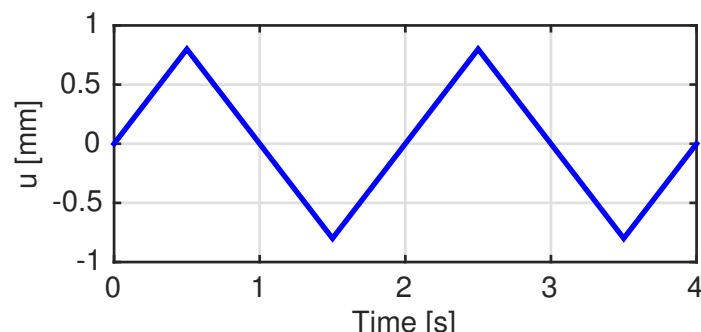


Figure 3 – Radial displacement u [mm] of the inner surface for 2 cycles

We will make some assumptions, commonly used and also in theoretical lectures,

- small deformations
- inertial effects neglected, the problem is thus called *quasi-static* in the inertia meaning, not because behavior would not depend on the *rate*: in fact, we will see that the rate has much consequences on behavior because of plasticity
- isothermal problem

The purpose of this study will be the analysis of several behaviors and the influence of numerical parameters:

- 1) elasto-plastic behavior with linear hardening
- 2) elasto-plastic behavior with non-linear hardening with Voce and Armstrong-Frederick models
- 3) elasto-viscoplastic behavior with Perzyna model
- 4) sensitive study of numerical parameters

This analysis of behaviors will depend also on the hardening law,

- no hardening
- isotropic hardening
- kinematic hardening
- mixed hardening

Numerical data for our problems are shown on table 1 for the geometry and on table 2 for the material. Material is very probably aluminium.

	R_1	R_2	u_{max}
Geometry 5	75	350	0.8

Table 1 – Geometry and loading [mm]

	ρ [kg/m ³]	E [MPa]	ν [-]	σ_y^0 [MPa]	h [MPa]	δ^* [-]	σ_y^∞ [MPa]
Material 2	2700	70000	0.33	100	6500	0.65	250

Table 2 – Material data

We will use the software `Metafor` to generate behaviors of the sphere, we simply modify the main Python file `sphere.py` to get relevant results and we export them into `Matlab` to display graphs.

Important remark `Metafor` uses its own axis system: cylindrical axis system of figure 2. We will must take this into account and make a conversion between `Metafor` and spherical coordinates.

2 Part 1 : Study of elasto-plastic behavior with linear hardening

2.1 Introduction

After having tried different meshes and time step in order to find the best combination that provides results accurate enough, we start to study the behavior of the sphere. The first part of the project consists in the study of the elasto-plastic behavior with linear hardening. This can be done by studying different loading and unloading cycles of the sphere. During those tests, different assumptions will be taken (no hardening, isotropic hardening, kinematic hardening and mixed hardening). The goal of this part is to study the influence of those assumptions on the different key parameters such as the current yield stress, the equivalent plastic strain, the equivalent back-stress et cetera.

2.1.1 No hardening model

First, we have studied the no hardening model, also called perfectly plastic. This model is characterised by a constant yield criterion and no Bauschinger effect, which can be traduced by the invariance of the yield surface. Thus, we didn't talk in this section about the equivalent backstress $\bar{\sigma}$ because it is always 0. We can visualize it on Fig. 4 [3] where it is also obvious that the yield surface doesn't change during hardening.

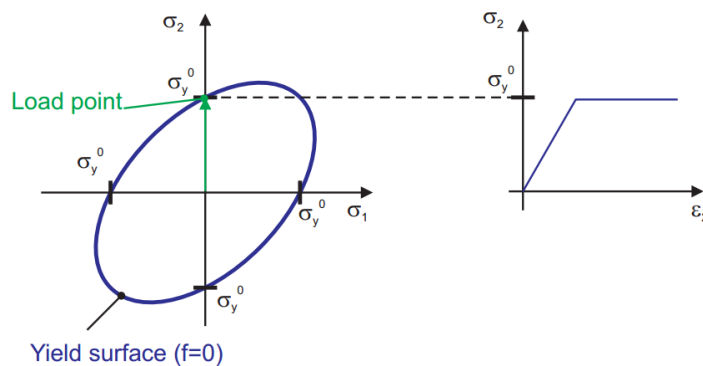


Figure 4 – Stress-strain and Haigh Westergaard's space evolution for no hardening model .

Von Mises' equivalent stress Here, we will talk without distinction about von Mises' equivalent stress and equivalent stress because of the absence of kinematic hardening in this model. Some observations can be made if we look at Fig. 5, that shows the evolution of the von Mises' equivalent stress at P1 (inner surface) and P2 (outer surface). First, if we consider P1, we can observe that the evolution of $\bar{\sigma}_{VM}$ is linear in the elastic region. When it enters in plasticity, we can see that as said before, the yield stress is constant because while the loading is still increased, $\bar{\sigma}_{VM}$ remains constant. As soon as the loading direction is inverted, $\bar{\sigma}_{VM}$ starts to decrease and reaches a zero value when the driven displacement hasn't reach the negative values. As a consequence, we can observe that there are some residual stresses. We can also notice that the first plasticity period of P1 is shorter than the other one. We can explain it considering the fact that there is no residual stress at the beginning of the simulation. Another important remark is that once the material is not virgin anymore, we can see that the minimal $\bar{\sigma}_{VM}$ in traction or compression are not the same, which can be explained by the fact that the path used is not the same depending on the loading direction. It is obvious to say that if we inverted the loading direction, we would just have the inversion of the apparition of the different values and we can extend this remark to every model and variable where this phenomenon is present. Now, if we look at P2, we can see that the equivalent stress never reach the yield criterion. Thus, this region is not submitted to plasticity and is only driven by elasticity. This way, we can easily have an

idea of the driven displacement according to the time.

However, it is important to notice that at P_1 , $\bar{\sigma}_{VM}$ never goes back to zero after the beginning of the first loading while it should be the case in the model. This phenomenon can be explained by the extrapolation of Gauss points values, that is described in the numerical parameters study. We could decrease, the amplitude of those minimal values by reducing the time step, but as we know the reason of those spurious values, we just ignore them in the analysis of the model.

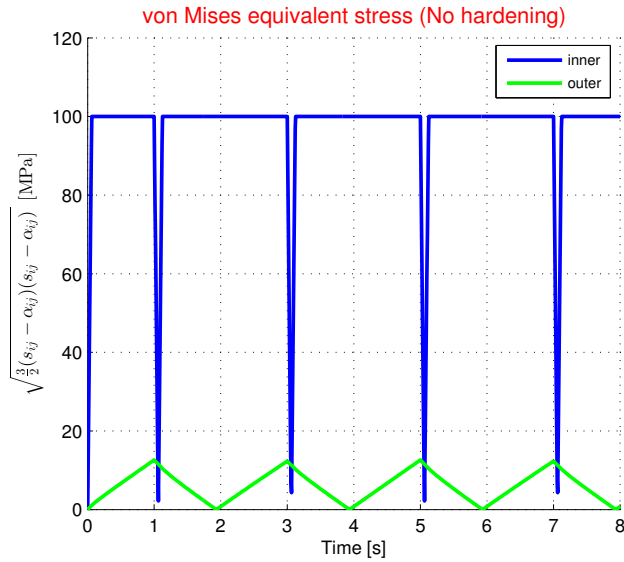


Figure 5 – Evolution of the von Mises' equivalent stress with respect to time.No hardening.

Seeing the important difference between the two points, we could wonder where is the limit between them, i.e. what is the critical radius so that just beyond we enter in plasticity. We will do that later in the paragraph about residual stresses.

We can also wonder about the behavior of the sphere before it enters in plasticity. Indeed, for this loading part, we have an analytical solution to compare with. If we display the analytical and numerical solutions, we can see on Fig. 6 that they are really close until it reaches plasticity.

Of course, the critical radius and the initial elastic behavior results can be extended to all the elasto-plastic models, because they are exactly the same until first plasticity zone is reached.

To calculate the analytical solution, we used the results given in Part 4. Thus, by using the geometry and the material properties, every unknown is determined. Using that $\bar{\sigma}_{VM} = \sigma_{\theta\theta} - \sigma_{rr}$ (loading along a principal axes means that Tresca equals Von Mises equivalent stress), if we arranged all the terms, we get the final expression we were looking for :

$$\bar{\sigma}_{VM}(t) = 1.2E \frac{R_2^3}{R_1^3} \frac{1}{1-2\nu} \frac{1}{R_1 + \frac{1-\nu}{2(1-2\nu)} \frac{R_2^3}{R_1^2}} t$$

Equivalent plastic strain The equivalent plastic strain refers to the total plastic deformation. This value either increases or remains constant but cannot decrease. The increase only appears if we are in the plastic domain. This value illustrates the history of the material. If we observe the curves of $\bar{\epsilon}_p$ for P1 and P2 over the time (Fig. 7), we can see that for the outer surface, it never increases because this zone never enters in plasticity while for the inner surface, we have a succession of plateaus and increases. We can notice that this succession is actually cyclic except at the beginning, where the plateau and the increase are shorter than the others. It is due as in the previous section to the fact that there is no residual stresses, i.e. the material is virgin before the first loading cycle begins.

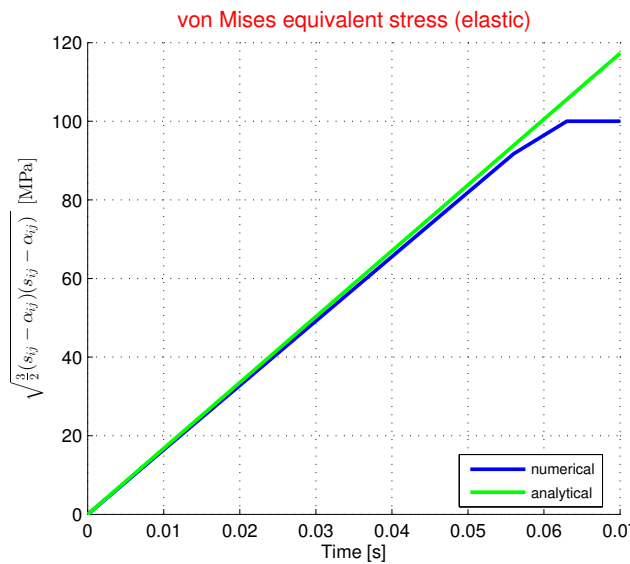


Figure 6 – Comparison between analytical and numerical solution for $\bar{\sigma}_{VM}$ in the elastic domain.

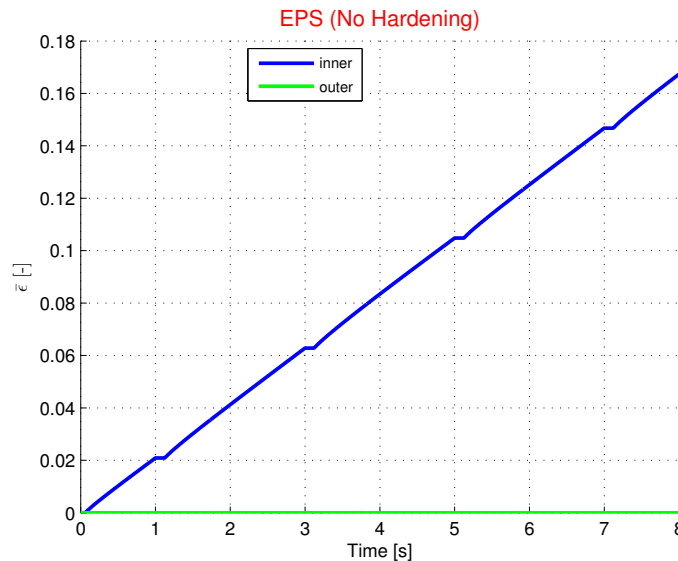


Figure 7 – Evolution of $\bar{\epsilon}_p$ with respect to time for no hardening model.

Reaction pressure *Remark :* The pressure is obtain by use of the reaction forces theorem if Newton. The sum of the forces at the surface must vanish. But this is not compulsory for our FEM model. We have use a kinematic model and not a dynamic model. This introduce some errors in our results but the accuracy of it was assume to be high enough and the extraction of the pressure by this way simplify a lot our calculations.

The pressure is obtained by extracting $-\sigma_{XX}$ at the point P1. Another way to extract the pressure would be the balancing of the part of sphere we study : the reaction forces must balance the inner pressure. Indeed, we can express $F_r = -\iint_S \vec{t} \cdot \vec{e}_r dS$. As we know that \vec{t} can be expressed by $-p \cos\phi \vec{e}_r - p \sin\phi \vec{e}_z$, we can perform the scalar product and if we add the jacobian ($r^2 \cos\phi$), we get this expression :

$$F_r = pR_1^2 \int_0^1 \int_0^{\pi/2} \cos^2\phi d\phi d\theta.$$

Finally, if we perform the integrations (The θ integration domain is one radian because it is computed by the software this way), we obtain the expression of the pressure :

$$p = \frac{4F_r}{\pi R_1^2}.$$

We could also use F_z in the same way. Anyway, the two methods give the same results, that are shown in Fig. 8, where we can see the evolution of the reaction pressure over the time for P1 et P2. We can observe that this pressure evolves linearly in the elastic domain while it is not anymore the case in plasticity. Indeed, in the elastic domain, we know that $\sigma_{rr}(R_1)$ is a linear function of the driven displacement and so also of the time.

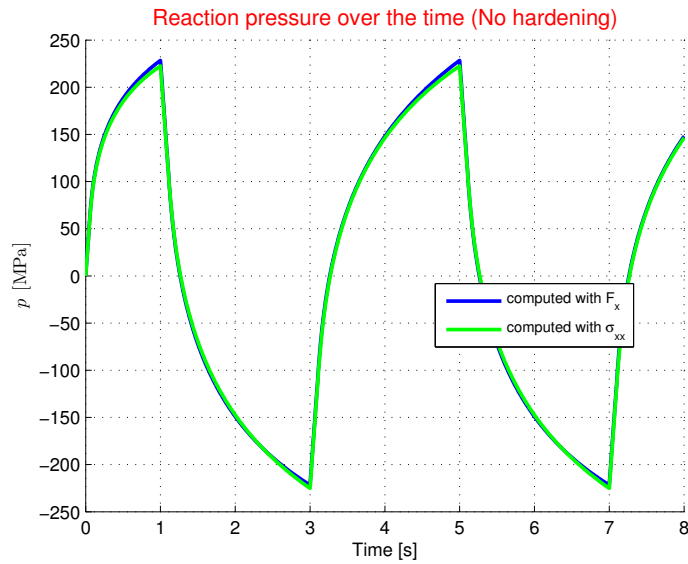


Figure 8 – Evolution of the reaction pressure with respect to time for no hardening model.

Now, if we analyse the evolution of the pressure as a function of the driven displacement (Fig. 9), we can observe the perfectly plastic assumption, which is such that there is no evolution in the plastic domain. This means that the elastic part will always be the same, even if multiple cycles are performed. Indeed, we can see that after the first loading part, the path is always the same.

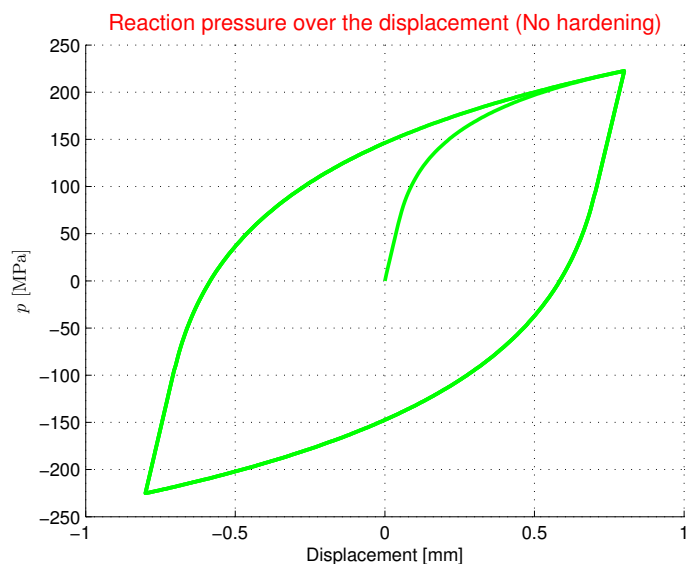


Figure 9 – Evolution of the reaction pressure with respect to displacement for no hardening model.

Initial yield pressure The initial yield pressure is the pressure such that the first hardening phase begins. This is the same for all behaviors. The first hardening phase at the inner radius begins at a reaction pressure of 66.25 [MPa]. We found this value by looking at the first non-zero value of the equivalent plastic strain at P1 and we computed the related reaction pressure. We also used a smaller time step than for the basic simulations to be as accurate as possible.

Because the value we're looking for is at the boundary between elastic and plastic behavior of the sphere, we could also use the analytical solution developed to determine the elastic part of the evolution of $\bar{\sigma}_{VM}$. If we do so, we find an analytical expression of the yield pressure :

$$p_e = \frac{2}{3} \left(1 - \frac{R_1^3}{R_2^3}\right) \sigma_y,$$

which gives if we use the data of our problem :

$p_e = 66.01$ [MPa], so that the relative error is negligible.

Ultimate pressure The ultimate pressure is the pressure such that the outer layer of the sphere comes in plasticity (the all sphere is thus in plasticity). In order to find this we have plotted the equivalent plastic strain at the outer radius in function of the inner pressure. We also used a uniform mesh to avoid too big mistake due to extrapolation in big elements. The equivalent plastic strain evolves only if the outer layer of the sphere enters in plasticity.

With this approach, we find a ultimate pressure of 287.75 [MPa].

Shakedown pressure The shakedown pressure is the maximum pressure that can be applied such that the unloading to a zero applied relative pressure is entirely elastic. And that if we load with a negative relative pressure this results in a plastic deformation.

To find it, we have increased the maximum displacement from a lower value than the initial one until we obtain the change at $p=0$ (by trial error process) of the behavior of $\bar{\varepsilon}_p$, meaning that it starts to increase at this point, as sees in Fig. 10.

We obtain a shakedown pressure of 131.98 [MPa].

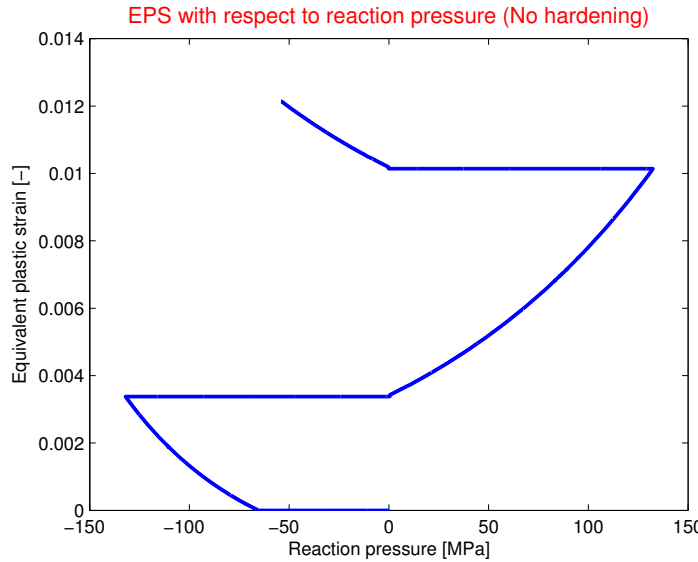


Figure 10 – Evolution of $\bar{\varepsilon}_p$ with respect to p for no hardening model.

Residual stresses We can analyse the residual stresses (stress level when the reaction pressure is back to a zero value) along C1. To do that, we first used a uniform mesh to determine the approximate value of the critical value. Then, we used a mesh where the density of the nodes was higher at the approximate value to increase the precision. The obtained results are shown in Fig. 11. We can see

that there is a special point where the von Mises' equivalent stress reaches a maximum. This special point is the critical radius, that separates the zone where plasticity has occurred and the one where it didn't. We obtain that the critical radius value is 172,2 [mm], with a 1 mm possible mistake, which give a very low relative error.

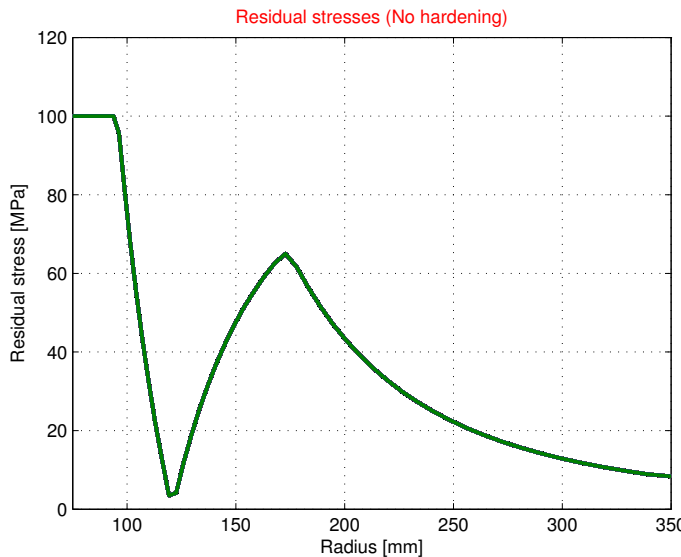


Figure 11 – Evolution of the residual stresses in the thick walled sphere for no hardening model.

Stress tensor components If we display the evolution of stress tensor components according to the time for P1 and P2 (Fig. 12) we can observe that P2 components always evolve linearly while P1 components have linear and non-linear parts because it enters in plasticity. Those non-linear parts highlight that even if the von Mises' equivalent stress is constant, this is not the case for the components. Indeed, even if when the yield criterion is full-filled and that we must stay on the yield surface, the principal directions can still evolve. We can also notice that the non-diagonals components are not zero, because of the plasticity.

We should also notice that non-diagonal components are not all zero. Indeed, the ones where radial direction is involved vary in a small range, while it would be zero if we were in elasticity everywhere. This proves that we don't have two independent parts before and after the critical radius, otherwise the outer non-diagonal components should be zero.

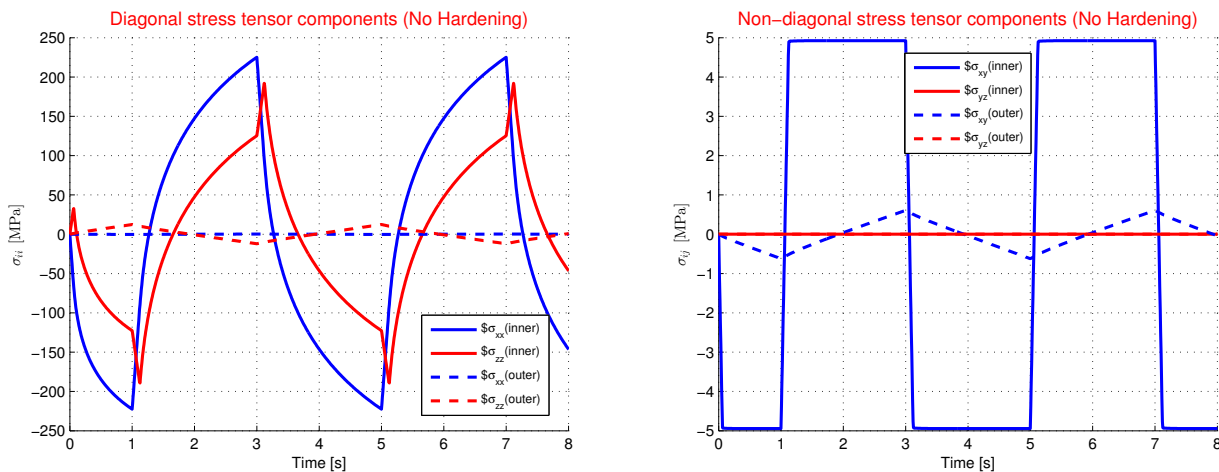


Figure 12 – Evolution of stress tensor components with respect to time for no hardening model.

Plastic energy dissipation If we analyse the plastic energy dissipation (Fig. 13), we can notice that except at the beginning, the dissipated energy is always the same, whatever the cycle we consider.

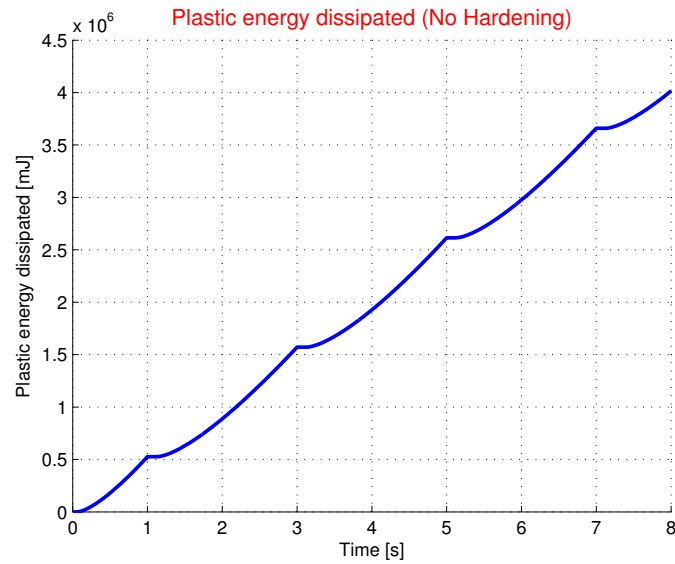


Figure 13 – Evolution of the plastic energy dissipation with respect to time for no hardening model.

2.1.2 Isotropic linear hardening

This assumption means that whatever the direction of the loading, if the yield criterion is satisfied and that the loading keeps increasing in that direction, the yield stress increases in all the direction, i.e. the subsequent yield surface will be of a greater size. As in the no hardening case, we still don't have any Bauschinger's effect with this model and so, the yield domain will remain symmetric. In our case, this means that even in tension as in compression, the yield stress increases symmetrically as observed on Fig. 14 [3].

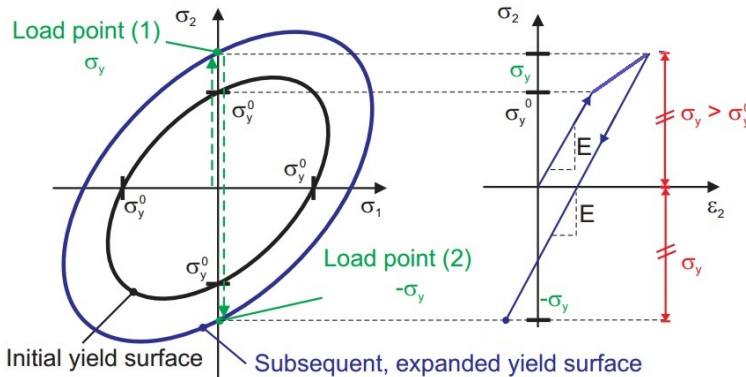


Figure 14 – Stress-strain and Haigh Westergaard's space evolution for isotropic linear hardening model.

For this model and the next ones, we will only focus on what's happening at P1, because we want to see the effect of the hardening model.

Von Mises' equivalent stress If we consider the evolution of $\bar{\sigma}_{VM}$ over the time at P1 (Fig. 15), several observations could be done. At the beginning of each cycle, we first meet an elastic loading : the evolution of the equivalent stress is linear. As soon as we enter into plasticity, the derivative of the

stress with respect to time changes, but stay positive. The equivalent stress follows the same evolution as the yield stress during the plastic phase. In case of isotropic hardening the yield stress evolves in the same way in tension and compression. This means that the unloading and reloading in the other direction are done in the elastic domain until the equivalent stress reaches the new yield stress value. This new value corresponds to the last equivalent stress reached at the maximum displacement of the last half-cycle. Because of the increase of the yield stress, the time in plasticity decreases at each half-cycle : the equivalent stress must reach a greater value before entering into plasticity. The evolution of the yield stress can be easily deduced from this evolution. Indeed, the only difference between them is that when the $\bar{\sigma}_{VM}$ decreases and increases when the P1 is in plasticity, the yield stress remains constant and increases again when plasticity occurs until the asymptotic value is reached. Now, if we consider the P2 state, we can notice that plasticity domain is never reached but also that the behavior of $\bar{\sigma}_{VM}$ is not cyclic and has its amplitude increased, even if we have a constant yield stress. That shows again the dependency between the two zones of the sphere.

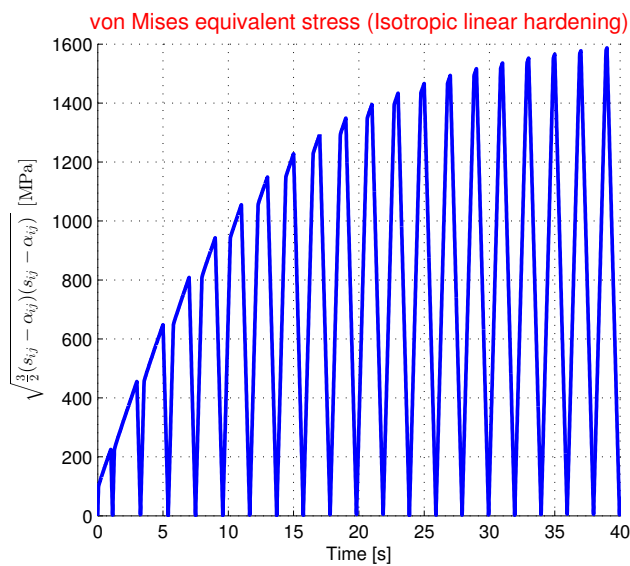


Figure 15 – Evolution of the von Mises' equivalent stress with respect to time. Isotropic linear hardening.

Equivalent plastic strain If we display $\bar{\varepsilon}_p$ (Fig. 16) for the inner surface, we can see that as the previous model, we have a succession of increases and plateaus. However, in this model, by the fact that the entering into plasticity is delayed by the increase of the yield stress, the duration of horizontal plateaus during the cycles increases with the number of loading cycle performed. The equivalent plastic strain doesn't evolve during the elastic phases. By the fact that the entering into plasticity is delayed and that the duration in plasticity decreases every new cycle, the evolution of the equivalent plastic stress is much weaker than in the perfectly plastic case. If the maximum displacement is not increased, after a bigger number of cycles there won't be any entering into plasticity anymore : the equivalent plastic strain will converge to a constant value.

For P2, the equivalent plastic strain remains obviously zero.

Reaction pressure If we observe the evolution of the reaction pressure over the time (Fig. 17), several observations can be done. First, we should notice that as the perfectly plastic model, we have a succession of linear and non-linear zones considering the fact that we are respectively in elasticity and plasticity. However, because of the increase of the yield stress occurs later and later with the number of cycles loading applied and finally, after a very high number of cycles, the evolution is only

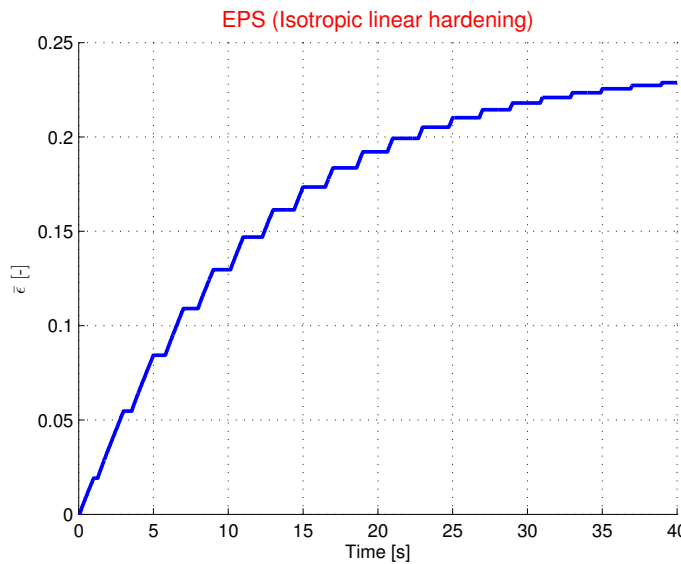


Figure 16 – Evolution of $\bar{\epsilon}_p$ with respect to time for no isotropic linear hardening.

linear. For the same reason, the intensity of the pressure increases and then stabilized over the time.

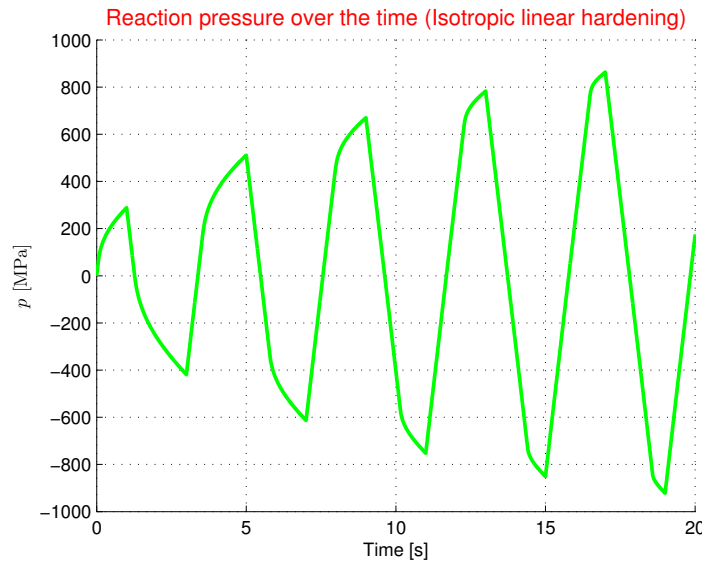


Figure 17 – Evolution of the reaction pressure with respect to time for isotropic linear hardening model.

We can also look at the evolution over the displacement (Fig. 18) and again, we see that the linear parts of the curve grows at each entering into plasticity.

If we compare with the perfectly plastic case, we see that the curve tends to rotate in the anti-clockwise direction and to extend : this come from the isotropic hardening : the slope of the curve $p(u)$ is bigger in elasticity than in plasticity and the hardening tends to expand the elastic domain. As the maximum displacement is fixed, the pressure evolves and may reach greater values.

Residual stresses As in the perfectly plastic model, if we have a look at $\bar{\sigma}_{VM}$ after a load cycle, when the reaction pressure is back to zero, we can observe on Fig. 19 the distribution of residual

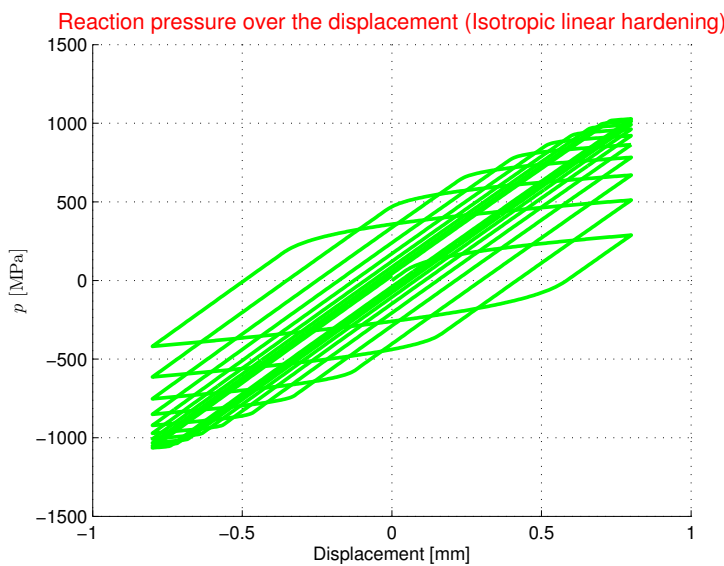


Figure 18 – Evolution of the reaction pressure with respect to displacement for isotropic linear hardening model.

stresses over the sphere, with a similar shape as in the previous model. The main difference lies in the fact that this distribution varies over the performed loading cycles, with a global decrease, until it approaches a zero value everywhere, when the behavior of the sphere is almost purely elastic.

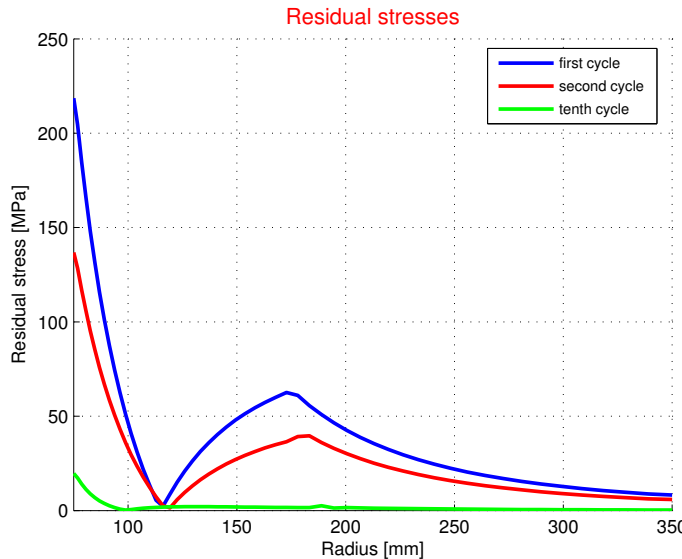


Figure 19 – Evolution of the residual stresses in the thick walled sphere for isotropic linear hardening model.

Plastic dissipation Because of the increasing energy needed to reach the hardening, we can see on Fig. 20 that the duration of the plateaus increase over the performed cycles so that after a very high number of cycles, there will be no more plastic dissipation.

2.1.3 Kinematic linear hardening

This model is quite different from the previous one. Indeed, in this case, the size of the yield surface doesn't change at all with plasticity, but the center of the surface is modified. This modification

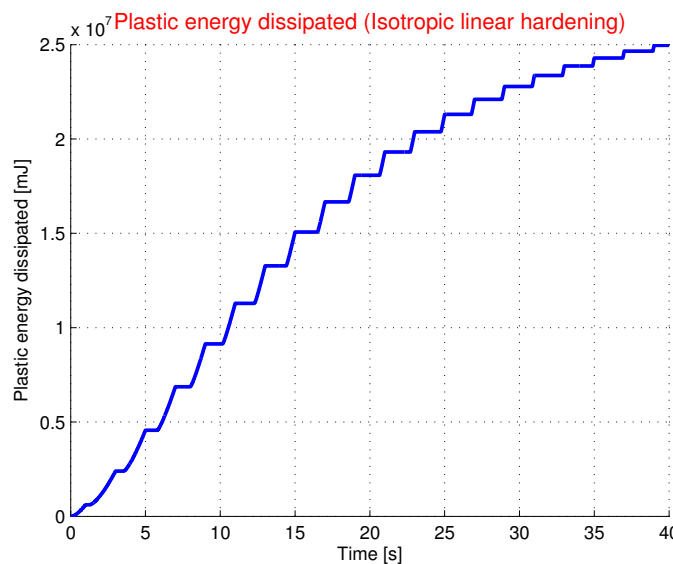


Figure 20 – Evolution of the plastic energy dissipation with respect to time for isotropic linear hardening model.

represents the Bauschinger's effect and to quantify it, we introduce the equivalent back-stress $\bar{\sigma}_p$, that is a measure of the length between the initial center and the subsequent center. This quantity is always positive. It is also important to notify that because the size of the yield surface never change in this model, the yield stress cannot be modified, whatever the loading. We can see those characteristics on Fig. 21 [3].

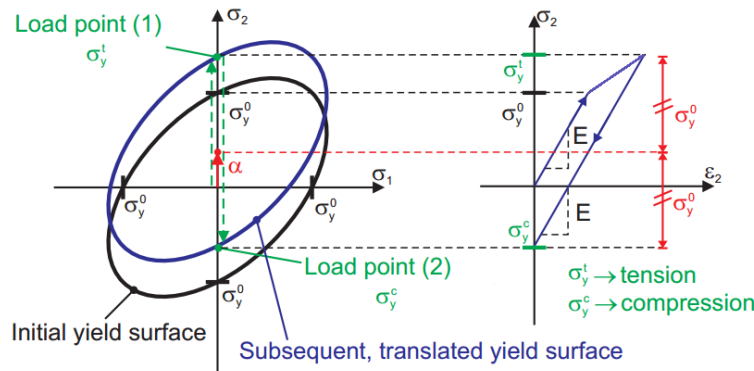


Figure 21 – Stress-strain and Haigh Westergaard's space evolution for kinematic linear hardening model.

Equivalent stress and von Mises' equivalent stress While for the no hardening model and the isotropic linear hardening model, equivalent stress and von Mises' stress were equals due to the zero back-stress tensor, it is not the case anymore.

The evolution of $\bar{\sigma}_{VM}$ for kinematic linear model is the same as the one of the no hardening model, because by definition, $\bar{\sigma}_{VM}$ is always equal to the yield stress during plasticity and that the yield stress doesn't change in this model.

For the equivalent stress, which can really highlight the particularity of this model, at each entering into plasticity, the elastic domain moves into the opposite direction as the last time. This leads to a "back and forth motion" for the range of admissible values of the equivalent stress. This means that the equivalent stress may take greater values than in the perfectly plastic case, but because of

the linearity, the limitation of the motion and its periodicity, the increase of admissible values of the equivalent stress over time stays limited. A part of the energy provided by the external forces during the plastic phases is used to translate the elastic domain in the same direction than the applied pressure. It results in a periodic behavior of the equivalent stress, as can be seen in Fig. 22

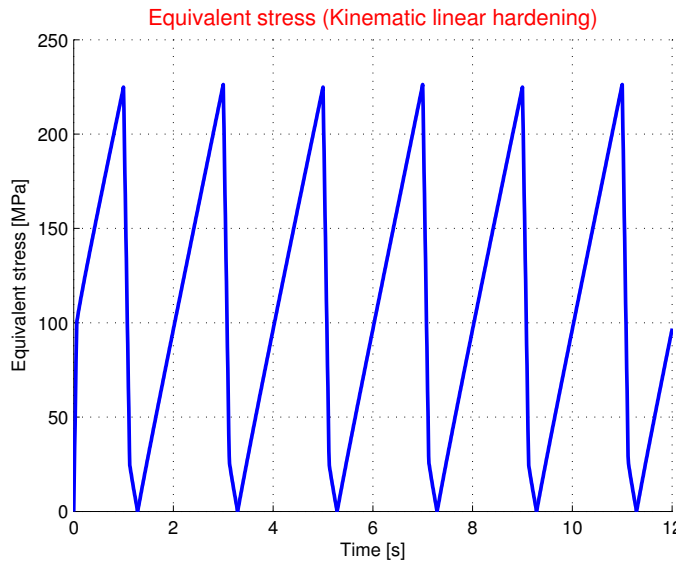


Figure 22 – Evolution of the equivalent stress with respect to time for kinematic linear hardening.

Equivalent plastic strain As we can see on Fig. 23, the kinematic hardening provides a lower equivalent plastic strain rate than the perfectly plastic case, even if their behavior are similar. This can be interpreted as an adaptation of the solid to the current loading. By moving the center of the elastic domain, a part of the energy is used to move the elastic domain. This leads to a lower slope during the plastic phases than the perfectly plastic case.

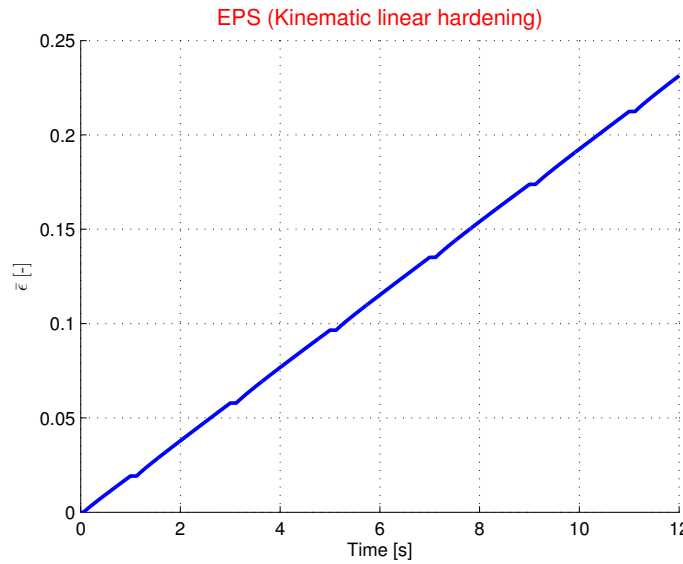


Figure 23 – Evolution of $\bar{\epsilon}_p$ with respect to time for kinematic linear hardening model.

Equivalent back-stress If we look at the evolution of the equivalent back-stress on Fig. 24, we can see that it follows the loading. The back-stress reaches its maximum when the displacement is

maximum. The little plateaus at the top of the peaks shows that there is no evolution of the equivalent back-stress during the elastic phases. And, thanks to the fact the criterion doesn't evolve, the duration of the elastic phases is constant. This leads to a cyclic evolution of $\bar{\alpha}$. However, it is important to notice that the period is from one entire compression-traction cycle, and not only a compression phase. Indeed, the maxima reached are different in traction. This can be explained by describing what's happening from the beginning. Indeed, due to the residual stresses after the first loading, the second elastic part corresponds to less than two times the first elastic displacement such that the second plastic part corresponds to more than two times the first plastic displacement. The new maximum backstress is higher than the first one and next displacement is the same as the second one in opposite way. By linearity, we get again the first maximum back-stress at U_{max} .

We should also notice that after the beginning of the simulation, $\bar{\alpha}$ never goes back to a zero value, again because of the extrapolation errors.

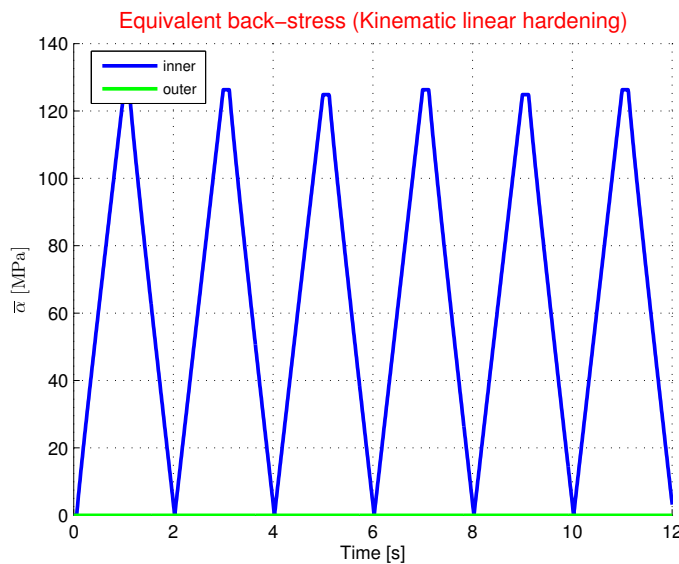


Figure 24 – Evolution of the equivalent back-stress with respect to time for kinematic linear hardening model.

Other important parameters As we did for the first models, we could study the evolution of the plastic energy dissipation but it is obvious that it is very similar to the one of the no hardening model because there is no evolution of the yield stress.

Another important parameter is the evolution of the residual stresses, but again, as the yield stress is constant, it doesn't evolve over the performed cycles (like the perfectly plastic model).

2.1.4 Mixed linear hardening

This model is a combination of the isotropic and kinematic hardening : the isotropic case use a part of the external work delivered from the external forces to increase the yield stress but the kinematic case use another part to translate the yield surface. This results in a increase of the yield stress but with a weaker "average slope" than in the purely isotropic case due to the energy used to translate the yield surface. We can see the combination of isotropic and kinematic effects on Fig. 25 [3].

Equivalent stress We will only study the equivalent stress, that is more representative of the kinematic hardening part and we compare it with those from kinematic and isotropic hardening. We can see on Fig. 26 that the expansion of the admissible values is slower than for the isotropic model, due

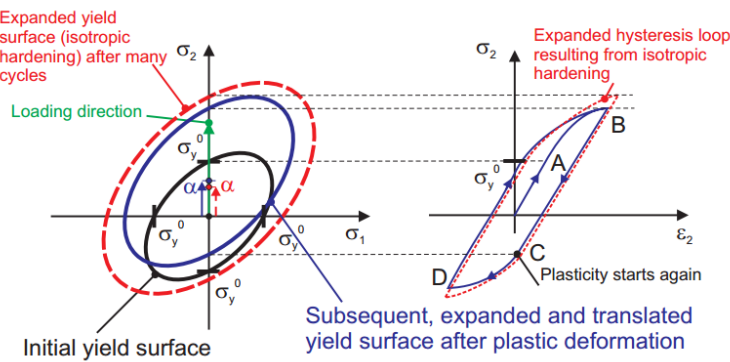


Figure 25 – Stress-strain and Haigh Westergaard's space evolution for mixed hardening model.

to the fact that a part of the external work is used to translate the elastic domain. That results in a slower expansion of the admissible values for the equivalent stress. As we will see for the yield stress, in the bi-linear case, the equivalent stress tends to the same we get in the isotropic case if the number of cycles is increased en tends to ∞

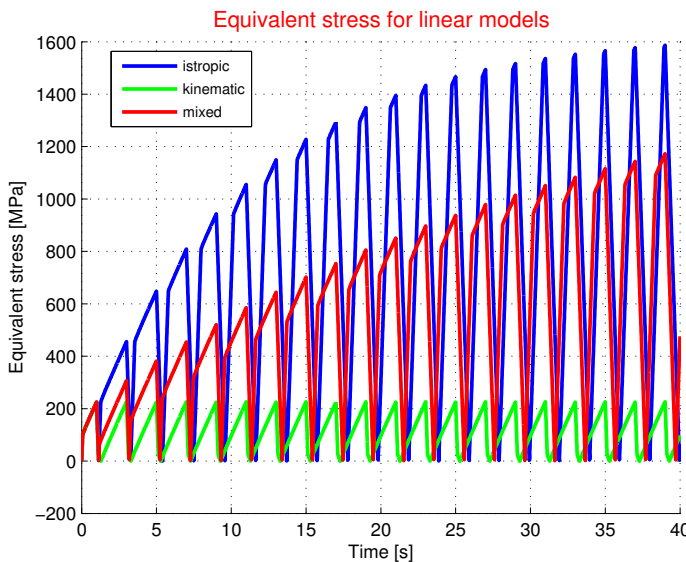


Figure 26 – Evolution of the equivalent stress with respect to time for mixed linear hardening.

However if we perform a very high number of cycles, the values reached at P1 and P2 are the same as the ones obtained for the isotropic linear hardening. Indeed, for P1 we obtain 1638.85 [MPa] and at P2, 17 [MPa]

Equivalent back-stress On Fig. 27, we can see the evolution of $\bar{\alpha}$ for the kinematic and mixed hardening. The back-stress evolves in a similar way as in the kinematic case but the amplitude tends to decrease because of the increase of the yield stress that makes the plastic domain harder to reach. Also, the increase of the yield stress increases the duration of the elastic phase. This leads to longer plateaus on the top of the peaks. The delay in time to recover a minimum back-stress in comparison with the kinematic case comes from the fact that the radius has increased and the delay before coming back into plasticity but in the opposite direction is bigger. So, a bigger equivalent Von Misses stress is needed to enter into plasticity and moves the center of the elastic domain in the other direction. Finally, we can notice, that the amplitude of the peaks tends to decrease to a zero value, thanks to the isotropic effect.

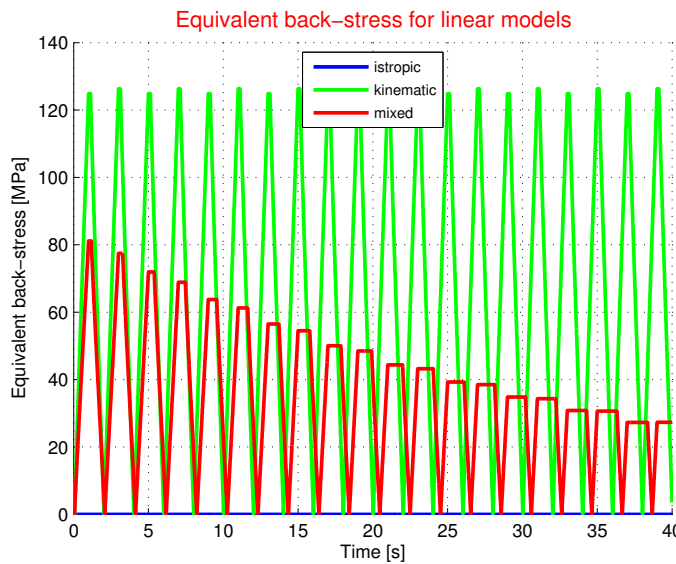


Figure 27 – Evolution of the equivalent back-stress with respect to time for mixed linear hardening.

Equivalent plastic strain If we compare the mixed hardening with the isotropic and kinematic, we can observe that there exists an increase of the duration of the plateau during a loading cycle but the equivalent plastic strain increases faster and more than in the perfectly isotropic case: the whole energy that is dedicated to the plastic effects is not fully used to increase the yield stress. A part is used for the displacement of the center of the elastic domain. So that the elastic domain doesn't increase as fast as for the isotropic hardening. The proportion of elastic displacement stays higher in time in mixed hardening than in isotropic hardening. So that, if the number of cycles performed increases, there is more plastic effect. Again, we can see the effects of both models on Fig. 28.

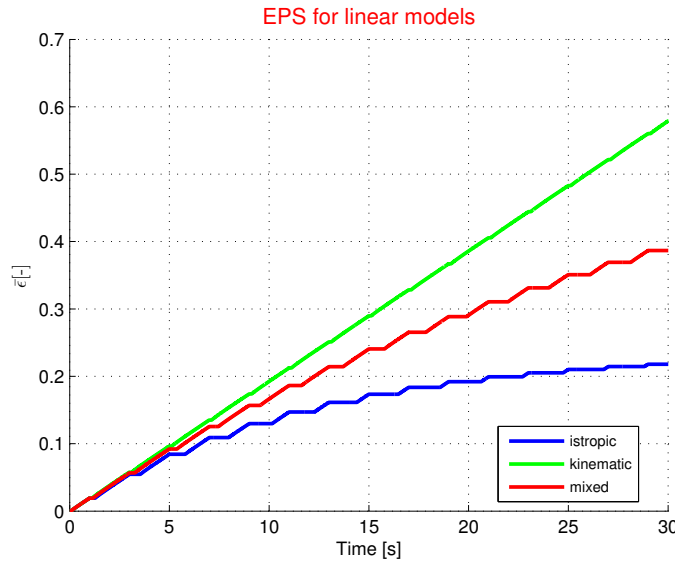


Figure 28 – Evolution of $\bar{\epsilon}_p$ with respect to time for mixed linear hardening model.

To explain the convergence of $\bar{\epsilon}_p$ for mixed and isotropic linear hardening while it is not the case for kinematic linear hardening (and no hardening), we should think about the decomposition of tensor \mathbf{D} . Indeed, we have : $\mathbf{D} = \mathbf{D}^e + \mathbf{D}^p$. For the small strains (which is the case here), we also have : $\boldsymbol{\epsilon} = \boldsymbol{\epsilon}^e + \boldsymbol{\epsilon}^p$. If we realize that after each cycle, $\boldsymbol{\epsilon}$ has to be the same because we impose displacements, it is easy to understand that because of the increase of the yield criterion with isotropic hypothesis,

the amplitude of ϵ^e keeps raising so that the amplitude of ϵ^p and to decrease over the cycles. That's why the increase of $\bar{\varepsilon}_p$ tends to zero after many cycles.

Other important parameters We won't discuss about the evolution of other variables that were already described in other models because it would be quite repetitive to remind that we always have the combination of isotropic and kinematic models that is driving the evolution of the variable we studied. However, it is useful to notice that we always have the convergence effect of isotropic hardening.

3 Part 2: Study of elasto-plastic behavior with non-linear hardening

3.1 Non-linear kinematic hardening

A nonlinear kinematic hardening is characterized by the evolution of the backstress tensor described by the Armstrong Frederick's evolution law (equation 3.1) and a constant yield stress $\sigma_Y = \sigma_Y^0$.

$$\dot{\alpha}_{ij} = \frac{2}{3}h_k D_{ij}^{vp} - \eta_k \dot{\bar{\varepsilon}}^{vp} \alpha_{ij} \quad (3.1)$$

We can decompose the right-hand-side term of the equation. The first term represents the linear evolution of the backstress tensor, characterized by the kinematic hardening factor h_k and the displacement induced by this term is in the same direction as D_{ij} (the plastic flow). The second terms represent the dynamic recovery of the backstress tensor. At first, we will determine the unit of the parameter η_k . The left-hand-side term of the evolution law is expressed in $\frac{MPa}{Sec}$. For the non-linear term, α is in MegaPascal and $\dot{\bar{\varepsilon}}^{vp}$ is Sec^{-1} such that η_k is without unit. As we can see, this term as an opposite sign to the linear term : it tends to bring back the backstress to its initial position. This recovery term depends on the dynamic recovery parameter η_k , in the equivalent plastic strain rate and in the current state of the backstress tensor. If those three values are great, the rate of change of the backstress tensor decreases and the non linear dependence will increase. This tends then to keep the elastic domain at its initial position. As we can see, if $\eta_k = 0$, we recover the linear kinematic hardening assumption. This term only influences during the plastic phases because of the dependence in the plastic strain rate.

We can also re-write this equation under the form 3.5

$$\dot{\alpha}_{ij} = \frac{2}{3}k_k D_{ij}^p - \eta_k \dot{\bar{\varepsilon}}^p \alpha_{ij} \quad (3.2)$$

$$= \frac{2}{3}h_k \lambda N_{ij} - \eta_k \sqrt{\frac{2}{3}} \lambda \alpha_{ij} \quad (3.3)$$

$$= \lambda \left(\frac{2}{3}h_k N_{ij} - \eta_k \sqrt{\frac{2}{3}} \alpha_{ij} \right) \quad (3.4)$$

$$\Rightarrow \dot{q}^k(\sigma, \alpha) = \lambda r^k(\sigma, \alpha) \quad (3.5)$$

For the We may now compute the plastic modulus : $H^p = \frac{1}{\lambda} \frac{\partial f}{\partial \sigma_{ij}} \sigma_{ij}$ by means of the consistency equation (equation 3.6).

$$\dot{f} = \frac{\partial f}{\partial \sigma_{ij}} \dot{\sigma}_{ij} + \frac{\partial f}{\partial q^k} \dot{q}^k = 0 \quad (3.6)$$

We get for the plastic modulus $H^p = -\frac{1}{\lambda} \frac{\partial f}{\partial q^k} \dot{q}^k = -\frac{1}{\lambda} \frac{\partial f}{\partial \alpha} \dot{\alpha}$. in the case of the Armstrong Frederick evolution law of the backstress we get the relation 3.7.

$$H^p = -\frac{\partial f}{\partial \alpha_{ij}} \left(\frac{2}{3}h_k N_{ij} - \eta_k \sqrt{\frac{2}{3}} \alpha_{ij} \right) \quad (3.7)$$

If we use the Von Mises Yield criterion : $f = \sqrt{\frac{3}{2}(s_{ij} - \alpha_{ij})(s_{ij} - \alpha_{ij})} - \sigma_y$ we can deduce the following equation.

$$\frac{\partial f}{\partial \alpha_{ij}} = -\sqrt{\frac{3}{2}} \frac{(s_{ij} - \alpha_{ij})}{\sqrt{(s_{ij} - \alpha_{ij})(s_{ij} - \alpha_{ij})}} \quad (3.8)$$

From eqn. 3.8 and eqn. 3.7 we get a final expression for H^p .

$$H^p = \left(\sqrt{\frac{3}{2}} \frac{(s_{ij} - \alpha_{ij})}{\sqrt{(s_{ij} - \alpha_{ij})(s_{ij} - \alpha_{ij})}} \right) \left(\frac{2}{3} h_k N_{ij} - \eta_k \sqrt{\frac{2}{3}} \alpha_{ij} \right) \quad (3.9)$$

$$= \frac{\sqrt{2}}{\sqrt{3}} h_k - \eta_k N_{ij} \alpha_{ij} \quad (3.10)$$

Asymptotic value for α_{ij} If we reach a stable state, there is no more rate of change for the backstress tensor. By substituting this in the equation 3.1 we get:

$$\eta_k \dot{\varepsilon}^p \alpha_{ij}^u = \frac{2}{3} h_k D_{ij}^p \quad (3.11)$$

$$\Rightarrow \alpha_{ij}^u = \frac{2 h_k \lambda N_{ij}}{3 \eta_k \lambda \sqrt{\frac{2}{3}}} \quad (3.12)$$

$$\Leftrightarrow \alpha_{ij} = \sqrt{\frac{2}{3}} \frac{h_k}{\eta_k} N_{ij} \quad (3.13)$$

So we find the equivalent asymptotic backstress :

$$\bar{\alpha}^u = \sqrt{\frac{3}{2} \frac{2}{3} N_{ij} N_{ij}} \frac{h_k}{\eta_k} = \frac{h_k}{\eta_k}$$

The higher the dynamic recovery parameter, the lower the asymptotic value for the equivalent backstress.

Influence of the dynamic recovery parameter From the Armstrong Frederick's evolution law (equation 3.1) we can deduce some information about the influence of the dynamic recovery parameter η_k .

In order to represent a recovering, it is compulsory to only consider positive values of η_k .

As we already said it, if we set the parameter at zero we get back the linear case of kinematic hardening. This means that there is no recovering of the material.

If we increase the value of η_k , we increase as well the weight of the non linear part of the evolution of the backstress tensor. This leads to a greater dynamic recovering. A very large value of η_k would lead to a model where only the non-linear part has influence on the results.

In order to better determine the influence of the parameter η_k , we will study the evolution of some parameters at the point $P1$ with different values of η_k .

n.b.: it is unnecessary to study the evolution of the equivalent Von Mises stress as the yield stress because these values take into account the position of the center of the elastic domain. The Von Mises equivalent stress only represents the distance of the equivalent stress with respect to the center of the elastic domain. And the yield stress, the radius of the elastic domain.

Equivalent plastic strain From the appendix of the project statement (eqn. 3.14), we can interpret the plastic modulus.

$$\dot{\sigma}_{ij} \dot{\varepsilon}_{ij}^p = \sqrt{\frac{3}{2}} (\dot{\varepsilon}^p)^2 H^p \quad (3.14)$$

However, as we have seen, H^p is not constant along the cycle. When we are in plasticity and when we approach the maximum displacement, the tensors $s_{ij} - \alpha_{ij}$ and α_{ij} are almost parallel. In the same direction. Because the parameter H^p is dependent in $-\eta_k N_{ij} \alpha_{ij}$, the value of the parameter H^p will decrease because of the quasi maximum of this product. When the loading reaches its maximum,

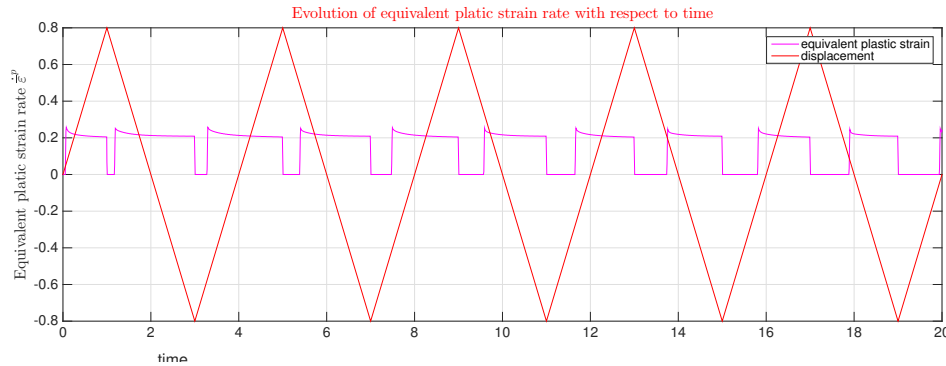


Figure 29 – Evolution of the time derivative of the equivalent plastic strain during a loading unloading cycle with a non linear kinematic hardening material.

crosses the elastic domain and then reaches the yield surface but at the opposite point of the previous one, the tensors $s_{ij} - \alpha_{ij}$ and α_{ij} are almost anti-parallel. This means that the product reaches its minimum and is negative. This will increase the value of the parameter H^p and the product $\dot{\sigma}_{ij}\dot{\varepsilon}_{ij}^p$ will reaches a maximum. This means that at each re-entry into plasticity, the plastic effects are stronger if there is a non-linear kinematic hardening. The behaviour described here above is easy to observe. Each re-entry in plasticity occur after the elastic phase $\dot{\varepsilon}^p = 0$, during the unloading (from maximum amplitude to a zero amplitude). Thanks to the formula of H^p we see that this effect is linear with respect to η_k . The higher the value of η_k the harder the effect of the non-linear kinematic hardening. This will be visible on all the graphs below, the plastic effect will be stronger at the beginning of each elasto-plastic phase. The values will stronger evolve at the beginning of the hardening.

Equivalent backstress The first value we will study is the equivalent backstress. As we can see on Figure 30, the higher the value of the parameter η_k , the less linear the evolution of the equivalent backstress, and the lower the maximum value of the equivalent backstress. The general evolution of the equivalent backstress during the hardening seems to follow a rule in $\alpha = \alpha_{max} * (1 - e^{-At})$. Where A is proportional to η_k and α_{max} inversely proportional to η_k . This comes from the negative influence of the current value of the backstress tensor on its evolution by the dynamic recovering term in the equation 3.1. A short conclusion based on this graph is the following : if η_k tends to zero then the behaviour tends to a linear kinematic hardening behaviour, if η_k tends to infinity, then the behaviour tends to a perfectly plastic behaviour.

The effect described here above is visible. The time derivative of the backstress tensor is proportional to $-\eta_k \dot{\varepsilon}^p \alpha_{ij}$. We can see that the slope of the equivalent backstress is much more steep at the re-entry in plasticity in the opposite direction than at the end of the previous elasto-plastic phase. As it was also said, but not shown, this effect is much stronger if the parameter η_k increases.

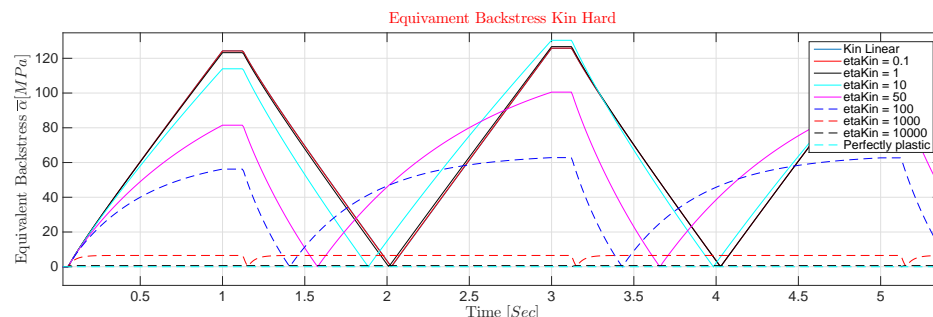


Figure 30 – Evolution of the equivalent backstress with respect to time with different values for η_k . Non linear kinematic hardening.

Equivalent stress We can not measure the influence of η_k on the equivalent Von Mises stress but we can measure it on the equivalent stress because it doesn't take into account the position of the center of the elastic domain. As we can see on Figure 31, the same conclusions as above can be taken. If η_k tends to infinity, the range of admissible values for the equivalent stress doesn't evolves and stays the same as the one for a virgin material : no hardening. If the value of η_k tends to zero, we get back the same behaviour as for a linear kinematic hardening assumption. As well as above, the equivalent stress seems to follow a rule in $\sigma = \sigma_{max} * (1 - e^{-At})$. Where A is proportional to η_k and σ_{max} inversely proportional to η_k .

On Figure 32 and Figure 33 the same conclusion can be taken (except for the shape of the rule for the

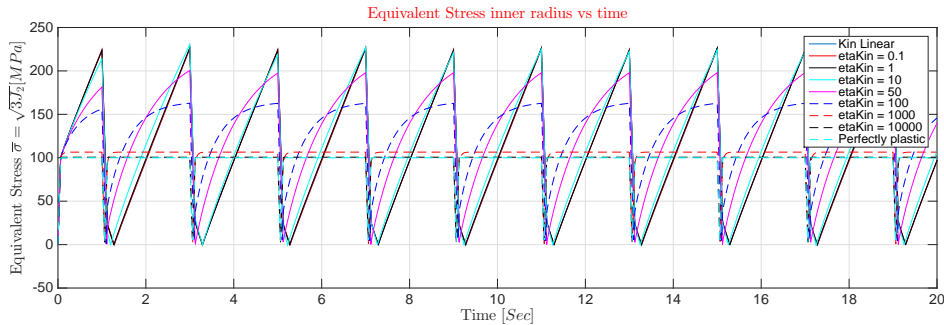


Figure 31 – Evolution of the equivalent stress with respect to time with different values for η_k . Non linear kinematic hardening.

equivalent plastic strain). This is why we won't go deeper into the influence of η_k on the behaviour of the material. The limitations of η_k are the following : if it tends to zero, we get back an linear kinematic hardening. If it tends to infinity, we recover a perfectly plastic behaviour.

Note that the equivalent plastic strain doesn't evolve linearly during the plastic phases : it evolves faster at the beginning of the hardening than at the end thanks to the non-linear kinematic hardening effect explained above. See Figure 29. The non linear effect are more visible if the parameter η_k increases. Remarks: all the data's shown on the graphs are computed at point P1.

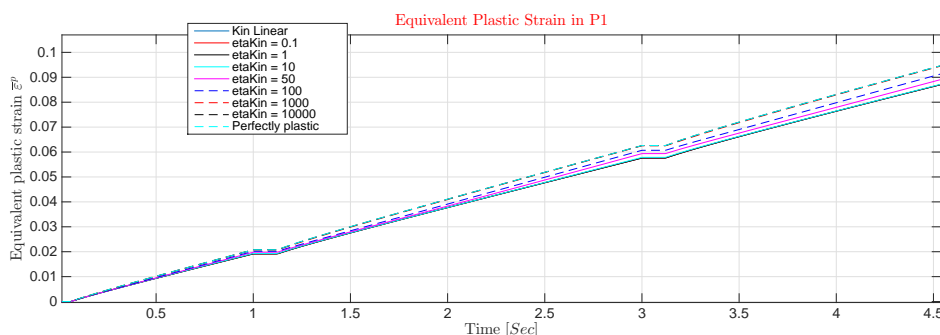


Figure 32 – Evolution of the equivalent strain with respect to time with different values for η_k . Non linear kinematic hardening.

By opposition with an isotropic hardening, the durations of the elastic and elasto-plastic phases stay constant in time. Even if more cycles are performed. This can be seen on Figure 32 (resp. Figure 30) where the horizontal plateaus occur at the same time for the different values of η_k and have the same length (duration). Remember that an horizontal plateau means no evolution of the equivalent plastic strain (resp. equivalent backstress) which corresponds to the elastic phases. This comes from the fact that a kinematic hardening doesn't enlarge the elastic domain : the size of it remains constant and correspond to a range of equivalent stress of same size, but shifted. Because the loading rate is the same, the time required to cross a range of stress value of same length in the elastic phase is the

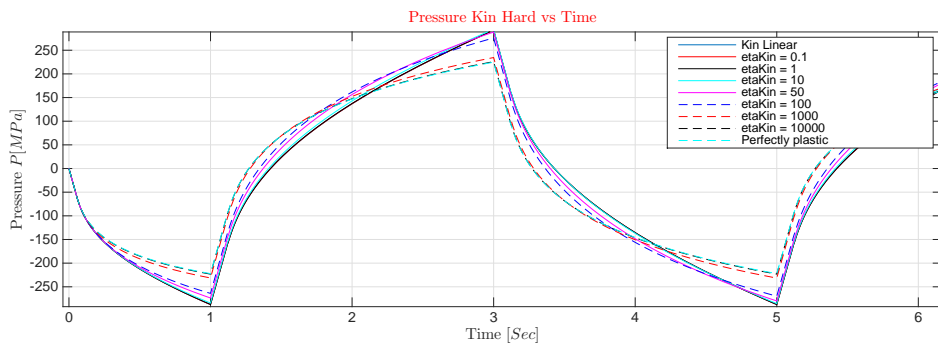


Figure 33 – Evolution of the pressure with respect to time with different values for η_k . Non linear kinematic hardening.

same. Even if the range is at a different place. This is to seen on Figure 31 : the duration of the linear (elastic) phase is the same and occurs at same time : the beginning of the unloading (from u_{max} or $-u_{max}$ to 0) but happens at different values of $\sqrt{3J_2}$ because the center of the elastic domain has moved of a different amplitude, but has not been enlarged.

Influence of u_{max} at fixed value of $\eta_k (=500)$. Basically, increasing the maximum displacement will lead to a greater ratio "elasto-plastic phase duration over elastic phase duration" for a loading unloading cycle. This will lead to the same phenomena but with a higher amplitude and occurs faster in the cycle. Further more, the difference in the evolution rate of the parameters at the beginning and the end of the hardening will increase.

Equivalent backstress The bigger the displacement the faster the maximum equivalent backstress reaches its maximum during a cycle. this maximum value of the backstress exists because of the shape of the evolution of the backstress during the hardening. This upper limit doesn't seem to depend on the maximum displacement. This can be seen on Figure 34. For the purple curve, the plateaus are linked with the elastic phase. Those kinds of plateaus are longer over a cycle if the maximum amplitude of the displacement is lower. It always begins with the elastic phase (beginning of unloading). For the other curve, there is plateau ahead of the elastic phase. This is a plateau coming from the fact that the equivalent backstress has reached its maximum value, asymptotic value. When the elastic domain is fully crossed, the equivalent backstress first drops to 0 (the loading occurs in the opposite way as just before and bring back the center of the yield surface to its initial position). And then cross its initial position and is "loaded" in the opposite way to reach its maximum value. When the displacement changes of direction the same phenomenon as above happens, but in the opposite directions. As we also can see on Figure 34, if the applied displacement has not a large enough amplitude to make the equivalent backstress converge to its upper limits, during the first cycle the horizontal plateaus of the equivalent backstress will not happen at the same value. But, yet for the second cycle, a "balance" is reached such as in the linear case.

The effect of the non-linear kinematic hardening is already visible. the slope of $\bar{\alpha}$ is steeper at the beginning of the hardening than at the end of the previous hardening phase. This effect increases with the increasing displacement amplitude. This comes from the dependence in the localisation of the backstress tensor for the value H^p . This phenomenon will also be visible for each values on the graphs below.

Thanks to the non linear kinematic hardening, the parameter H^p depends on $-\eta N_{ij} \alpha_{ij}$. This means that at the first loading (to u_{max}) at the beginning, H^p is not affected by this term : $\alpha_{ij} = 0$. during the loading, N_{ij} and α_{ij} are in the same direction in the Haigh-Weistergaard's space. So that H^p decrease : $\dot{\bar{\varepsilon}}$ is less important. This during the whole first hardening. This leads to a relative low equivalent backstress. At the beginning of the unloading, after the elastic phase that we will not discuss, the

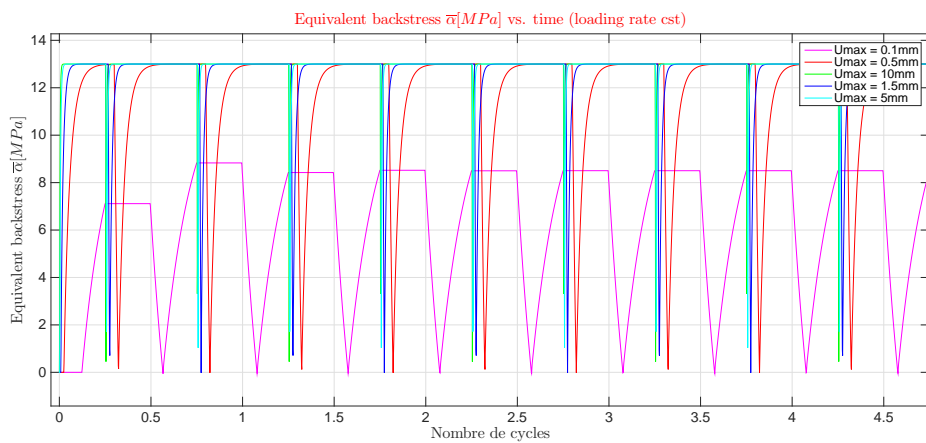


Figure 34 – Influence of the maximum displacement on the equivalent backstress for a non-linear kinematic hardening.

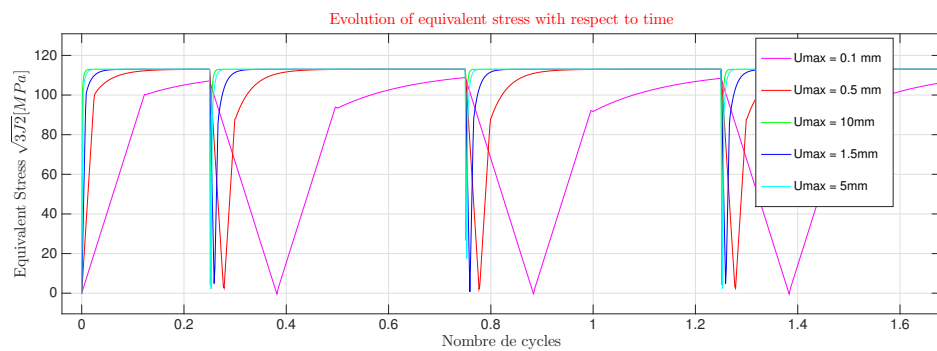


Figure 35 – Influence of the maximum displacement on the equivalent stress for a non-linear kinematic hardening.

tensor N_{ij} and α_{ij} are in opposite directions. Their product is then negative : the plastic modulus increases. The rate of equivalent plastic strain increases. Moreover, α_{ij} is different from zero and is opposite with N_{ij} , D_{ij} . All this factors will increase the rate of the backstress tensor in the same direction as N_{ij} . This will make come back the backstress tensor to its initial position faster than when it did in the opposite way. It will be back at 0 and the remaining displacement in the same direction is larger than the plastic displacement of the first hardening. The imposed displacement to $-u_{max}$ will provide a backstress tensor in the opposite direction than the one corresponding to the first hardening phase. This will lead the backstress tensor to a position that is more away from the zero position at $-u_{max}$ than at u_{max} . We have the same for the next unloading but the distance to cross in order to reach the zero position is bigger. That will lead to a smaller amplitude of the equivalent back stress at the next u_{max} than at the previous $-u_{max}$ but bigger than the previous u_{max} . This scheme will repeat such that an equilibrium position will be found. All this is shown on Figure 34. To sum up : if the imposed stress is in the opposite direction to the backstress tensor, the displacement of the backstress tensor is faster. So that it takes less time to cross the same distance to go back to zero. The remaining displacement to perform is then larger than the plastic displacement of the first hardening phase and will be done along the "same way" that will result in a larger equivalent backstress.

Equivalent Stress For the equivalent stress, exactly the same conclusions can be taken that for the equivalent backstress : the bigger the displacement the faster into plasticity and the more plastic effect we get on a cycle. There also exists a maximum plateau for the equivalent stress, for the same reasons as for the equivalent backstress. Here, the elastic phases are represented with linear parts of the graph. The horizontal plateau is linked to the existence of a maximum equivalent backstress and

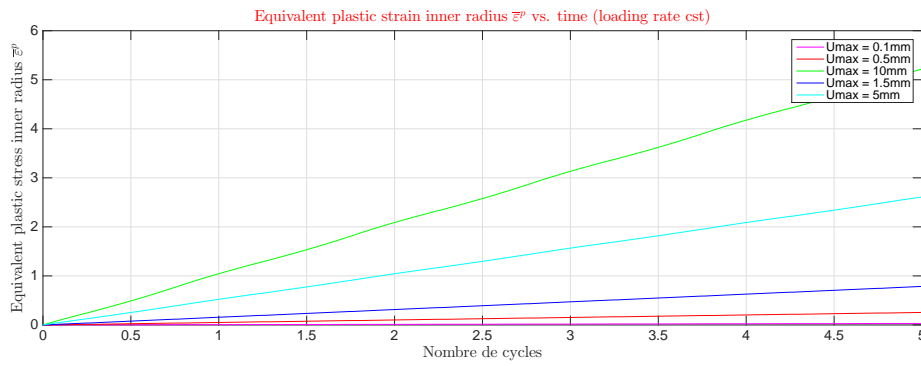


Figure 36 – Influence of the maximum displacement on the equivalent plastic strain for a non-linear kinematic hardening.

the constant yield stress for a non-linear kinematic hardening. Important to note that the maximum equivalent stress is always lower or equal to the equivalent Von Mises stress plus the equivalent backstress if we have a kinematic hardening (or mixed).

The maximum equivalent stress can be bounded in the Haigh-Westergaard's space thanks to the triangular inequality.

$$\sqrt{3J_2} = \sqrt{\frac{3}{2}s_{ij} : s_{ij}} \quad (3.15)$$

$$= \sqrt{\frac{3}{2}\|s\|} \quad (3.16)$$

$$= \sqrt{\frac{3}{2}\|(s - \alpha) + \alpha\|} \quad (3.17)$$

$$\leq \sqrt{\frac{3}{2}(\|s - \alpha\| + \|\alpha\|)} \quad (3.18)$$

$$\Rightarrow \sqrt{3J_2} \leq \sigma_{VM} + \bar{\alpha} \quad (3.19)$$

If we want to generalize to mixed hardening, we must remember that the equivalent Von Mises stress is always lower or equals to the yield stress. So we get the general upper bound of the equivalent stress.

$$\Rightarrow \sqrt{3J_2} \leq \sigma_Y^0 + \bar{\alpha} \quad (3.20)$$

Here, the equivalent stress is effectively bounded by $100MPa + 13MPa = 113MPa$.

This means that, if we want to keep evolving the state stress while the equivalent backstress and the yield stress have reached their asymptotic values, we must apply a loading that is not perpendicular to the yield surface : the components of the stress state evolve thanks to the tangent components of the loading to the yield surface but the equivalent stress doesn't evolve. It stays on the yield surface.

Equivalent plastic strain As it can be expected, the equivalent plastic strain evolves much more on a loading-unloading cycle if the maximum displacement has a bigger amplitude, the elastic plateaus tends to disappear if the ratio elastic phase over elasto-plastic phase tends to zero. It is important to note that if the amplitude is not great enough to make the inner layer of the sphere into plasticity, there would not be any plastic effect. All this is to seen on Figure 36.

The non linear effects are also visible and even more if the amplitude of the displacement is bigger. The rate of the equivalent plastic strain is bigger at the re-entry in the elasto-plastic domain.

3.2 Non-linear kinematic hardening combined with linear isotropic hardening

Such a behaviour is characterized by the equation 3.1 (the Armstrong Frederick's evolution law for the backstress tensor) and the equation 3.21 for the evolution of the backstress.

$$\dot{\sigma}_y = \sqrt{\frac{2}{3}}\lambda h_i; \dot{\bar{\varepsilon}}^p = \sqrt{\frac{2}{3}}\lambda \quad (3.21)$$

Which leads to $\sigma_Y = \sigma_Y^0 + h_i \bar{\varepsilon}^p$. with h_i constant. If we derive this function with respect to time we get the equation 3.2.

$$\dot{\sigma}_Y = h_i \dot{\bar{\varepsilon}}^p \quad (3.22)$$

We can find an expression of the generalized plastic modulus H^p for this case by means of the consistency equation and the definition of the plastic modulus.

$$H^p = \frac{1}{\lambda} \frac{\partial f}{\partial \sigma_{ij}} \dot{\sigma}_{ij} \quad (3.23)$$

$$\dot{f} = \frac{\partial f}{\partial \sigma_{ij}} \dot{\sigma}_{ij} + \frac{\partial f}{\partial q^k} \dot{q}^k \quad (3.24)$$

$$= \frac{\partial f}{\partial \sigma_{ij}} \dot{\sigma}_{ij} + \frac{\partial f}{\partial \alpha} \dot{\alpha} + \frac{\partial f}{\partial \bar{\varepsilon}} \dot{\bar{\varepsilon}}^p = 0 \quad (3.25)$$

From this we get the following for the plastic modulus.

$$H^p = -\frac{1}{\lambda} \frac{\partial f}{\partial \alpha} \dot{\alpha} - \frac{1}{\lambda} \frac{\partial f}{\partial \bar{\varepsilon}^p} \dot{\bar{\varepsilon}}^p \quad (3.26)$$

Which leads us to the following.

$$H^p = -\frac{1}{\lambda} \frac{\partial f}{\partial \alpha} \left(\frac{2}{3} h_k N_{ij} - \eta_k \sqrt{\frac{2}{3}} \alpha_{ij} \right) - \frac{\partial f}{\partial \bar{\varepsilon}^p} \sqrt{\frac{2}{3}} \quad (3.27)$$

If we use the Von Mises Equivalent stress in the criterion we have, by replacing the yield stress with its expression in the linear isotropic hardening we get the equation 3.28.

$$f = \sqrt{(s_{ij} - \alpha_{ij})(s_{ij} - \alpha_{ij})} - \sigma_Y^0 - h_i \bar{\varepsilon}^p \quad (3.28)$$

Which leads us to :

$$\frac{\partial f}{\partial \alpha_{ij}} = -\sqrt{\frac{3}{2}} \frac{(s_{ij} - \alpha_{ij})}{\sqrt{(s_{ij} - \alpha_{ij})(s_{ij} - \alpha_{ij})}} \quad (3.29)$$

$$\frac{\partial f}{\partial \bar{\varepsilon}^p} = -h_i \quad (3.30)$$

By use of this two equations above in equation 3.26, we finally get the expression of the plastic modulus (equation 3.31).

$$H^p = \frac{\sqrt{2}}{\sqrt{3}} h_k - \eta_k N_{ij} \alpha_{ij} + h_i \sqrt{\frac{2}{3}} \quad (3.31)$$

Remark :

- such that the parameter h_i is constant, we see that the yield stress evolves linearly with the equivalent plastic strain. This will be shown hereafter 37.

- all what we said about the effect of the non-linear kinematic hardening will stay the same because there is no change in the dependence of H^p with respect to $\eta_k, N_{ij}, \alpha_{ij}$.
- for the mixed hardening, we define a parameter δ such that $h_k = \delta h$ and $h_i = (1 - \delta)h$. In our case we have $\delta = 0.65$. The hardening will have a greater kinematic component than isotropic component. This will stay the same in all the mixed behaviour if the opposite is not specified.
- such the equivalent plastic strain doesn't evolve linearly with time during the hardening phases, the yield stress doesn't evolve linearly with time during the plastic phases. The yield stress is linearly dependent in the equivalent plastic strain.

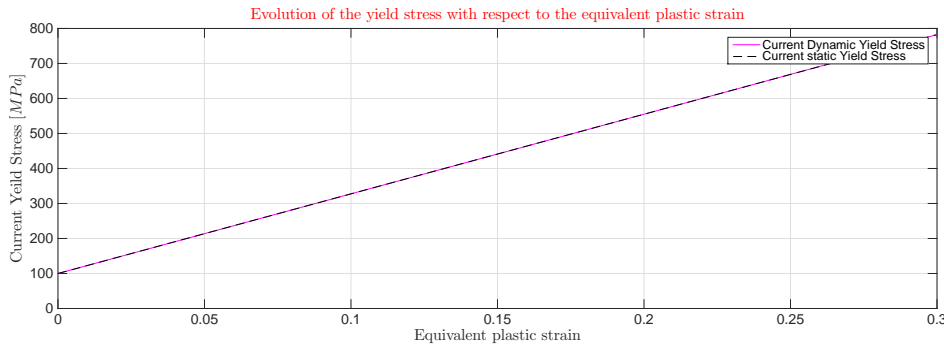


Figure 37 – Evolution of the yield stress with respect to the equivalent plastic strain in a non-linear kinematic and linear isotropic hardening assumption.

Influence of u_{max} at fixed value of $\eta_k = 500$

Equivalent Backstress As we can see on Figure 38, the maximum value of the equivalent backstress decreases with time. This comes from the fact that the elastic domain enlarges and there is deformation at each cycle in the elasto-plastic domain. It takes more time in case of great displacement to decrease because the ratio duration in elasto-plastic over duration in elastic is greater at the beginning of one cycle. Furthermore, we can compare the Figure 38 with the figure 34. In the non-linear kinematic hardening case, the maximum equivalent backstress reaches directly a fixed value and doesn't evolve anymore. This value is also much bigger than in the mixed case. In the mixed case, the maximum value tends to zero.

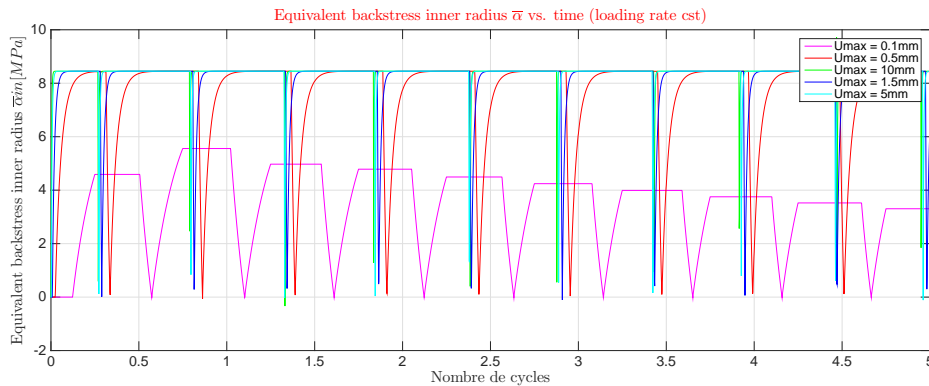


Figure 38 – Evolution of the equivalent backstress in case of non-linear kinematic linear isotropic hardening.

Equivalent plastic strain, current yield stress and equivalent Von Mises stress Because the yield stress depends linearly with the equivalent plastic strain, we can study both graphs simultaneously. We see that at the beginning of the studied phases, the elastic (horizontal) plateaus of both values are little and with the increasing of time and yield stress the elastic phases take more time and limit the evolution of both values. This will lead to an asymptotic value for both. This value will increase with the amplitude of the displacement. The horizontal plateau will be greater at the same time if the displacement is smaller. On Figure 39 and 40 we can easily observe the linear correlation of both quantities. This behaviour is also visible on the evolution of the equivalent Von Mises stress

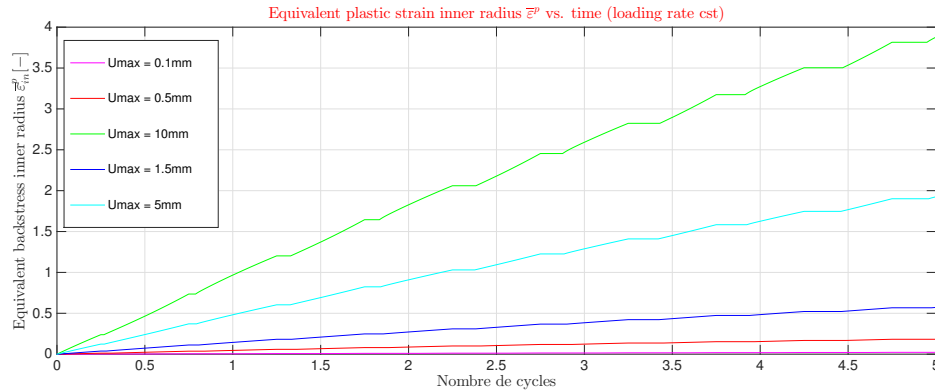


Figure 39 – Evolution of the equivalent plastic strain in case of non-linear kinematic linear isotropic hardening.

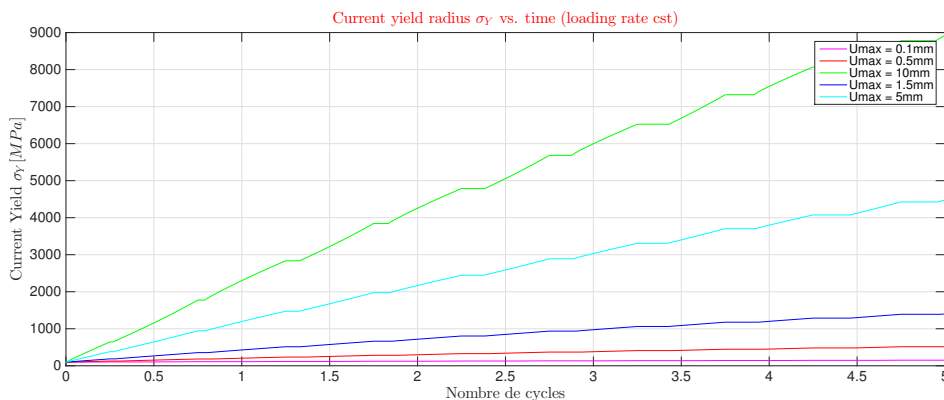


Figure 40 – Evolution of the current yield stress in case of non-linear kinematic linear isotropic hardening.

(Figure 41). The elastic phases take more time at each new cycle by opposition of the elasto-plastic hardening phases. The maximum equivalent Von Mises stress increases with time and will converge to the stress corresponding to a fully elastic displacement. This evolution is faster in case of greater value of u_{max} . The non linear kinematic effect are visible on the graph 39. The slope of the equivalent plastic strain is steeper at the beginning of the hardening than at the end.

Equivalent Stress On Figure 42 we can see the evolution of the equivalent stress with respect to time. If the amplitude of the displacement is bigger, the isotropic effects appear faster. The bigger the amplitude the faster the increase of the equivalent stress. It is important to see that the equivalent stress evolves linearly with the equivalent plastic strain during the elasto-plastic phases. This comes from the fact that the yield stress evolves linearly with the equivalent plastic strain and leads the equivalent stress during hardening. We can see that the plastic phases become longer with time : the elastic

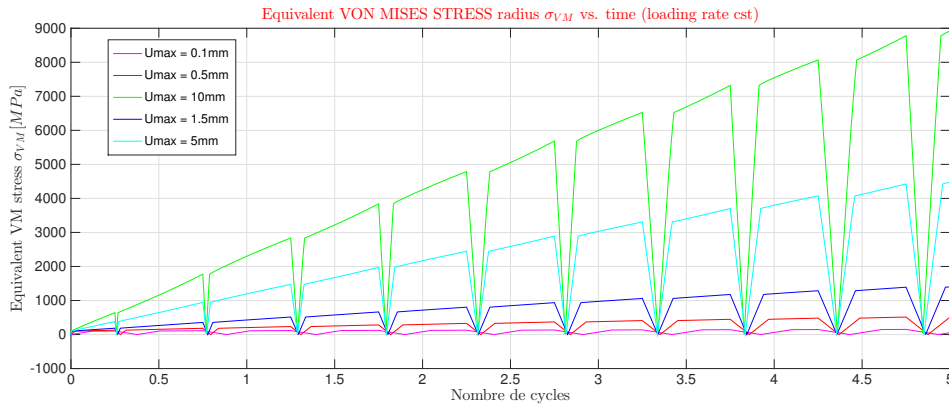


Figure 41 – Evolution of the Von Mises equivalent stress in case of non-linear kinematic linear isotropic hardening.

domain expands thanks to the isotropic hardening. Because the isotropic hardening is linear, and that the amplitude of the displacement is fixed, the yield stress will converge to a fixed value in time such that the whole displacement happens in the elastic domain. There won't be hardening anymore. As

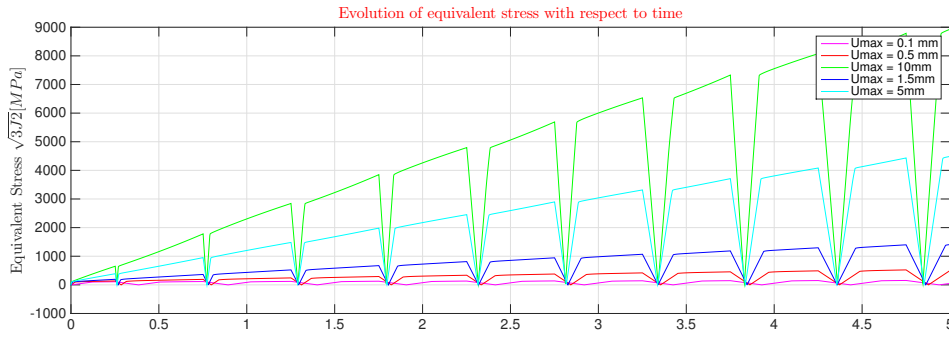


Figure 42 – Evolution of the equivalent stress in case of non-linear kinematic linear isotropic hardening.

we have seen during the non linear kinematic hardening, the equivalent stress is bounded by the sum of the yield stress and the equivalent backstress. At fixed maximum displacement, the asymptotic value of the equivalent backstress is zero and the yield stress converges to a finite value depending on the maximum displacement. So the equivalent stress will converge to the yield stress.

3.3 Non-linear kinematic hardening combined with a non-linear isotropic hardening

By comparison with the previous section, the law that describes the evolution of the yield stress changes. The rule that drives the evolution of the backstress tensor is still the Armstrong Frederick's evolution law (eqn. 3.1) but the yield stress follow the equation 3.32.

$$\sigma_Y = \sigma_Y^\infty - (\sigma_Y^\infty - \sigma_Y^0) e^{-\frac{h_i \bar{\varepsilon}^{vp}}{\sigma_Y^\infty - \sigma_Y^0}} \quad (3.32)$$

Remark :

- This corresponds to a non linear evolution of the yield stress with respect to the equivalent plastic strain. For a fully plastified material, the yield stress will converge to σ_Y^∞ . This convergence is done with a negative exponential rate with respect to the equivalent plastic strain.

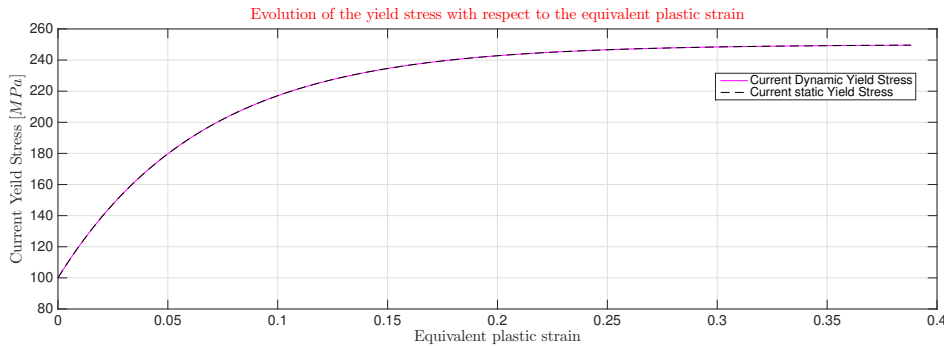


Figure 43 – Evolution of the yield stress with respect to the equivalent plastic strain

- All the effects on the rate of the $\dot{\bar{\varepsilon}}^p$ linked to the non linear kinematic hardening are still valid. As we can see on equation 3.35, the modification on the generalized plastic modulus only concerns the isotropic hardening which is no more constant.

If we want to obtain the expression of the generalized plastic modulus the development is the same as above but we must change the evolution rule of the yield stress. We can still use the equations 3.27 and 3.29. The expression of the yield criterion becomes 3.33.

$$f = \sqrt{(s_{ij} - \alpha_{ij})(s_{ij} - \alpha_{ij})} - \left(\sigma_Y^\infty - (\sigma_Y^\infty - \sigma_Y^0) e^{-\frac{h_i \bar{\varepsilon}^{vp}}{\sigma_Y^\infty - \sigma_Y^0}} \right) \quad (3.33)$$

Equation 3.33 leads us to equation 3.34.

$$\frac{\partial f}{\partial \bar{\varepsilon}^{vp}} = -h_i e^{-\frac{h_i \bar{\varepsilon}^{vp}}{\sigma_Y^\infty - \sigma_Y^0}} \quad (3.34)$$

Thanks to this we can express the generalized plastic modulus with equation 3.35.

$$H^p = \frac{\sqrt{2}}{\sqrt{3}} h_k - \eta_k N_{ij} \alpha_{ij} + h_i e^{-\frac{h_i \bar{\varepsilon}^{vp}}{\sigma_Y^\infty - \sigma_Y^0}} \sqrt{\frac{2}{3}} \quad (3.35)$$

As we can see, the non linear isotropic term has the opposite sign of the non linear kinematic term. If we accept that the equivalent plastic strain represents the level of hardening, we can see that if it increases, H^p decreases. This means that there exists a kind of saturation linked to the non linear isotropic hardening.

The figure 43 shows that the yield stress is absolutely not linear with respect to the equivalent plastic strain. As we can see, the higher the equivalent plastic strain the less steep is the slope and the yield stress converges to $\sigma_Y^\infty = 250 \text{ MPa}$.

Influence of u_{max} at fixed value of $\eta_k = 500$

Equivalent backstress As we can see on Figure 44 there are two different behaviours. If it is possible to make the whole displacement in elasticity, it means that the equivalent Von Mises stress corresponding to the maximum displacement is lower than σ_Y^∞ (it exists a state such that the whole displacement happens in the elastic domain) then the equivalent backstress will converge to zero if several loading unloading cycles are performed. If the Von Mises equivalent stress corresponding to the maximum displacement is equal to σ_Y^∞ (it doesn't exist a state where the total displacement take place in the elastic domain, if we multiply the young modulus with the deformation that provides the displacement, the result is bigger than the saturation stress) then there will always be a plastic phase

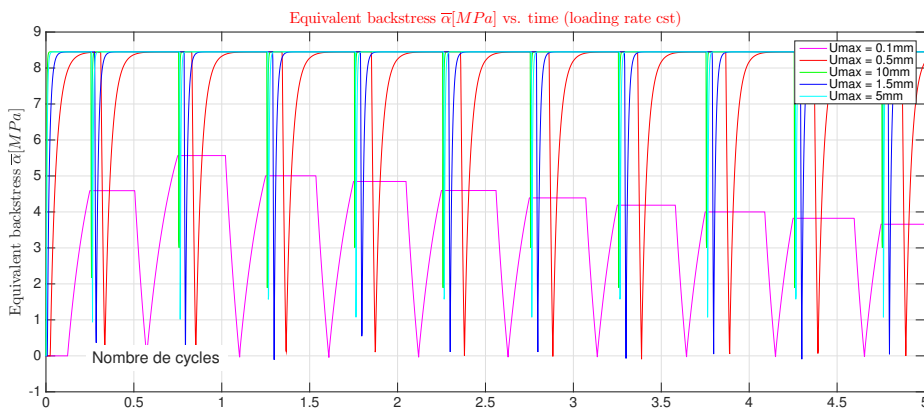


Figure 44 – Evolution of the equivalent backstress with the number of achieved cycles. Non linear mixed hardening.

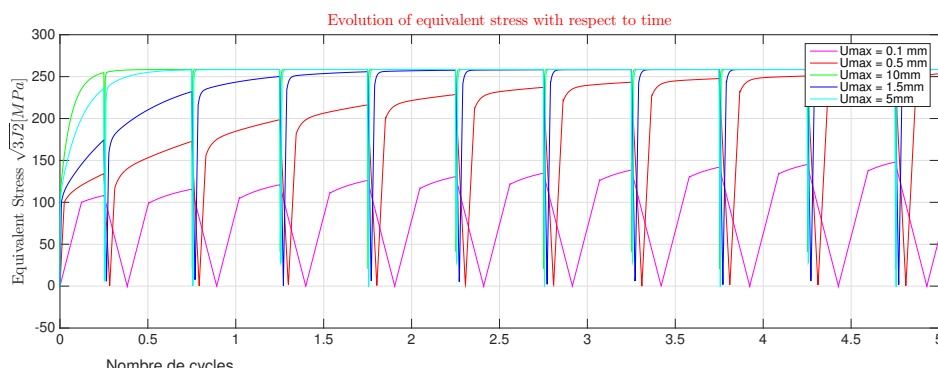


Figure 45 – Evolution of the equivalent stress with the number of achieved cycles. Non linear mixed hardening.

and a kinematic hardening even if the isotropic hardening is saturated. This means that the yield surface will "keep moving" at certain moments during the loading unloading cycle. There will exists a maximum equivalent backstress different from zero even if the number of cycles tends to infinity. If u_{max} is too large, the equivalent back stress will not converge to zero.

Equivalent stress If we compare the figure 45 with the figure 42 we can see that the evolution of the maximum equivalent stress doesn't evolve on the same way. This comes from the fact that the yield stress doesn't follow the same rule. As yet said, the maximum equivalent stress is lower or equal to the yield stress plus the equivalent backstress. There are here two cases to study. The first is when the displacement can be fully elastic. In this case, the equivalent stress converge to the asymptotic value of the yield stress : $\sigma_Y^\infty = 250 MPa$. If the displacement is too large to be performed fully elastically, the backstress doesn't converge to a finite value.

Current yield stress As we can see on Figure 46, the yield stress evolves, (during the plastic phases) in a negative exponential shape to the saturation yield stress σ_Y^∞ if the displacement is large enough to harden the material to its limit. We can also observe the horizontal plateaus occurring during the elastic phases if the yield stress is lower than the saturation yield stress. One the yield stress has reached its saturation value, the material behaves like a non-linear kinematic hardening material with a yield stress equal to the yield stress limit. The figure 47 also shows that the derivative of the yield stress with respect to the equivalent plastic strain decreases if the equivalent plastic strain increases. This explains the effect of the thirst term in the expression of H^p .

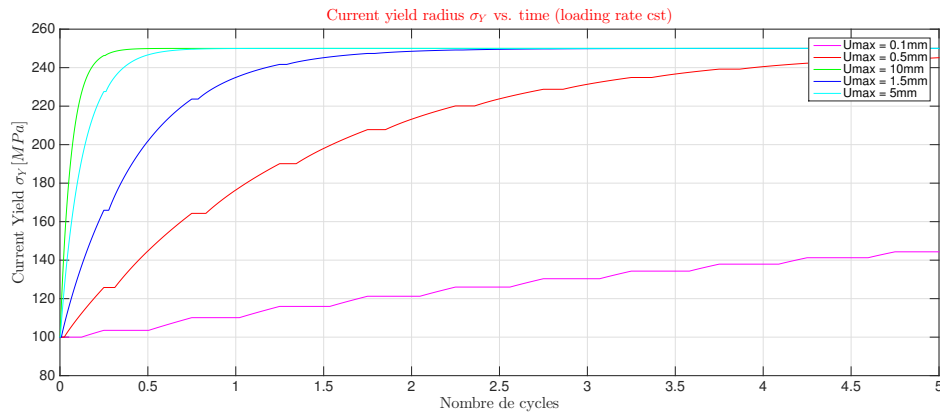


Figure 46 – Evolution of the yield stress with the number of achieved cycles. Non linear mixed hardening.

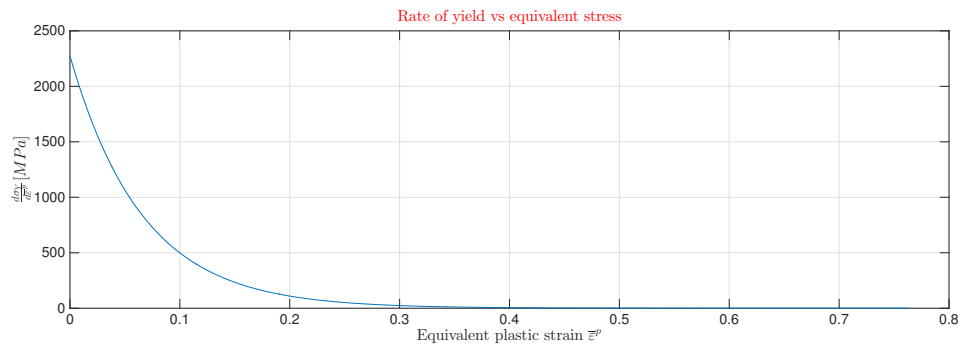


Figure 47 – Evolution of the derivative of the yield stress with respect to the equivalent plastic strain.

Equivalent plastic strain As we can see on Figure 48, the equivalent plastic strain increases with time much faster if the displacement is bigger. The evolution of the equivalent plastic strain is not exactly linear. It increases faster at the beginning of each hardening phase than at the end.

3.4 Non linear kinematic hardening in the case of a simple tension test

In this case, the backstress tensor may be expressed only in function of its first component as well as the plastic stain tensor. Their equivalent values are then the absolute value of this component.

$$\bar{\varepsilon}^p = |\varepsilon^p| \quad (3.36)$$

$$\bar{\alpha} = |\alpha| \quad (3.37)$$

In this case, the equation 3.1 becomes the following.

$$\dot{\alpha} = h_k \dot{\bar{\varepsilon}}^p - \bar{\varepsilon}^p \eta_k \alpha \quad (3.38)$$

If we assume that $\alpha(\bar{\varepsilon}^p = 0) = 0$ we get at the end of the next expression for α in tension ($\dot{\varepsilon}^p > 0$).

$$\alpha = \frac{1}{\eta_k} (h_k - e^{\alpha_0 - \eta_k \bar{\varepsilon}^p}) \quad (3.39)$$

Where α_0 is the backstress at the end of the previous loading. In compression ($\dot{\varepsilon}^p < 0$)we get the next one.

$$\alpha = \frac{1}{\eta_k} (e^{\alpha_0 + \eta_k \bar{\varepsilon}^p} + h_k) \quad (3.40)$$

Knowing that $\frac{d\sigma}{d\varepsilon^p} = \sqrt{\frac{3}{2}} H^p$ and that, in non linear kinematic hardening $H^p = \sqrt{\frac{2}{3}} h_k - \eta_k \alpha$. We can deduce the derivative of σ with respect to ε^p in compression and tension.

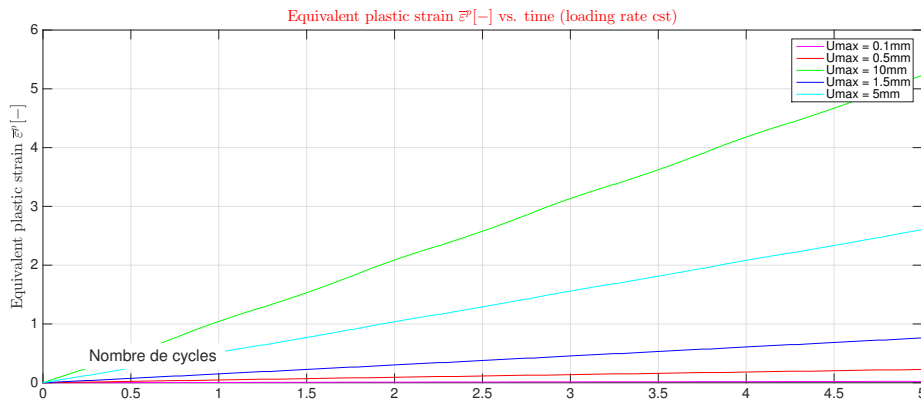


Figure 48 – Evolution of the equivalent plastic strain with time in case of a non linear mixed hardening.

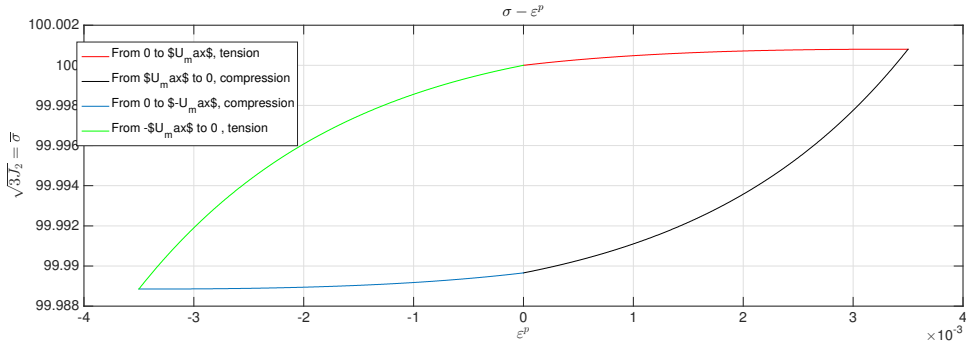


Figure 49 – Evolution of the equivalent stress in the plastic phases. Tensile test.

- Tension

$$\frac{d\sigma}{d\varepsilon^p} = h_k \left(1 - \sqrt{\frac{3}{2}}\right) + \sqrt{\frac{3}{2}} e^{\alpha_0 - \eta_k \varepsilon^p}$$

This leads us to, by integration.

$$\sigma(\varepsilon^p) = A + h_k * \varepsilon^p \left(1 - \sqrt{\frac{3}{2}}\right) - \frac{\sqrt{\frac{3}{2}} h_k}{\eta_k} e^{\eta_k \varepsilon^p} \quad (3.41)$$

- Compression

$$\frac{d\sigma}{d\varepsilon^p} = h_k \left(1 - \sqrt{\frac{3}{2}}\right) - \sqrt{\frac{3}{2}} e^{\alpha_0 + \eta_k \varepsilon^p}$$

This leads us to the following formula.

$$\sigma(\varepsilon^p) = B + h_k * \varepsilon^p \left(1 - \sqrt{\frac{3}{2}}\right) - \frac{\sqrt{\frac{3}{2}} h_k}{\eta_k} e^{-\eta_k \varepsilon^p} \quad (3.42)$$

Where A and B are chosen in order to ensure the continuity of the slope and the initial conditions. If we plot the corresponding curve we get the figure 49. On Figure 49 we can deduce some interesting behaviour. If we assume that the backstress tensor is directly proportional to the plastic strain tensor, we deduce that the evolution of the equivalent stress (if the yield stress is constant, all the evolution of the equivalent stress comes from the evolution of the backstress tensor) is much more important when the applied loading is in the opposite direction than the current plastic strain tensor (or backstress tensor). This is suitable with the non-linear effect that we have already explained : H^p increase if $(s_{ij} - \alpha_{ij}) : \alpha_{ij}$ is negative : loading in the opposite direction than the current plastic deformation.

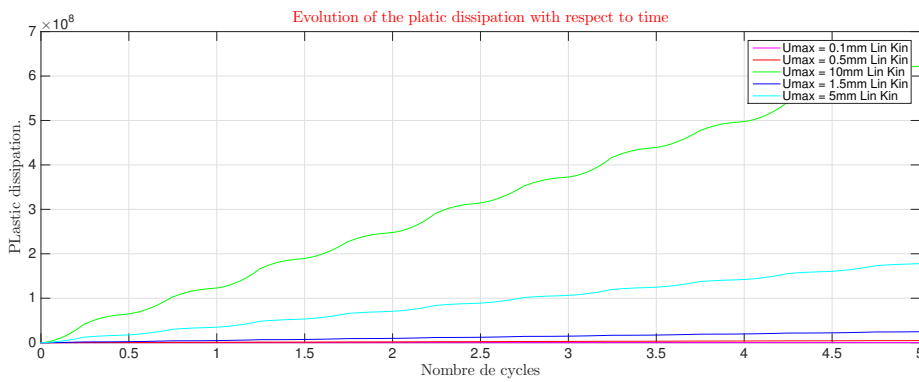


Figure 50 – Plastic dissipation linear kinematic model.

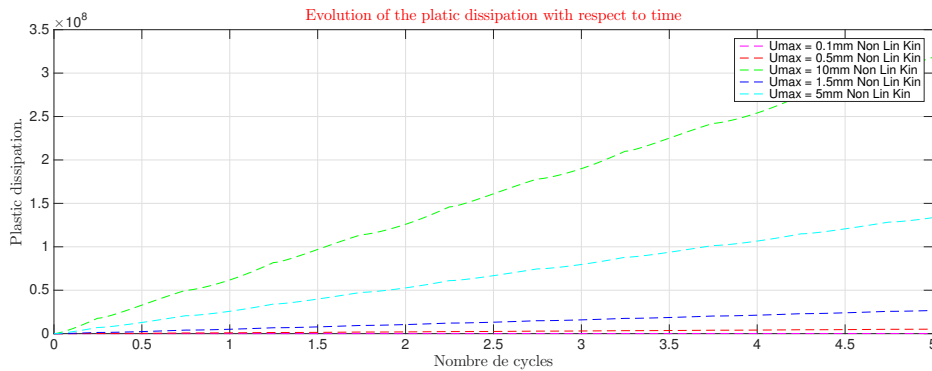


Figure 51 – Plastic dissipation non-linear kinematic model.

On Figure 49 we can also see that the curve is closed : if the plastic deformation vanishes after a whole cycle, the backstress tensor will come back to the initial condition. The same behaviour is visible on Figure 35: the equivalent stress decreases much more faster than it increases once the the hardening begins. This means that the yield surface moves much more easier when the loading is in the opposite way to the current plastic deformation/backstress tensor.

3.5 Dissipation energy

On Figure 50(linear kinematic hardening) and Figure 51(non-linear kinematic hardening) we can see the evolution of the plastic dissipation. If we compare both figures, we directly see that the the evolution is non linear and non constant over a cycle. For both models, there is no dissipation during the elastic phases. As we can see on both figure, the rate of the dissipation evolves during the loading-unloading cycle. The dissipation is maximum at the time just before the elastic phase, when the product $(s_{ij} - \alpha_{ij}) : \alpha_{ij}$ is maximum, (when the plastic modulus is minimum for the non-linear kinematic hardening). As we ca, also see, the dissipation is bigger if the model is linear. There is no recovery term. The hardening law has no "brake"-term. This allows to dissipate a greater amount of the energy into the plastic hardening phase.

Because there is no saturation of the hardening in this model and we will never reach a state where there is only elastic deformation (if linear isotropic hardening or non linear with maximum displacement providing a deformation that can be fully performed in elastic phase), there will always be energy dissipated during the remaining plastic phases. If there is as scheme that repeats at each cycle (no hardening, kinematic hardening) the amount of energy dissipated at each cycle is constant.

For the non linear mixed hardening, there is a transient phase where the amount of dissipated energy decreases with the number of load. At the end, the same asymptotic scheme repeats at each cycle : same amount of energy is dissipated at each cycle.

If for isotropic linear hardening, or non linear with fully deformation in elastic phases as asymptotic scheme, there is a transient phase where σ_Y is increasing and energy is dissipated. When the asymptotic fully elastic cycle is reached, there is no more energy dissipated.

4 Part 3: Study of elasto-viscoplastic behavior

In this section, we will study an elasto-viscoplastic behavior with isotropic and mixed linear hardening. We will show the influence of the viscosity parameter η and determine limit cases. To do that, we will divide our study firstly into 2 types of loading: normal sawtooth (like the one of previous sections) and sawtooth with plateau at $u_{max}, 0, -u_{max}$ of 1 [s]. This will be done in the 2 first sections. We will study linear isotropic and mixed hardening for both loadings. After, we will compute stress components in elastic and elasto-viscoplastic zones for a "relaxation loading": one cycle of loading/unloading followed by a constant displacement $u_{max}/2$. Then, demonstration of asymptotic values of σ^{VM} . At the end, we will discuss the evolution of the sigmum distance with the loading speed and compute the hydrostatic pressure inside the sphere.

Previous sections (elasto-plastic behavior) show that there are permanent deformations, depending on time of loading. Here, we will see that elasto-viscoplasticity introduces a *rate* of loading dependence. The general elasto-viscoplasticity in 1D case is shown on Fig. 52. We see already that the elastic part is the same for all strain rate (E remains quite constant). Nevertheless, the higher the strain rate, the higher the "brittleness" will be. In fact, the initial yield stress increases with the strain rate and the ductility decreases (chapter 2 of [3]).



Figure 52 – Influence of strain rate on the shape of $\sigma - \bar{\epsilon}$ curve (1D case in viscoplasticity), comparison with plasticity

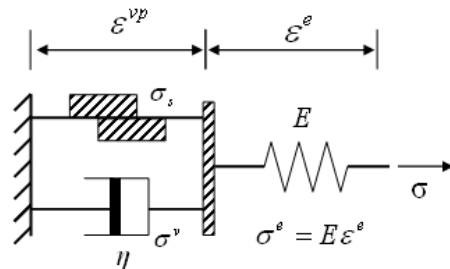


Figure 53 – Equivalent model for elasto-viscoplasticity

To modelize this kind of behavior, we need a viscoplastic model, Perzyna's model do it and define a *plastic multiplier* λ (slide 9 of chapter 8 of [3]),

$$\lambda = \sqrt{\frac{3}{2}} \left\langle \frac{\bar{\sigma}^{VM} - \sigma_y}{\eta(\bar{\varepsilon}^{vp})^n} \right\rangle^{1/m} \approx \sqrt{\frac{3}{2}} \left\langle \frac{\bar{\sigma}^{VM} - \sigma_y}{\eta} \right\rangle, \text{ for } n \rightarrow 0 \text{ and } m = 1 \quad (4.1)$$

With,

- $\langle x \rangle = \frac{1}{2}(x + |x|)$ is the McAuley notation, also x_+ : this means 0 if $x < 0$ and x if $x \geq 0$
- η the viscosity parameter express the viscosity in this model

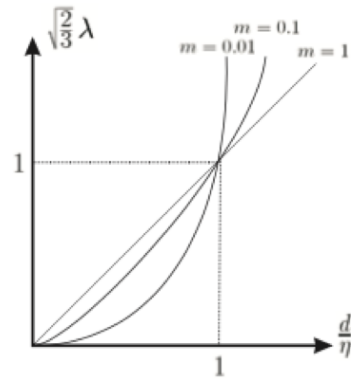


Figure 54 – Evolution of $\sqrt{\frac{2}{3}}\lambda$ for several m as a function of $\frac{d}{\eta}$

We will discuss the influence of this parameter by means of generate the equivalent Von Mises stress $\bar{\sigma}^{VM}$ and the equivalent viscoplastic strain $\dot{\varepsilon}^{vp}$ (both at inner surface) for several values of η (as powers of 10: 0, 10^2 , 10^3 , 10^4 , 10^5 , 10^6 , 10^7 , 10^8 [MPa.s]).

We can also define the *signum distance*, knowing that $\dot{\varepsilon}^{vp} = \sqrt{\frac{3}{2}}\lambda$

$$d = \langle \bar{\sigma}^{VM} - \sigma_y \rangle = \sqrt{\frac{3}{2}}\lambda\eta = \dot{\varepsilon}^{vp}\eta \quad (4.2)$$

So,

$$\eta = \frac{d \text{ [MPa]}}{\dot{\varepsilon}^{vp} \text{ [s}^{-1}\text{]}} \Rightarrow \eta \text{ [MPa.s]} \text{ (dynamic viscosity units)} \quad (4.3)$$

Finally, the yield function \bar{f} becomes for viscoplasticity (slide 17 of chapter 8 of [3]),

$$\bar{f} = \bar{\sigma}^{VM} - \sigma_y - \eta(\dot{\varepsilon}^{vp})^n(\dot{\varepsilon}^{vp})^m = \bar{\sigma}^{VM} - \sigma_y - \eta(\dot{\varepsilon}^{vp}) = 0 \quad (4.4)$$

Note that $\eta = 0$ [MPa.s] is a particular case where we recover elasto-plasticity.

4.1 Sawtooth loading

4.1.1 Linear isotropic hardening

(First limit case $\eta = 0$ [MPa.s] The most simple case is $\eta = 0$ [MPa.s] and corresponds to elasto-plasticity (without viscous effect). In that case, we obtain same graphs as previous section. Viscous effects are only visible from $\eta > 10^2$ [MPa.s]. Mathematically,

$$\lim_{\eta \rightarrow 0} \lambda = \lim_{\eta \rightarrow 0} \frac{d}{\eta} \Rightarrow d = 0 \text{ to have a finite } \lambda \quad (4.5)$$

The extended consistency condition (generalized) becomes,

$$\bar{f} = \bar{\sigma}^{VM} - \sigma_y = 0 = f \quad (4.6)$$

So we have always an elasto-plasticity behavior.

Increase of η [MPa.s] For $\eta = 10^4$ [MPa.s], viscous effects are clearly visible, with smooth shape characteristic of viscosity due to friction and time offset. Indeed, as η increases, a time offset increases as well between zero equivalent stresses. Zero equivalent stresses are the manifestation that the stresses change their sign because of change of loading direction (unloading). Viscosity introduce a decay in the response of the material: this decay is also loading speed (rate) dependent as we will see in this section. The hardening with a higher η introduce additional stresses and increases stresses with η . Moreover, the viscosity allows to increase the current yield stress σ_y during the plastic part (after the elastic part) and this lengthens the elastic part which occurs at the beginning of the unloading. This elastic part is linear. Thanks to hardening and sufficient viscosity, σ_y will increase during the several cycles of loading/unloading as we can see on Fig. 55. We see that at each cycle, the current yield stress increases which lengthens the elastic part at the beginning of the unloading. For a long time, all cases of viscosity will converges towards the same limit value of the equivalent stress. Viscosity tends also to decrease residual stresses as the cycles occur. We will see in section 4.5 that the loading time/speed also increases stresses. To harden a material we have thus 2 cases with a linear isotropic hardening:

- take a low η and wait a sufficient long time to get the maximal value of the equivalent stress
- take a huge η to have directly the maximum equivalent stress

For an intermediate viscosity, we see thus that the stress deviates progressively from elastic zone with slope E and the plastic zone characterized by a linear isotropic hardening of slope E_T . This is no more a sudden transition between E and E_T like in previous sections (elasto-plasticity) but a smooth one thanks to viscosity and time offset. This is clearly visible for $\eta = 10^4$ [MPa.s] and this is why we will keep this value as a reference to represent elasto-viscoplasticity in the rest of the section (when we will study phenomena with no comparison of η).

Second limit case $\eta \rightarrow +\infty$ [MPa.s] If η increases much and in the limit case, $+\infty$, we see that the equivalent stress becomes linear because the viscosity is so much high and the smooth transition between E and E_T leads to have no more E_T and only E (elasticity). In fact, the current yield stress which increases with η is so much high that $\bar{f} < 0$ always. The current yield stress is too high to have plasticity: however stresses $\bar{\sigma}^{VM}$ are huge, σ_y are so huge that only elasticity occurs. For $\eta = 10^8$ [MPa.s] (which leads to $\theta \rightarrow +\infty$), stresses are linear. The viscosity induces a decay in the flow, a resistance (friction). Theoretically, a infinite viscosity stops plastic flow and there remains only elasticity. Mathematically, we have

$$\lim_{\eta \rightarrow +\infty} \lambda = \sqrt{\frac{3}{2}} \frac{d}{\eta} = 0 \quad (4.7)$$

$$\dot{\varepsilon}^{vp} = \sqrt{\frac{2}{3}} \lambda = 0 \Rightarrow \dot{\varepsilon}^{vp} \text{ cst} \quad (4.8)$$

$$\dot{\sigma}_y = h_i \dot{\varepsilon}^{vp} = 0 \Rightarrow \sigma_y = \sigma_y^0 \text{ cst} \quad (4.9)$$

Or,

$$\lim_{\eta \rightarrow +\infty} \bar{f} = \bar{\sigma}^{VM} - \sigma_y - \eta(\dot{\varepsilon}^{vp}) = 0 \Rightarrow \lim_{\eta \rightarrow +\infty} d = \bar{\sigma}^{VM} - \sigma_y = \lim_{\eta \rightarrow +\infty} \eta \dot{\varepsilon}^{vp} \approx 1511 \text{ [MPa]} \quad (4.10)$$

$$\dot{\varepsilon}^{vp} \rightarrow 0 \text{ if } \eta \rightarrow +\infty \text{ in order to have } \eta \dot{\varepsilon}^{vp} \text{ finite} \quad (4.11)$$

And because we assume that $\dot{\varepsilon}^{vp}(t_0) = 0$ and the form of $\dot{\varepsilon}^{vp}$ is, (from tips of the report)

$$\dot{\varepsilon}^{vp}(t) = \dot{\varepsilon}^{vp}(t_0) + \int_{t_0}^t |\dot{\varepsilon}^{vp}| dt = 0 \quad (4.12)$$

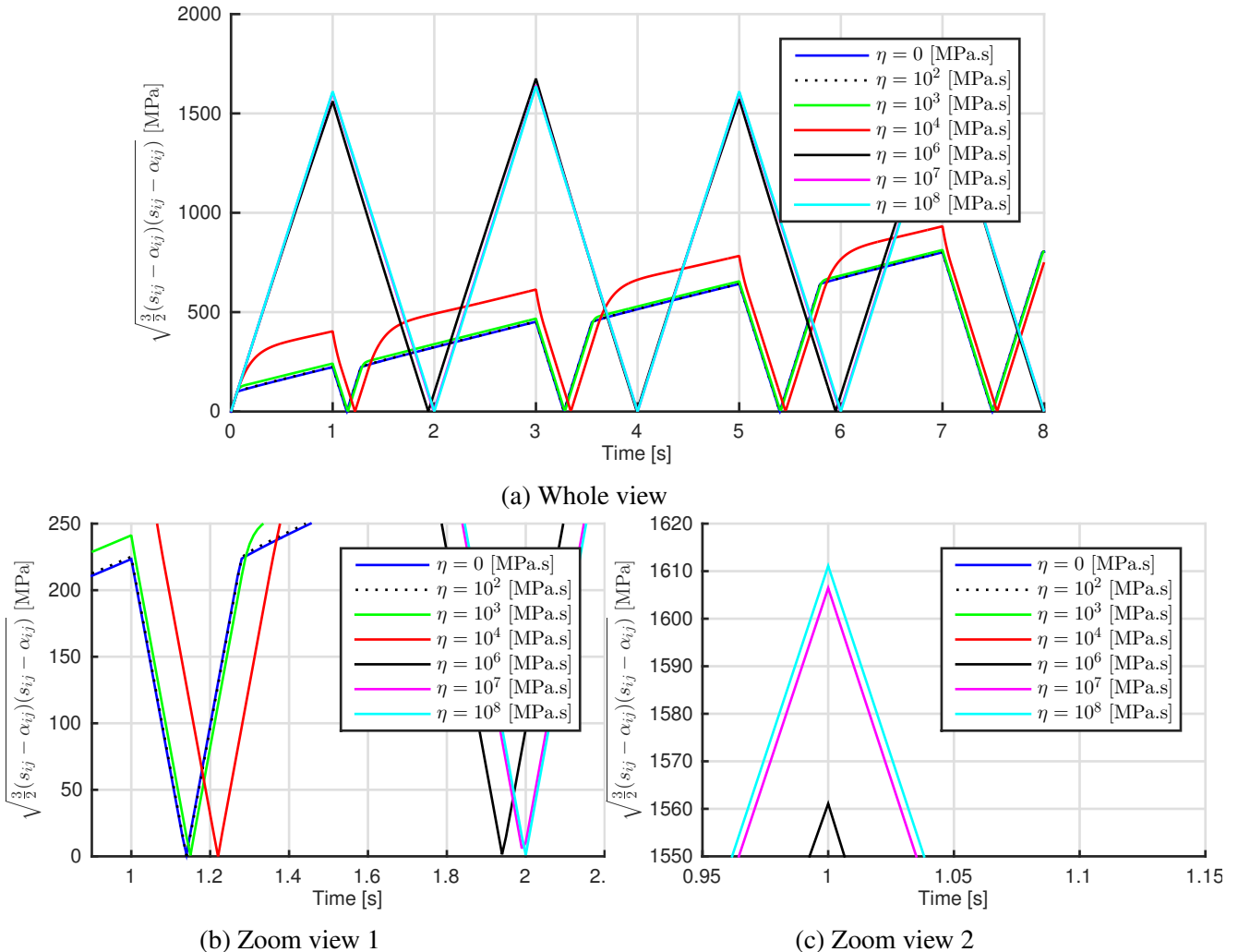


Figure 55 – Temporal variation of the Von Mises equivalent stress $\bar{\sigma}^{VM}$ [MPa] at inner surface for several viscosity parameters η [MPa.s] with linear isotropic hardening for 2 cycles of loading/unloading in sawtooth

This is thus a limit case of (pseudo)-elasticity. We see thus that $\bar{\varepsilon}^{vp} \rightarrow 0$ when $\theta \rightarrow +\infty$ and this is well observable on Fig. 56. We theoretically tends to 0. Remember that practically, an infinite viscosity is not possible, this is just a limit case. Strain rate is indeed inversely proportionnal to η .

A third kind of graph which can shows the effect of the viscosity is the pressure $p[\text{MPa}]$ versus the displacement $u [\text{mm}]$ (Fig. 57). This comparison is more accurate and has a real meaning compared to $\sigma - \varepsilon$ graphs difficult to interpretate. Remember that we can express the pressure p as $-\sigma_{XX}$ for point P1 (where $\sigma_r = \sigma_{XX}$). This curves begin with a huge "hystereris" (first limit case, elasto-plasticity) for low values of η and as viscosity increases, this "hysteresis" becomes much thinner to be a straight line (second limit case, elasticity). This is a manifestation that elasto-viscoplasticity does not follow the same path at each cycle: combination of isotropic linear hardening and viscosity increases the current yield stress. The decay between "hysteresis" curves remembers the time offset seen for Von Misses stresses.

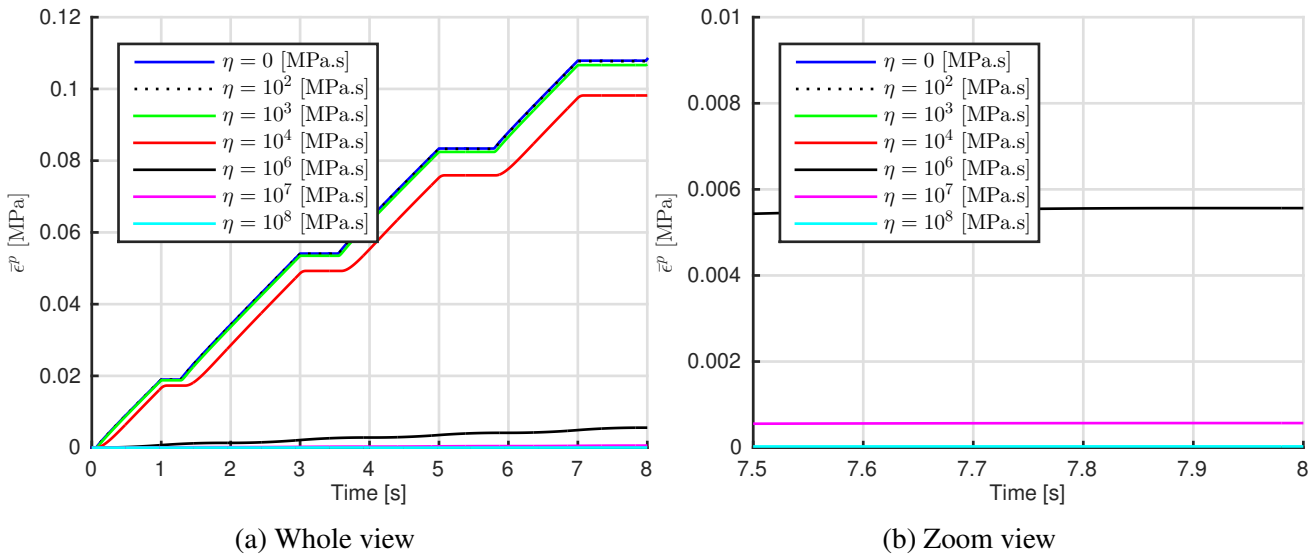


Figure 56 – Temporal variation of the equivalent viscoplastic strain $\bar{\varepsilon}^{vp}$ [-] at inner surface (extrapolated at the inner left node P1 on curve C4) for several 1 parameters η [MPa.s] with linear isotropic hardening for 2 cycles of loading/unloading in sawtooth

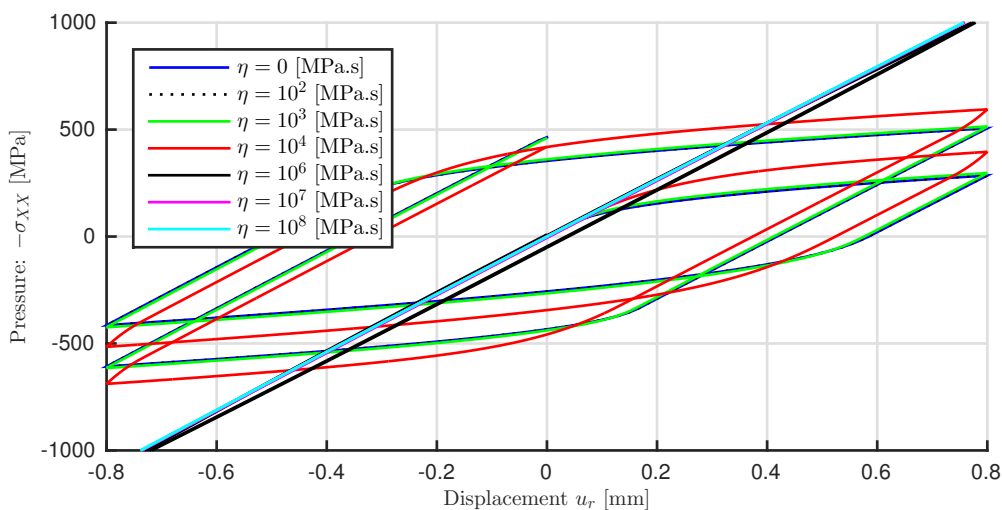


Figure 57 – Temporal variation of the pressure $-\sigma_{XX}$ [MPa] at inner surface (extrapolated at the inner left node P1 on curve C4) for several 1 parameters η [MPa.s] with linear isotropic hardening for 2 cycles of loading/unloading in sawtooth

4.1.2 Mixed hardening

Conclusions for the effect of viscosity on the material behavior for mixed hardening are similar than those for linear isotropic hardening. In fact, the mixed hardening takes into account both linear isotropic and kinematic hardening with a bigger proportion of kinematic hardening because of $\delta = 0.65$: $h_k = \delta h > h_i = (1 - \delta)h$. Values of Von Mises stresses are slightly different because of their definition, (Fig. 59)

$$\bar{\sigma}^{VM} = \sqrt{\frac{3}{2}(s_{ij} - \alpha_{ij})(s_{ij} - \alpha_{ij})} \quad (4.13)$$

Where backstresses α_{ij} were = 0 for linear isotropic hardening but not for kinematic hardening so also not for mixed hardening. Fig. shows equivalent backstresses for several η , (slide 30 of chapter 5 [3]),

$$\bar{\alpha} = \sqrt{\frac{3}{2}\alpha_{ij}\alpha_{ij}} \quad (4.14)$$

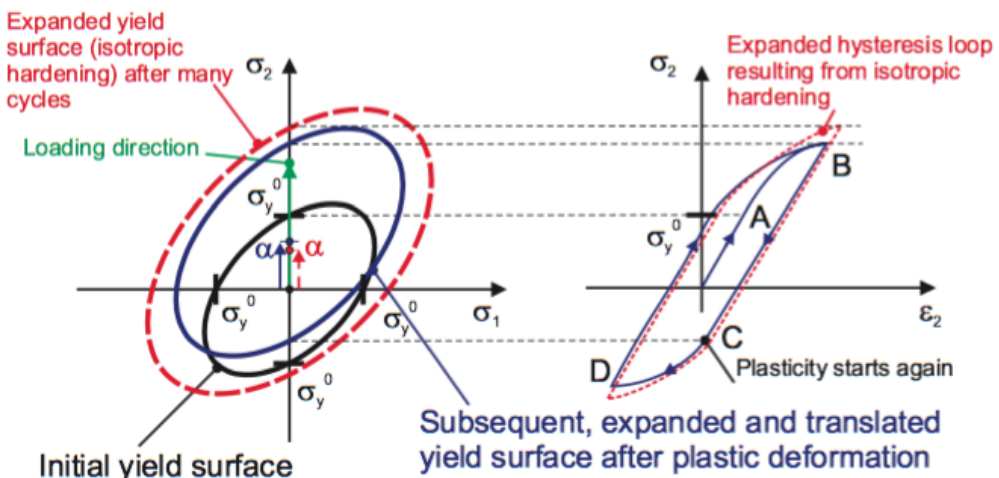


Figure 58 – Mixed hardening, in which the yield surface expands and translates with plastic deformation, and the corresponding uniaxial stress-strain curve in case of strain imposed resulting in cyclic plasticity (in 3D plane stress state) [3]

Fig. 58 shows a schematic view of the effect of mixed hardening: α is the location of the center of the yield stress, mixed hardening takes isotropic hardening to describe the expansion of the yield surface and kinematic hardening to represent the center of the yield surface α .

Viscosity tends to decrease backstresses, reduce their effect because the viscoplastic zone is reduced in f if η increases. For $\eta = 10^8$ [MPa.s], $\bar{\alpha} \ll$ so there is almost no difference with isotropic linear hardening, this is not true for lower values of η . Note that the definition of the current yield stress is the same that the one for linear isotropic hardening but as $h_i = h$ for isotropic hardening and $h_i = (1 - \delta)h$ for mixed hardening, the current yield stress decreases so d increases and for a same value of η leads to a higher λ and so higher $\dot{\varepsilon}^{vp}$ and $\dot{\sigma}_y$. Note also that equivalent backstresses decreases in time during the several cycles. As the hardening increases stresses, it decreases backstresses. Finally, we see that the effect of time and viscosity is the opposite for equivalent stresses and backstresses.

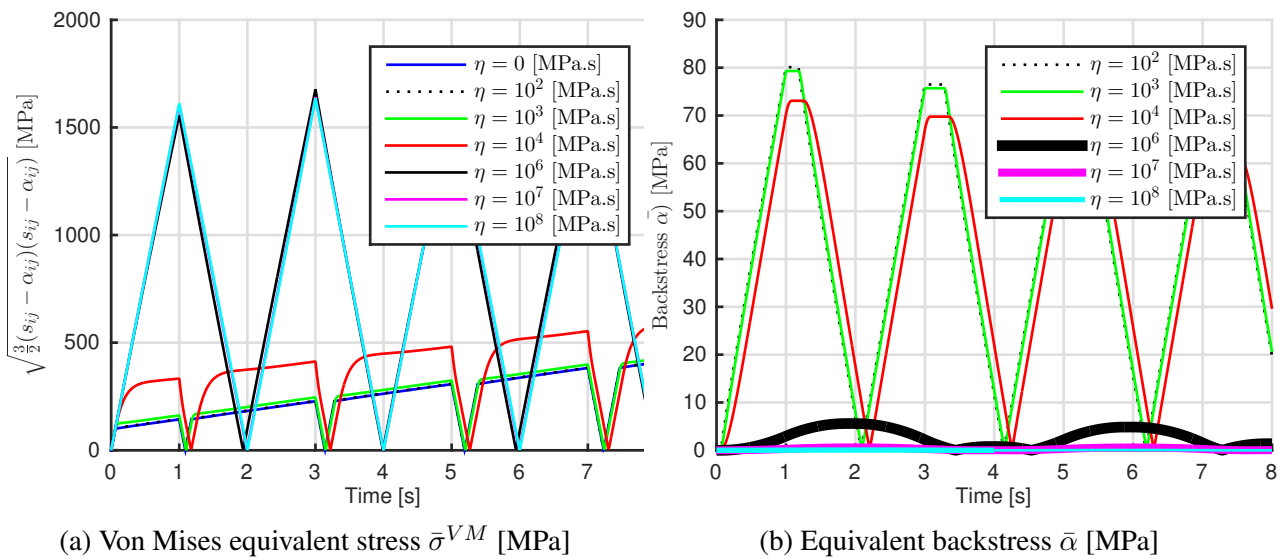


Figure 59 – Temporal variation of ... at inner surface (extrapolated at node P1 on curve C4) for several 1 parameters η [MPa.s] with mixed hardening for 2 cycles of loading/unloading in sawtooth

4.2 Sawtooth loading with plateaus of 1 [s]

This kind of loading will introduce little "relaxation" in the material behavior (because constant displacements are imposed at $u_{max}, -u_{max}, 0$ during 1 [s]).

4.2.1 Linear isotropic hardening

We see on Fig. 60 that influence of viscosity is the same for the *general* evolution of Von Mises stresses. Nevertheless, we see that *plateaus* introduce different behavior. In fact, the viscosity decays the response so the stresses are not suddenly constant when the displacement is constant: there is an decreasing exponential evolution with an inverse proportionality on η (see section on "relaxation" 4.3). When η increases, plasticity is "slowed" and the time needed to decrease is much longer than the one for lower η . For a high viscosity, the material has not enough time to adapt itself because of slowly plastic flow. For the first limit case, there is no "relaxation" because of no viscous effect. For the second limit case, the time needed to decrease the stress is infinite. In fact, the stress is constant when the displacement is constant: elasticity.

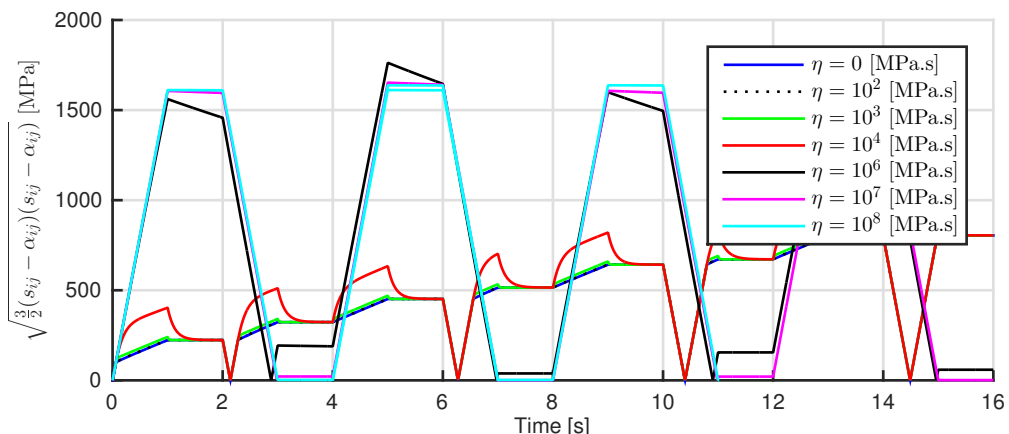


Figure 60 – Temporal variation of the Von Mises equivalent stress $\bar{\sigma}^{VM}$ [MPa] at inner surface for several viscosity parameters η [MPa.s] with linear isotropic hardening for 2 cycles of loading/unloading in sawtooth with plateaus of 1 [s] for $u_{max}, 0, -u_{max}$

Fig. 61 shows the displacement used. It shows also backstresses which are all null because of isotropic linear hardening (fortunately). The pressure versus the displacement is very similar to the sawtooth loading but there are only small decay of pressure for constant displacement (visible for small η but not for higher). Again the equivalent visco-plastic strain tends to zero when η increases but we see that it is not necessary constant when u is constant: viscosity introduces a decay (as attended). It becomes constant (see the plateaus) a little bit after the displacement.

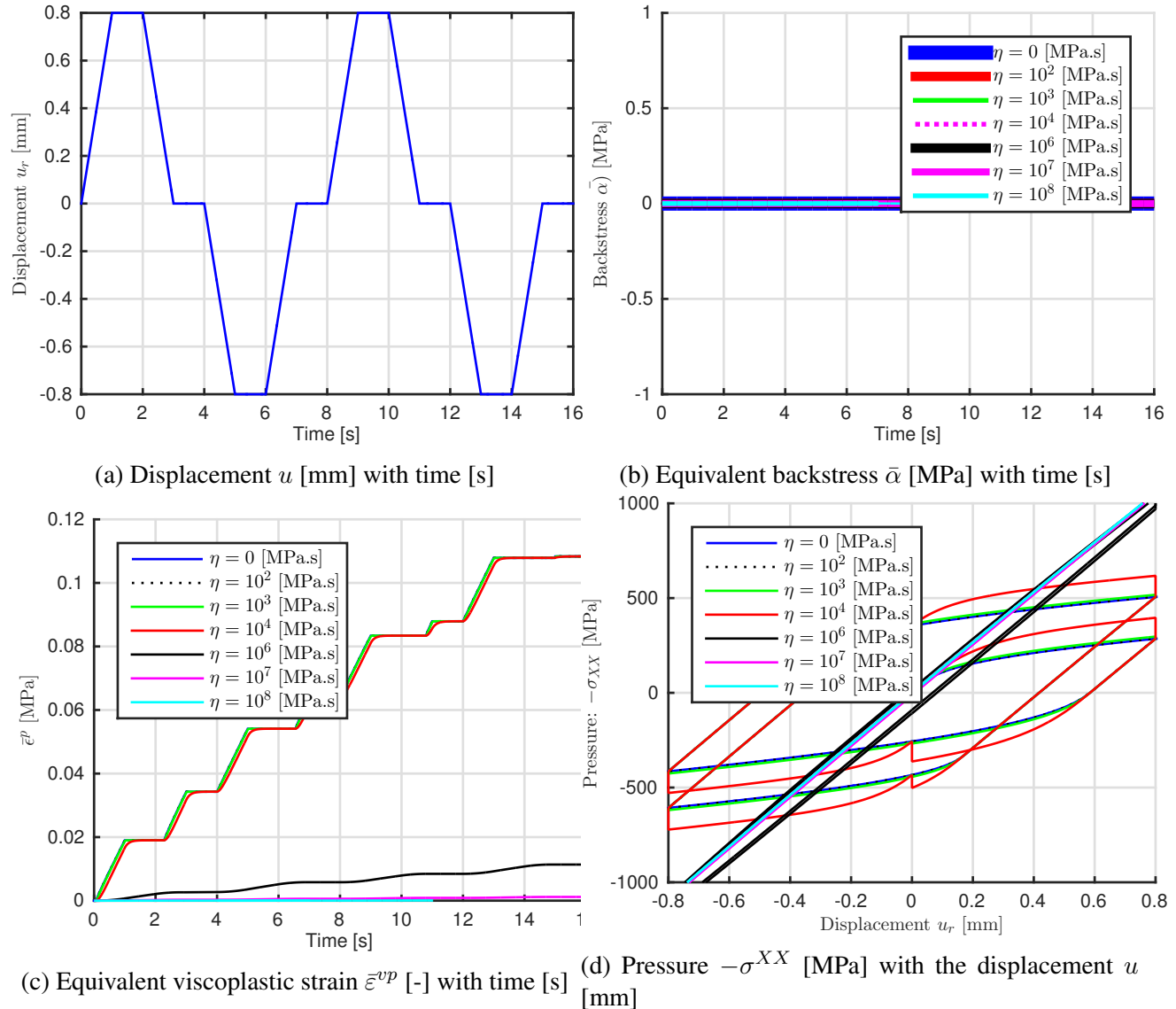


Figure 61 – Variation of ... at inner surface (extrapolated at the inner left node P1 on curve C4) for several viscosity parameters η [MPa.s] with linear isotropic hardening for 2 cycles of loading/unloading in sawtooth with plateaus of 1 [s] for $u_{max}, 0, -u_{max}$

4.2.2 Mixed hardening

Conclusions of previous section on effect on viscosity are still true for mixed hardening except for backstresses which are no more null. Here again we observe same characteristics of backstresses than those of sawtooth loading without plateaus but the shape is quite different: the maximum values of $\bar{\alpha}$ are higher than previously, there is a longer plateaus at these values. For low η , backstresses are not always in sawtooth but there are small plateaus corresponding to the plateaus of the displacement.

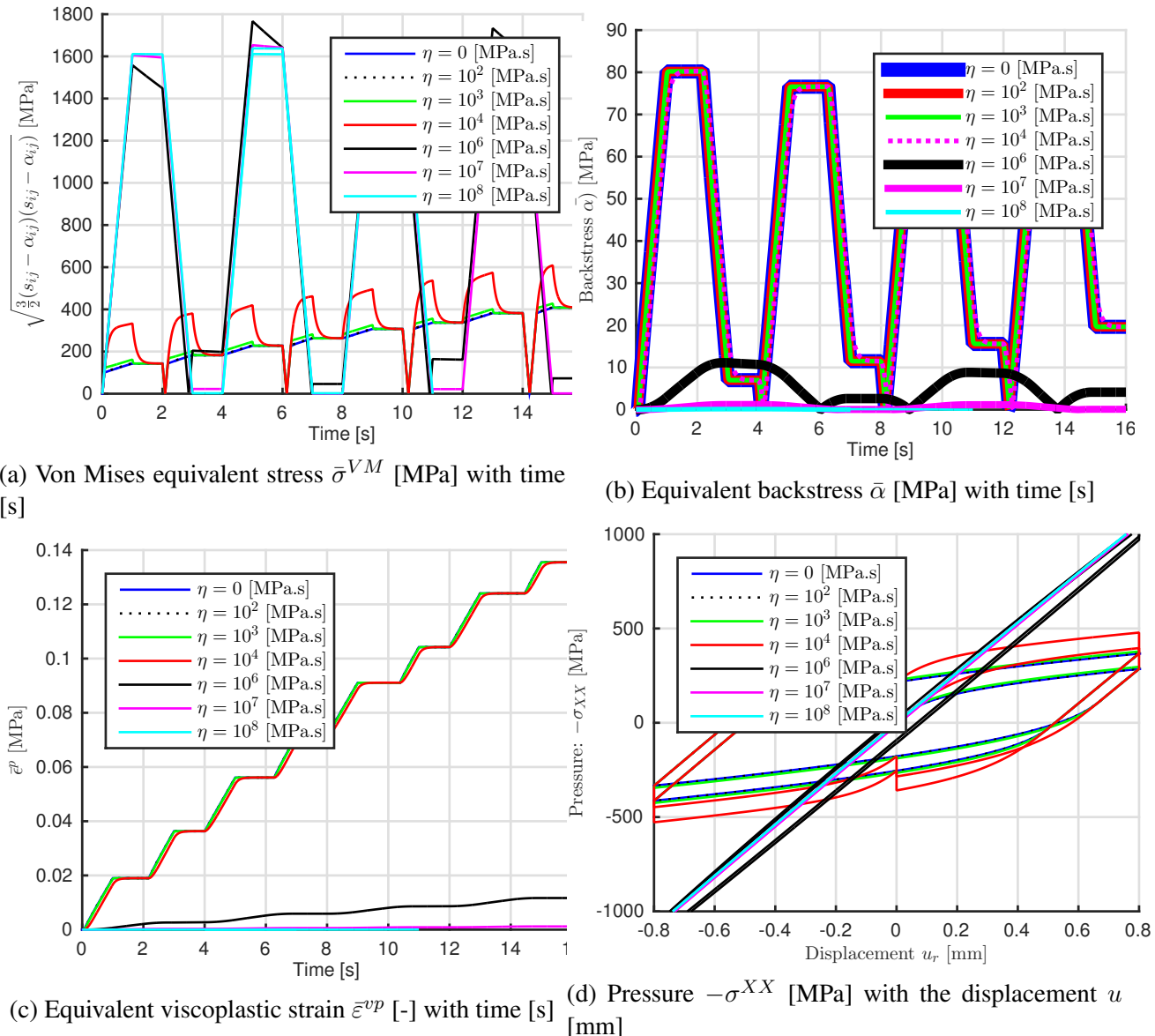


Figure 62 – Variation of ... at inner surface (extrapolated at the inner left node P1 on curve C4) for several viscosity parameters η [MPa.s] with mixed hardening for 2 cycles of loading/unloading in sawtooth with plateaus of 1 [s] for $u_{max}, 0, -u_{max}$

4.3 One cycle of sawtooth loading followed by constant $\frac{u_{max}}{2}$: "relaxation"

4.3.1 Variation of stress components ($\eta = 10^4$ [MPa.s], linear isotropic hardening)

In this section, we will study stress components for one cycle of loading/unloading in sawtooth followed by a constant value u_{max} , which leads to an "relaxation" (ε cst and $\sigma(t)$). In the case of viscosity, the relaxation gives a shape like Fig. 63 and σ decreases exponentially to 0.

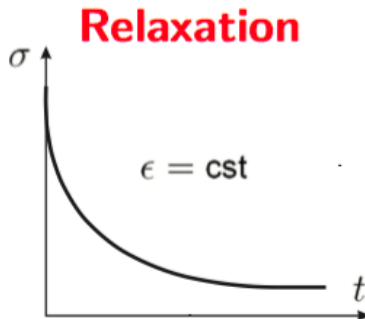


Figure 63 – Relaxation phenomenon ($\sigma(t)$) and ε constant

We have displayed stress components [MPa],

- $\bar{\sigma}^{VM}$: equivalent Von Mises stress
- $\sigma_{XX} = \sigma_r, \sigma_{YY} = \sigma_{ZZ} = \sigma_\theta = \sigma_\phi$: stress tensor components at point P1, the fixed axis system of Metafor is superposed to the spherical axis system $O(r\theta\phi)$ with $\theta = \phi = 0$ and $r = R_1$

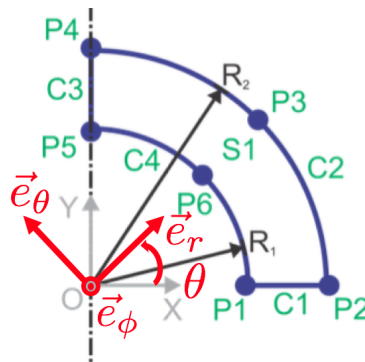


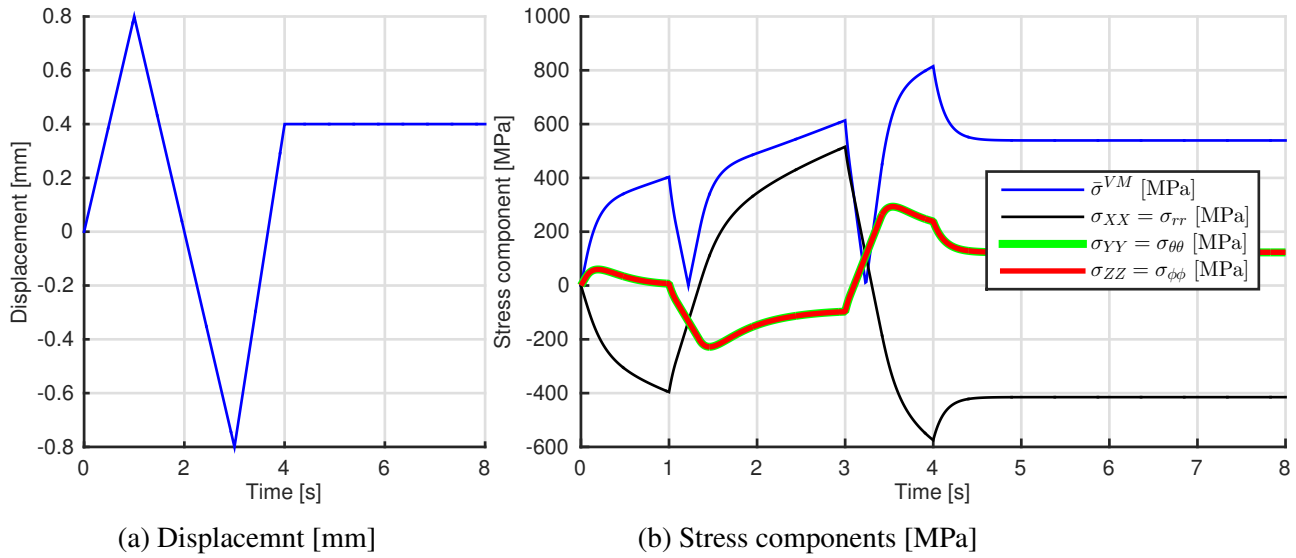
Figure 64 – Metafor axis system and spherical axis system

We will compare these stress components for the elasto-viscoplastic zone (at inner surface, the displacement u exceeds $u_y^0 = 0.05$ [mm] (limit value of u for elasticity, see section 5.1 for analytical developments) on Fig. 65a). We will also consider the elastic zone (at outer surface, u does not exceed u_y^0 as shown on Fig. 65b).

For the elasto-viscoplastic zone, we see that the shape of the components is quite complex: at the beginning of the loading (elasticity), stresses are linear and after u_y^0 , plasticity occurs and the viscosity makes the shape as a decreasing exponential due to friction, stresses increase but slower and slower. At u_{max} , the displacement is reversed and elasticity occurs again at the beginning and then viscoplasticity and so on... We see also the phenomenon of relaxation (asymptotic value of stresses reaches for a long time when we keep a constant displacement (decreasing exponential), see next section). Note that in elasto-viscoplasticity, radial stresses are predominant in the Von Mises equivalent stress

compared to circumferential.

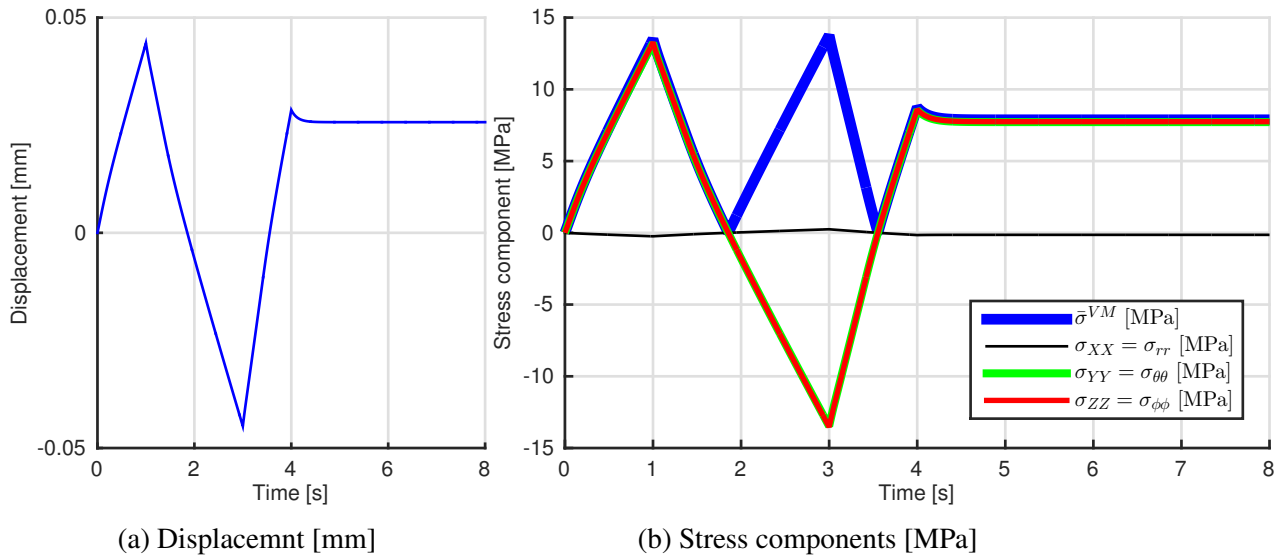
At the opposite, in the elastic zone, radial components are negligible compared to circumferential. Moreover, stresses are linear and follow well the displacement (linear relation between stress and strain leads well to elasticity). Note that the displacement computed at the outer surface is below u_y^0 but has a slightly different shape than the one for the inner surface: after the cycle of loading/unloading, there is a slight decrease of u before reaching a constant value for a long time. This decrease is due to the relaxation of elasto-viscoplasticity part occurring near the elasticity zone and influence slightly this displacement. Stresses follow thus linearly this displacement/strain. Nevertheless, mention that there are residual stresses due to the residual strain occurring at elasto-viscoplasticity zone.



(a) Displacemnt [mm]

(b) Stress components [MPa]

Figure 65 – Temporal variation of ... at inner surface (extrapolated at the inner left node P1 on curve C4) for $\eta = 10^4$ [MPa.s] with linear hardening for one cycle of sawtooth loading followed by constant $\frac{u_{max}}{2}$



(a) Displacemnt [mm]

(b) Stress components [MPa]

Figure 66 – Temporal variation of ... at outer surface (extrapolated at the inner left node P2 on curve C2) for $\eta = 10^4$ [MPa.s] with linear hardening for one cycle of sawtooth loading followed by constant $\frac{u_{max}}{2}$

We will now compute analytically these asymptotic values of $\bar{\sigma}^{VM}$ due to this "relaxation".

4.3.2 Asymptotic value of $\bar{\sigma}^{VM}$ without hardening ($\eta = 10^4$ [MPa.s])

Note that mathematical and mechanical relations of this sections are extracted from chapter 5 of theoretical lectures [3]. We will demonstrate towards which value tends the equivalent Von Mises stress $\bar{\sigma}^{VM}$ [MPa] if we apply a displacement u_{max} for an infinitely long time. This will be done for elasto-viscoplastic behavior without hardening. We start with splitting the constitutive law in hydrostatic p and deviatoric s parts,

$$\dot{\sigma}_{ij} = \dot{p}\delta_{ij} + \dot{s}_{ij} = \dot{\sigma}_{ii} + \dot{s}_{ij} = \mathbb{H}_{ijkl}(D_{kl} - D_{kl}^{vp}) \quad (4.15)$$

We make the assumption that $D_{kl} \cong \dot{\varepsilon}_{kl} \cong \dot{p} \cong 0$ when $u(t) = u_{max}$ and we will verify it in Metafor. In fact, the strain during the relaxation is much lower than during the first load. As seen in chapter 8, slide 3 of [3],

$$\dot{s}_{ij} \cong -\mathbb{H}_{ijkl}D_{kl}^{vp} \quad (4.16)$$

$$= \left(K\delta_{ij}\delta_{kl} + G \left(\delta_{ik}\delta_{jl} + \delta_{il}\delta_{kj} - \frac{2}{3}\delta_{ij}\delta_{kl} \right) \right) D_{kl}^{vp} \quad (4.17)$$

$$= -2GD_{ij}^{vp} \quad (4.18)$$

Because $D_{kk}^{vp} = \lambda N_{kk} = \sigma_{kk} - p = 0$. \mathbf{N} is a unit outward normal ($\mathbf{N} : \mathbf{N} = 1$). Anyway, it is possible to prove that $\dot{p} \cong 0$ (using similar developments than the previous one),

$$\dot{p} = \frac{\dot{\sigma}_{ii}}{3} = -\mathbb{H}_{iilk}D_{kl}^{vp} = -KD_{ii}^{vp} = 0 \quad (4.19)$$

Using $D_{ij}^{vp} = \lambda N_{ij}$ and $N_{ij} = \frac{\frac{\partial f}{\partial \sigma_{ij}}}{\left| \frac{\partial f}{\partial \sigma_{ij}} \right|} = \frac{\frac{\partial \bar{\sigma}^{VM}}{\partial s_{ij}}}{\left| \frac{\partial \bar{\sigma}^{VM}}{\partial s_{ij}} \right|} = \frac{s_{ij}}{|s_{ij}|}$ (slide 8 of chapter 8 of [3]) because

$N_{ij} = \frac{\phi_{ij}}{\sqrt{\phi_{ij}\phi_{ij}}}$ with $\phi_{ij} = s_{ij} - \alpha_{ij}$ with $\alpha_{ij} = 0$,

$$\dot{s}_{ij} = -2G\lambda N_{ij} = -2G\lambda \frac{s_{ij}}{\sqrt{s_{ij}s_{ij}}} \quad (4.20)$$

We can now compute, with equation 4.20,

$$\dot{\bar{\sigma}}^{VM} = \frac{d}{dt} \sqrt{\frac{3}{2}s_{ij}s_{ij}} = \frac{1}{2\sqrt{\frac{3}{2}s_{ij}s_{ij}}} \frac{3}{2}(\dot{s}_{ij}s_{ij} + s_{ij}\dot{s}_{ij}) = \sqrt{\frac{3}{2}} \frac{\dot{s}_{ij}s_{ij}}{\sqrt{s_{ij}s_{ij}}} = -\sqrt{6}G\lambda \quad (4.21)$$

By combining equations 4.21 and 4.1,

$$\dot{\bar{\sigma}}^{VM} = -3G \left\langle \frac{\bar{\sigma}^{VM} - \sigma_y}{\eta} \right\rangle \quad (4.22)$$

We are in the viscoplastic case such that $f = \bar{\sigma}^{VM} - \sigma_y > 0$ so $\langle \bar{\sigma}^{VM} - \sigma_y \rangle = \bar{\sigma}^{VM} - \sigma_y$ and,

$$\dot{\bar{\sigma}}^{VM} + \frac{3G}{\eta} \bar{\sigma}^{VM} = \frac{3G}{\eta} \sigma_y \quad (4.23)$$

Here, there is no hardening so we are in *perfect* plasticity and the yield stress remain constant $\sigma_y = \sigma_y^0$. The solution of this first order linear differential equation for $\bar{\sigma}^{VM}$ is composed of an homogeneous and particular solutions, with C_0 a constant depending on initial condition,

$$\bar{\sigma}^{VM}(t) = \bar{\sigma}^{VM} \cdot e^{-\frac{3G}{\eta}t} + \sigma_y^0 \quad (4.24)$$

Taking a infinite long time, the decreasing exponential is a transient part and vanishes,

$$\lim_{t \rightarrow +\infty} \bar{\sigma}_0^{VM} \cdot e^{-\frac{3G}{\eta} t} + \sigma_y^0 = \sigma_y^0 \quad (4.25)$$

On Fig. 67, we have compared this transient part several values of η [MPa.s]. If we take $\eta = 0$ [MPa.s], we are in the elasto-plastic case and without hardening, the material has no time to increase the stress, with equation 4.24 we see that the exponential $\rightarrow 0$ when $\eta \rightarrow 0$. For $\eta = 10^8$ [MPa.s], which leads to " $\eta \rightarrow +\infty$ ", we are in perfect plasticity and there is no transient part, the stress increase until $C_0 + \sigma_y^0$ (if $\eta \rightarrow +\infty$) and remains constant after loading. For intermediate values pf η , we see that the lower η , the faster the transient stress vanishes. Finally, we verify well that $\bar{\sigma}^{VM}$ tends to $\sigma_y^0 = 100$ [MPa].

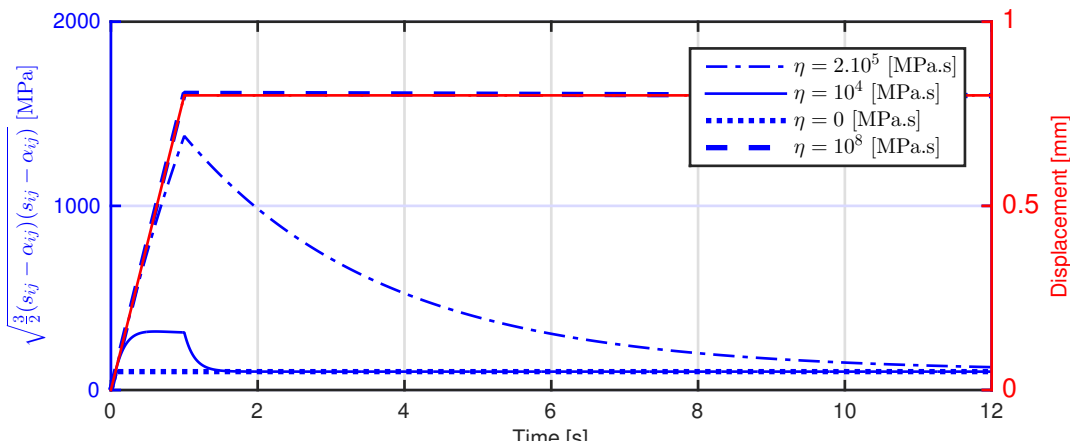


Figure 67 – Temporal variation of the equivalent Von Mises stress $\bar{\sigma}^{VM}$ [MPa] at inner surface (extrapolated at the inner left node P1 on curve C4) for several viscosity parameters η [MPa.s] with no hardening for 1 cycles of loading until u_{max} during 12 [s], displacement [mm] is in red

4.3.3 Asymptotic value of $\bar{\sigma}^{VM}$ with linear isotropic hardening and extrapolation for mixed hardening ($\eta = 10^4$ [MPa.s])

Linear isotropic hardening Note that mathematical and mechanical relations of this sections are extracted from chapter 5 of theoretical lectures [3]. As done in the previous section, we will find a first order linear differential equation for $\bar{\sigma}^{VM}$ and the value of $\bar{\sigma}^{VM}$ for an infinitely long time. The difference here is that we have a linear hardening so the yield stress σ_y is no more constant ($\dot{\sigma}_y \neq 0$) and is defined in the Perzyna's model ($\dot{\varepsilon}^{vp}$ defined in slide 12 of chapter 8 of [3]),

$$\begin{cases} \dot{\sigma}_y &= \frac{d}{dt}(\sigma_y^0 + h_i \dot{\varepsilon}^{vp}) = \sqrt{\frac{2}{3}} h_i \lambda = \sqrt{\frac{2}{3}} h_i \sqrt{\frac{3}{2}} \left\langle \frac{\bar{\sigma}^{VM} - \sigma_y}{\eta} \right\rangle \\ \alpha_{ij} &= 0 \end{cases} \quad (4.26)$$

We must thus resolve a system of differential equations for $\bar{\sigma}^{VM}$ and $\dot{\sigma}_y$, note that we are in the viscoplastic zone so $\bar{\sigma}^{VM} > \sigma_y$ and,

$$\begin{cases} \dot{\sigma}_y + \frac{3G}{\eta} \bar{\sigma}^{VM} = \frac{3G}{\eta} \sigma_y \\ \dot{\sigma}_y = h_i \left\langle \frac{\bar{\sigma}^{VM} - \sigma_y}{\eta} \right\rangle \end{cases} \Leftrightarrow \begin{cases} \dot{\bar{\sigma}}^{VM} + \frac{3G}{\eta} \bar{\sigma}^{VM} &= \frac{3G}{\eta} \sigma_y \\ \dot{\sigma}_y + \frac{h_i}{\eta} \sigma_y &= \frac{h_i}{\eta} \bar{\sigma}^{VM} \end{cases} \quad (4.27)$$

As suggested in the tips of the report instruction, we rewrite the system into a matrix form,

$$\dot{\mathbf{y}} = \mathbf{A}\mathbf{y} \Leftrightarrow \begin{pmatrix} \dot{\bar{\sigma}}^{VM} \\ \dot{\sigma}_y \end{pmatrix} = \begin{pmatrix} -\frac{3G}{\eta} & \frac{3G}{\eta} \\ \frac{h_i}{\eta} & -\frac{h_i}{\eta} \end{pmatrix} \begin{pmatrix} \bar{\sigma}^{VM} \\ \sigma_y \end{pmatrix} \quad (4.28)$$

Equation 4.28 is a matricial, homogenous, linear differential equation of first order. Matrix \mathbf{A} is constant so we can express the solution (we consider that the solution is of the same form as the scalar case but here we will have a matricial exponential),

$$\mathbf{y} = \mathbf{y}_0 e^{-\mathbf{A}t} \quad (4.29)$$

With initial conditions allows to find the constant vector \mathbf{y}_0 . Tips suggest also to use *diagonalization* properties of matricial exponential, note that these properties were seen in *Modélisation et analyse des systèmes* of 2nd bachelor [5],

$$e^{\mathbf{At}} = \mathbf{V} e^{\mathbf{Dt}} \mathbf{V}^{-1} \quad (4.30)$$

Where \mathbf{V} is a square matrix containing eigenvectors of \mathbf{A} and \mathbf{D} is a diagonal matrix containing eigenvalues of \mathbf{A} . We find thus,

$$\mathbf{V} = \begin{pmatrix} 1 & -\frac{3G}{h_i} \\ 1 & 1 \end{pmatrix} \quad \mathbf{D} = \begin{pmatrix} 0 & 0 \\ 0 & -\frac{3G+h_i}{\eta} \end{pmatrix} \quad (4.31)$$

Finally, we find the solution

$$\begin{cases} \bar{\sigma}^{VM}(t) &= C_1 e^{-\frac{(3G+h_i)}{\eta}(t-t_0)} + C_2 \\ \sigma_y(t) &= C_3 e^{-\frac{(3G+h_i)}{\eta}(t-t_0)} + C_4 \end{cases} \quad (4.32)$$

$$\begin{cases} \bar{\sigma}^{VM}(t) &= \frac{3G(\bar{\sigma}_0^{VM} - \sigma_y^0)e^{-\frac{(3G+h_i)}{\eta}(t-t_0)} + h_i \bar{\sigma}_0^{VM} + 3G\sigma_y^0}{3G+h_i} \\ \sigma_y(t) &= \frac{h_i(\sigma_y^0 - \bar{\sigma}_0^{VM})e^{-\frac{(3G+h_i)}{\eta}(t-t_0)} + h_i \bar{\sigma}_0^{VM} + 3G\sigma_y^0}{3G+h_i} \end{cases} \quad (4.33)$$

The second constant is the result of $Ce^0 = C$. With initial conditions chosen in $t = t_0$ [s] (correspond to the time at which relaxation begins, usually at 1 [s] for the loading used in Fig. 68, bring by Metafor),

$$\begin{cases} \bar{\sigma}^{VM}(t_0) &= \bar{\sigma}_0^{VM} \\ \sigma_y(t_0) &= \bar{\sigma}_y^0 = \sigma_y^0 + h_i \bar{\varepsilon}^{vp} \end{cases} \quad (4.34)$$

The coefficients near the decreasing exponential are different for $\bar{\sigma}^{VM}(t)$ and $\sigma_y(t)$ but this term vanishes for an infinitely long time $t \rightarrow +\infty$ and constants C_2 and C_4 are equal so in total,

$$\lim_{t \rightarrow +\infty} \bar{\sigma}^{VM}(t) = \lim_{t \rightarrow +\infty} \sigma_y(t) = \frac{h_i \bar{\sigma}_0^{VM} + 3G\bar{\sigma}_y^0}{3G + h_i} = \frac{6500 \cdot 403.5 + 3 \frac{70000}{2(1+\nu)} \cdot 208.1}{3 \frac{70000}{2(1+\nu)} + 6500} = 222.9 \text{ [MPa]} \quad (4.35)$$

As done in the previous section, we will simulate this relaxation in Metafor to compare it with analytical attended results. We see that results are in agreement with analytical solution: $\bar{\sigma}_{VM}$ and σ_y reaches the same constant value after a certain time. In the numerical simulation, this value is 223.5 [MPa], very close to the analytical one. As observed in previous section, this value does not depend on viscosity parameter η [MPa.s], only the time needed to reach this value depends on η (towards the exponential). We see thus that this value is greater than the one obtained without hardening. This is obvious since the hardening increase the stress to harden the material. Equivalent backstress is obviously zero because of isotropic hardening (linear or non linear) also with no hardening because $\bar{\alpha}$ is a kinematic hardening property.

We have demonstrate the asymptotic value for a linear isotropic hardening but we have also displayed non-linear isotropic and mixed hardening on Fig. 68 to compare it. We see that the asymptotic value for non-linear isotropic is below the one for linear isotropic and the one for mixed is below the

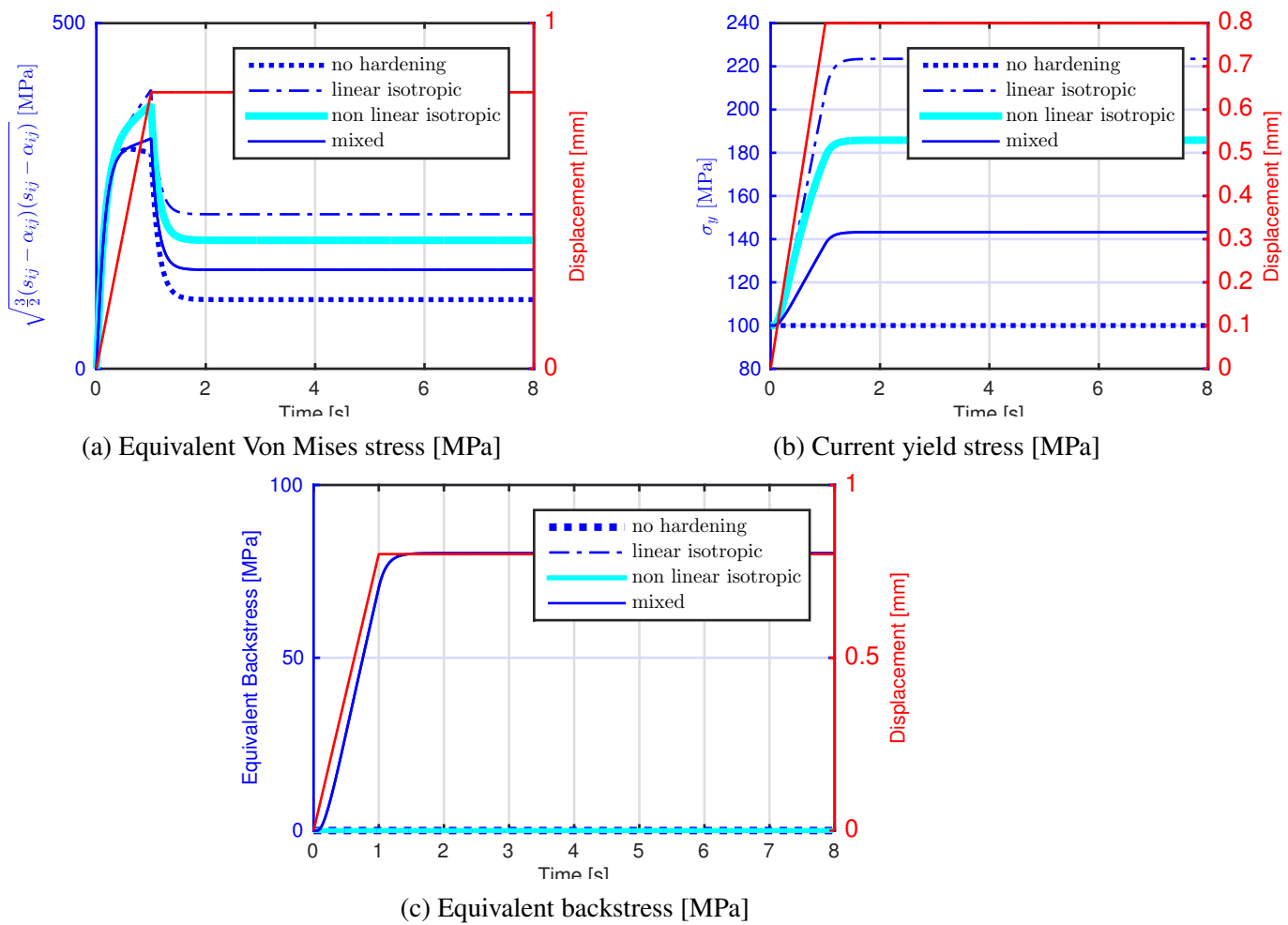


Figure 68 – Temporal variation of ... at inner surface (extrapolated at the inner left node P1 on curve C4) for $\eta = 10^4$ [MPa.s] with linear isotropic, mixed and no hardening for 1 cycles of loading until u_{max} during 8 [s], displacement [mm] is in red

one for non-linear isotropic. Linear isotropic hardening is thus the most "efficient" hardening because it gives the greater asymptotic value.

Non linear isotropic hardening For this hardening, we can keep the differential equation for $\bar{\sigma}^{VM}$ but the one for σ_y changes because of non-linear isotropic hardening,

$$\dot{\sigma}_y = \frac{d}{dt} \left(\sigma_y^\infty - (\sigma_y^\infty - \sigma_y^0) e^{\left(-\frac{h_i \varepsilon^{vp}}{\sigma_y^\infty - \sigma_y^0} \right)} \right) \quad (4.36)$$

The differential system becomes more complex because of ε^{vp} and thus λ and thus $\bar{\sigma}^{VM} - \sigma_y$ in the exponential. Such a system is not solvable analytically, as indicated by its name it is non-linear and numerical resolution is needed so no comparison is available. Anyway, the backstress is also zero and the center of the yield surface does not change its position. This hardening provides a smaller asymptotic value than the one for linear isotropic hardening, plastic flow is non-linear. The plastic range is no longer represented by a straight line but by a decreasing slope curve.

Mixed hardening This hardening supposes a combination of linear isotropic and kinematic hardening: now, there is a kinematic variable and the backstress are no longer zero and the center yield surface can change its position. Evolution of the yield stress follows the one of isotropic hardening. The hardening law becomes,

$$\sigma_y = \sigma_y^0 + h_i \bar{\varepsilon}^{vp} \quad (4.37)$$

$$\dot{\alpha}_{ij} = \frac{2}{3} h_k D_{ij}^{vp} = \frac{2}{3} h_k \lambda N_{ij} \quad (4.38)$$

$$\bar{\alpha} = \sqrt{\frac{3}{2} \alpha_{ij} \alpha_{ij}} \quad (4.39)$$

$$h_i = \delta h = 0.65 \cdot 6500 \quad (4.40)$$

$$h_k = (1 - \delta)h = 0.35 \cdot 6500 \quad (4.41)$$

So, development of sections 4.3.2 and 4.3.3 are no more valid because,

$$\bar{\sigma}^{VM} = \sqrt{\frac{3}{2} (s_{ij} - \alpha_{ij})(s_{ij} - \alpha_{ij})} \neq \sqrt{\frac{3}{2} s_{ij} s_{ij}} \quad (4.42)$$

In fact, if we are in the Haigh-Westergaard space (see Fig. 71), $\bar{\sigma}^{VM}$ is outside de yield surface for a displacement $u_{max} = 0.8$ [mm] and will return on this surface, this is a potential (plasticity) expressed by \bar{f} and d (signum distance, see next section).

Mathematical development are more general and much more complex so we will only express what is append physically: because $\delta = 0.65$, kinematic hardening is predominant compared to isotropic hardening, so the difference of asymptotic values on Fig. 68 is quite visible but not huge. In fact, it is lower for mixed hardening because of backstress of kinematic hardening which represent the position of the center of the yield surface. *As the back-stress α_{ij} changes due to plastic flow, the yield surface translates in the stress space while maintaining its initial shape and size.*[3] When $\bar{\sigma}^{VM} - \sigma_y$ decreases, the plastic flow to. Note that equivalent backstress increases during relaxation (Fig. 68c). Finally, the shape of current yield stress is not the same as the equivalent Von Mises stress but their asymptotic values are still equal. The hardening has as effect to increase this current yield stress (backstress has the opposite effect).

4.4 Internal (hydrostatic) pressure

In this section, we will analyse the evolution of the hydrostatic pressure with the time at the inner surface and depending on the hardening. Remember that,

$$p = \frac{\text{tr}\boldsymbol{\sigma}}{3} \quad (4.43)$$

At inner surface, on P1, we have $\sigma_r = \sigma_{XX}$ and $\sigma_\theta = \sigma_\phi = \sigma_{YY}$, so

$$p = \frac{\sigma_{XX} + 2\sigma_{YY}}{3} \quad (4.44)$$

We impose one loading until u_{max} and keep this displacement during 2 [s]. We see on Fig. 70 that this pressure becomes rapidly constant when u is maintain constant. This validate our assumption $\dot{p} = 0$ in section 4.3.2. This pressure is quite equal for linear isotropic and mixed hardening. In fact, the hydrostatic pressure p in section 4.3.2 does not depend directly on the hardening so it is attended. Not that the pressure begins positive (in elasticity, corresponding to traction¹). In fact, we have seen the evolution of stress diagonal components in section 4.3.1. We have seen that σ_{XX} is always negative during the loading (compression) but σ_{YY} is positive at the beginning (traction). When plasticity becomes (after a displacement $u_y^0 = 0.05$ [mm], see section 5.1.6), σ_{XX} decreases due to this plasticity and as σ_{XX} is more negative than σ_{YY} is positive, the hydrostatic pressure becomes

¹during the loading, $\sigma_r < 0$ so there is compression and as $\sigma_r = p + s_r$, with $\sigma_r < 0$ and $p > 0$, s_r is more negative

rapidly negative after a short time of elasticity.

Finally, we see that $\eta = 10^8$ [MPa.s] is an illustration of $\eta \rightarrow +\infty$ leads to theoretically a purely elastic case, because

$$\lim_{\eta \rightarrow +\infty} \lambda = \sqrt{\frac{3}{2} \frac{d}{\eta}} = 0 \quad (4.45)$$

So,

$$\dot{\varepsilon}^{vp} = \sqrt{\frac{2}{3}} \lambda = 0 \Rightarrow \dot{\varepsilon}^{vp} \text{ cst} \quad (4.46)$$

$$\dot{\sigma}_y = h_i \dot{\varepsilon}^{vp} = 0 \Rightarrow \sigma_y = \sigma_y^0 \text{ cst} \quad (4.47)$$

Or,

$$\lim_{\eta \rightarrow +\infty} \bar{f} = \bar{\sigma}^{VM} - \sigma_y - \eta(\dot{\varepsilon}^{vp}) = 0 \Rightarrow \lim_{\eta \rightarrow +\infty} d = \bar{\sigma}^{VM} - \sigma_y = \lim_{\eta \rightarrow +\infty} \eta \dot{\varepsilon}^{vp} \approx 1511 \text{ [MPa]} \quad (4.48)$$

$$\dot{\varepsilon}^{vp} \rightarrow 0 \text{ if } \eta \rightarrow +\infty \text{ in order to have } \eta(\dot{\varepsilon}^{vp}) \text{ finite} \quad (4.49)$$

And because we assume that $\dot{\varepsilon}^{vp}(t_0) = 0$ and the form of $\dot{\varepsilon}^{vp}$ is, (from tips of the report)

$$\dot{\varepsilon}^{vp}(t) = \dot{\varepsilon}^{vp}(t_0) + \int_{t_0}^t |\dot{\varepsilon}^{vp}| dt = 0 \quad (4.50)$$

This is thus a limit case (pseudo-elasticity). We see on Fig. 69 that we have well $\dot{\varepsilon}^{vp} \rightarrow 0$ when $\eta \rightarrow +\infty$ (10^8). Moreover, stress tensors components followed the displacement and are linear (shape of an elastic case) but are huge ! Normally this kind of values for stresses leads to plasticity but with this linear shape, we call it "pseudo-elasticity". In fact, we see that $2\sigma_{YY}$ compensate σ_{XX} to make p positive: an always positive hydrostatic pressure makes us think of elasticity (but of a lower value than the real elasticity, see 4.3.1 where $\sigma_{YY} >> |\sigma_{XX}|$ at outer surface where elasticity occurs so $p > 0$ (higher value than the one for "pseudo-elasticity"). Physically, $\eta \rightarrow +\infty$ is not possible but makes an "infinite" viscous plasticity and avoid plasticity effect even the equivalent stress exceeds the initial yield stress.

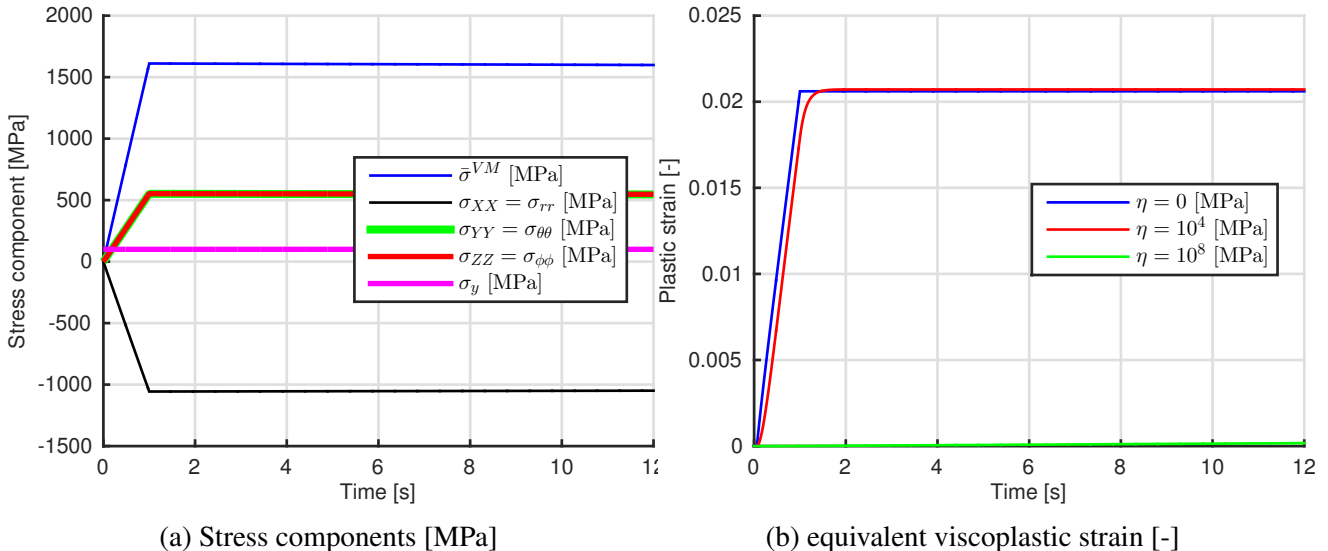


Figure 69 – Temporal variation of ... at inner surface (extrapolated at the inner left node P1 on curve C4) for several η [MPa.s] 1 cycle of loading until u_{max} during 8 [s]

Finally, we have displayed the hydrostatic pressure for $\eta = 0$ [MPa.s], which corresponds to elasto-viscoplasticity and perfectly plasticity at inner surface. The behavior is the same for elasticity

part ($p > 0$) but after, p drops faster than the one of viscoplasticity (the "braking" is a property of viscosity). When u_{max} is reached, p is directly constant while the one for viscoplasticity need a short time to reach its constant value. This is the main difference between plasticity and viscoplasticity: rate dependence due to friction (viscosity).

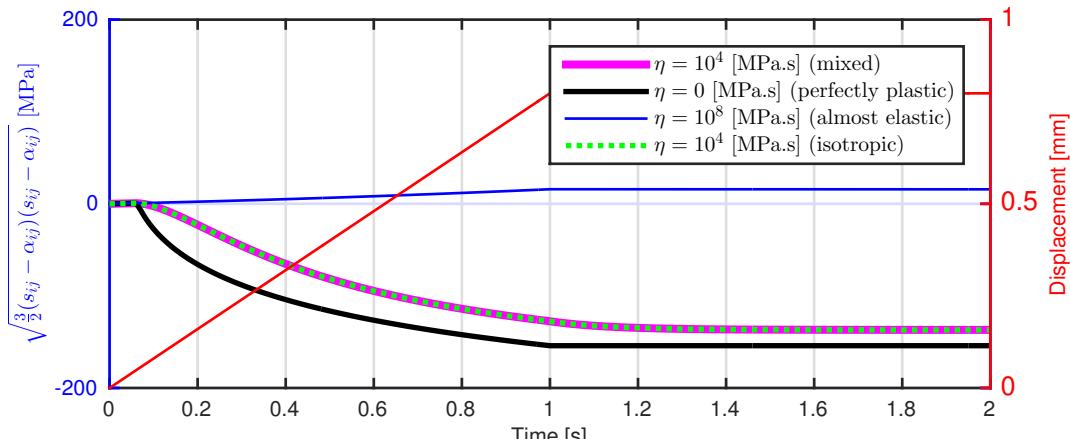


Figure 70 – Temporal variation of the hydrostatic pressure $\bar{\sigma}_{VM}$ [MPa] at inner surface (extrapolated at the inner left node P1 on curve C4) for $\eta = 10^4$ [MPa.s] with linear isotropic and mixed hardening for 1 cycles of loading until u_{max} during 2 [s], displacement [mm] is in red, comparison with "almost elastic" case $\eta = 10^8$ [MPa.s]

4.5 Signum distance ($\eta = 10^4$ [MPa.s], linear isotropic hardening)

This section will study the signum distance, defined previously as,

$$d = \langle \bar{\sigma} - \sigma_y \rangle \quad (4.51)$$

Where $\bar{\sigma} = \sqrt{\frac{3}{2}s_{ij}s_{ij}}$ is the equivalent stress. Remember that in elasto-viscoplasticity, a stress state ($\bar{\sigma}$) out of the yield hypersurface $\bar{\sigma} - \sigma_y$ so with $d > 0$. Note that it does not mean that $\bar{f} > 0$ because it is impossible and because the generalized \bar{f} for elasto-viscoplasticity is (extended consistency condition from slide 17 of chapter 8 [3]),

$$\bar{f} = \bar{\sigma}^{VM} - \sigma_y - \eta(\dot{\varepsilon}^{vp})^n(\dot{\varepsilon}^{vp})^m = \bar{\sigma}^{VM} - \sigma_y - \eta(\dot{\varepsilon}^{vp}) = 0 \quad (4.52)$$

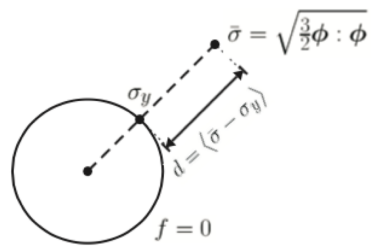
d is called "distance" but actually, this is only a difference between stresses (equivalent Von Mises and current yield) so d [MPa]. Nevertheless, in the Haigh-Westergaard space, it is well a "distance" (Fig. 71). Metafor does not give directly the values of d but we can compute it by difference of $\bar{\sigma}$ (IF_EVMS)² and σ_y (IF_STATIC_YIELD). This will be done for two types of loading: cycles of sawtooth loading/unloading during 4 [s] and 1 loading followed by a constant displacement of u_{max} during 2 [s]. We will study also the influence of the loading rate on this signum distance (more particularly for d_{max}). Note that because of linear isotropic hardening, $\alpha_{ij} = 0$. Thus the yield surface is centered at (0,0).

4.5.1 Sawtooth loading

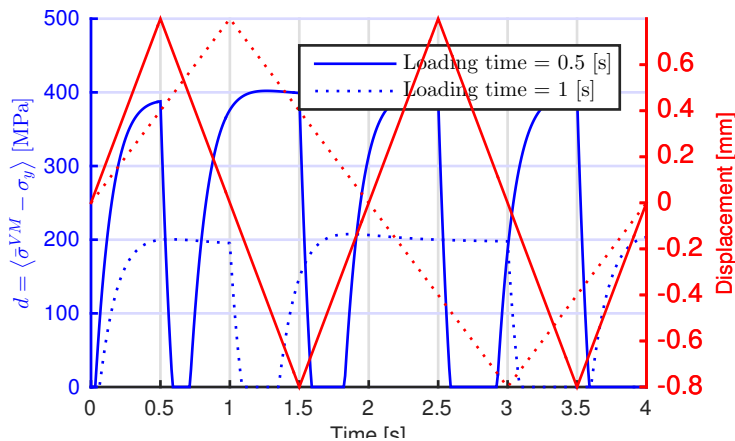
We observe on Fig. 72 that the shape of d is characterized by 3 phases:

- d is null in the elastic domain (first part of the loading domain, when $u < u_y^0$) because in that case plasticity is not reached and $\bar{\sigma} < \sigma_y$ so $d < 0 \Rightarrow d = 0$

²Note that $\bar{\sigma} = \bar{\sigma}^{VM}$ for linear isotropic hardening because in that case $\alpha_{ij} = 0$ and we can take also IF_CRITERION

Figure 71 – Schematic representation of the signum distance d

- Then, d increases fast from zero due to radial displacement in plasticity (we see that d is higher and increase faster if the loading time is lower and thus the loading speed is greater). d_{max} increases with the loading speed. Then, there is a slower increase of d because plastic flow increases so much compared to $\bar{\sigma}$ that σ_y is enough high to slow the increase of d . Then, d reaches a "limit" point: d_{max} where $\bar{\sigma}$ increases by the same rate than σ_y (it corresponds to u_{max}).
- After, the unloading cycle begins and d decreases rapidly (short time of adaptation to the unloading, $\bar{\sigma}$ decreases compared to σ_y and d becomes less and less positive). Then, d becomes null because we reach elasticity for a short time and $\bar{\sigma}$ recovers the yield surface ($\bar{f} = 0 \Rightarrow$ elasticity). d remains null during elastic phase and increase when plasticity begins in the unloading cycle and so on...

Figure 72 – Temporal variation of the signum distance d [MPa] at inner surface for several loading time [s] with linear isotropic hardening for cycles of loading/unloading in sawtooth for $\eta = 10^4$ [MPa.s]

The evolution of d with η is related to the evolution of $\bar{\sigma}$ with η : when η increases, $\bar{\sigma}$ and thus d increases. For $\eta \rightarrow +\infty$ (10^8) [MPa.s] and $\bar{\sigma}$ follows the displacement in absolute value so d to. In fact, we see that d increases when we increase η after 10^8 [MPa.s] but of a negligible amount, d reaches thus a maximum there. We have called this behavior as "pseudo-elasticity". Which corresponds to the fact that,

$$\lim_{\eta \rightarrow +\infty} \bar{f} = \bar{\sigma}^{VM} - \sigma_y - \eta(\dot{\varepsilon}^{vp}) = 0 \Rightarrow \lim_{\eta \rightarrow +\infty} d = \bar{\sigma}^{VM} - \sigma_y = \lim_{\eta \rightarrow +\infty} \eta \dot{\varepsilon}^{vp} \approx 1511 \text{ [MPa]} \quad (4.53)$$

$$\dot{\varepsilon}^{vp} \rightarrow 0 \text{ if } \eta \rightarrow +\infty \text{ in order to have } \eta(\dot{\varepsilon}^{vp}) \text{ finite} \quad (4.54)$$

Indeed, the shape of equivalent stress looks like elasticity but with higher value. In fact, the yield stress becomes constant for $\eta \rightarrow +\infty$ (σ_y^0) and the equivalent stress is linear but huge so $\bar{\sigma} \gg \sigma_y^0$ so

$d >> 0$ with high value (converges through 1511 [MPa]).

As the overstress d is a property of elasto-viscoplasticity so it increases when the viscosity (illustrated by η) increases. If $\eta = 0$ and no more viscosity (only elasto-plasticity, and just plasticity at inner surface), d is always null. $\bar{\sigma}$ is always equal to the current yield stress in elasto-plasticity (slide 17 of chapter 8 of [3]):

$$\bar{f} = \bar{\sigma}^{VM} - \sigma_y - \eta(\dot{\varepsilon}^{vp}) = 0, \text{ with } \eta = 0 \Rightarrow \bar{f} = \bar{\sigma}^{VM} - \sigma_y = 0 \Rightarrow d = 0 \quad (4.55)$$

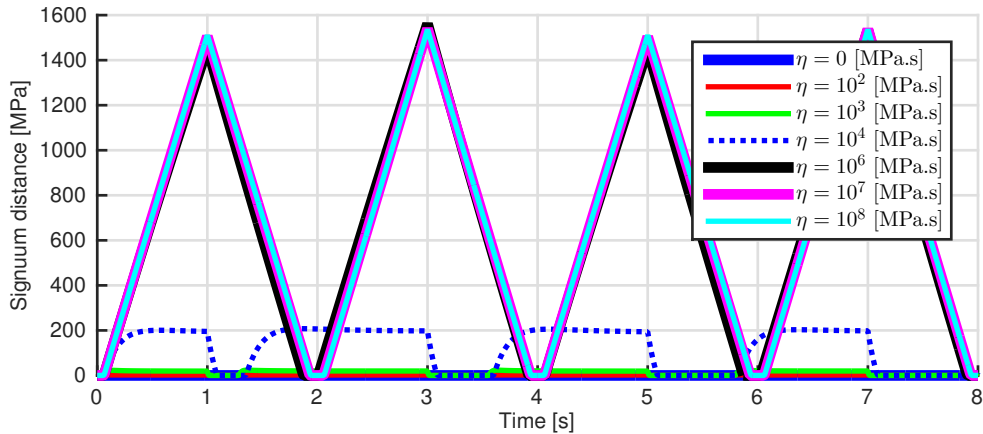


Figure 73 – Temporal variation of the signum distance δ [MPa] at inner surface for several loading time [s] with linear isotropic hardening for cycles of loading/unloading in sawtooth depending on η [MPa.s]

4.5.2 One loading followed by constant u_{max}

We will now study the evolution of d for a loading followed by constant u_{max} during 2 [s]. Similarly to previous case, we see 3 phases (2 firsts are identical to those of previous section because the first loading is the same):

- $d = 0$ while elasticity occurs
- d increases fast and stabilizes progressively until the end of the augmentation of the loading ($\bar{\sigma}$ increases as fast as σ_y finally)
- this phase is different than the one of sawtooth loading because the displacement remains constant. For u_{max} , λ is high so $\dot{\varepsilon}^{vp}$ to. Because of the definition of linear isotropic hardening, $\sigma_y = \sigma_y^0 +$ increases to. Then, $d = \bar{\sigma} - \sigma_y$ decreases fastly. Because of viscosity, we have seen that σ_y decreases when we impose a constant u_{max} (see section 4.3.3) so d continues to decrease but slowly because of decreasing of σ_y slower than the one of $\bar{\sigma}$. At the end (for a long time), we have seen that $\bar{\sigma}$ and σ_y have the same asymptotic values so $d = 0$ finally: it follows the shape of decreasing exponential of section 4.3.3 so d takes an infinite time to reaches 0.

As elasto-viscoplasticity depends on the strain/displacement rate, the signum distance to (Fig. 72, 74, 75). We see on Fig. 75 that d_{max} decreases with the loading time (increases with the loading speed). The relation between loading time and speed is:

$$v_{loading} = \frac{u_{max}}{t_{loading}} \quad (4.56)$$

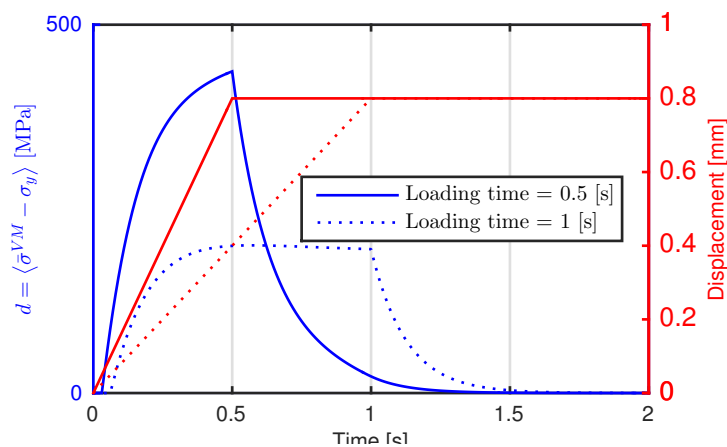


Figure 74 – Temporal variation of the signum distance δ [MPa] at inner surface for several loading time [s] with linear isotropic hardening for one loading followed by constant u_{max} for $\eta = 10^4$ [MPa.s]

Note that we have seen that the equivalent stress increases more when the strain rate increases (see Fig. 52) than the yield stress increases. As the stress increases more than the yield stress, d increases to. As the loading speed increases, $\bar{\sigma}$ increases much more than σ_y and d increases to a higher value. When the loading speed increases, the material has less time to adapt itself and the stress increases. The same phenomena occurs if you increase η . Thus, d_{max} increases with η . This is in accord to the general evolution of $\bar{\sigma}$ (increase) for elasto-viscoplasticity model (Fig. 53) when $\dot{\varepsilon}$ increases. Even if $\dot{\varepsilon}$ increases, σ_y^0 does not increase as much as $\bar{\sigma}$. Here \dot{u} increases and $d = \bar{\sigma} - \sigma_y$ increases as well.

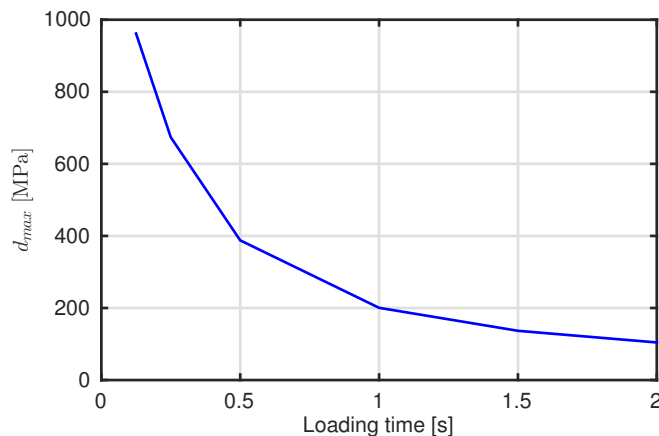


Figure 75 – Variation of the maximal signum distance δ_{max} [MPa] at inner surface for several loading time [s] with linear isotropic hardening for one loading followed by constant u_{max}

5 Part 4: Sensitive study of numerical parameters

5.1 Analytical solution

5.1.1 Introduction

Here, we will study the analytical solution for the elastic thick sphere under pressure where the pressure is replaced by an imposed displacement u at the inner surface. We assume spherical coordinates (Fig. 76) and *axisymmetric* problem (Fig. 1).

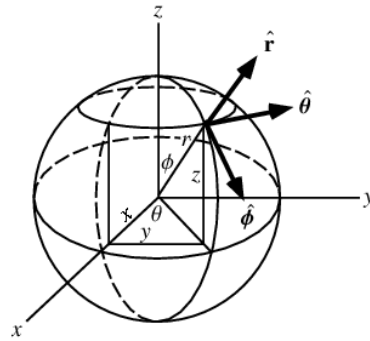


Figure 76 – Spherical coordinates [4]

These results are extracted from [1], *Mécanique du solide* in bachelor 2 [2] and from repetition 3 of *Advanced solid mechanics* [3].

Because of symmetry, non-diagonal terms of tensors are null, $\sigma_{r\theta} = \sigma_{r\phi} = \sigma_{\phi\theta} = \varepsilon_{r\theta} = \varepsilon_{r\phi} = \varepsilon_{\phi\theta} = 0$. Remaining stress/strain does not depend on θ and ϕ . We assume *small strain* so undeformed ($\vec{X}(R, \Theta, \Phi)$) and deformed ($\vec{x}(r, \theta, \phi)$) configuration are equivalent,

$$\vec{X}(R, \Theta, \Phi) \approx \vec{x}(r, \theta, \phi) \quad (5.1)$$

$$R_1 \approx R_1^0 \text{ and } R_2 \approx R_2^0 \quad (5.2)$$

$$\text{If } \varepsilon_{rr} \ll 1 \quad \varepsilon_{\theta\theta} \ll 1 \quad \varepsilon_{\phi\phi} \ll 1 \quad (5.3)$$

5.1.2 Boundary conditions

All boundary conditions are static. The general expression valid for all surfaces of the sphere,

$$\vec{t} = \vec{t}^* \quad \forall \vec{x} \in \mathbb{S}_\sigma \quad (5.4)$$

With,

- \vec{t} is the applied surface traction vector
- \vec{t}^* is the surface traction vector from the stress field σ

Inner surface

$$r = R_1 \quad \vec{n}^{(i)} = (-1 \ 0 \ 0)^T \quad (5.5)$$

By definition,

$$\vec{t}^{(i)} = \boldsymbol{\sigma}^{(i)} \cdot \vec{n}^{(i)} = \begin{pmatrix} \sigma_{rr} & 0 & 0 \\ 0 & \sigma_{\theta\theta} & 0 \\ 0 & 0 & \sigma_{\phi\phi} \end{pmatrix} \Big|_{r=R_1} \times \begin{pmatrix} -1 \\ 0 \\ 0 \end{pmatrix} = \begin{pmatrix} -\sigma_{rr} \\ 0 \\ 0 \end{pmatrix} \Big|_{r=R_1} \quad (5.6)$$

And we know that,

$$\vec{t}^{(i)} = \begin{pmatrix} p \\ 0 \\ 0 \end{pmatrix} \quad \forall(\theta, \phi) \in [0, \pi] \times [0, 2\pi] \quad (5.7)$$

Because $p \neq f(\theta) \neq f(\phi)$: pressure uniformly distributed inside the sphere. So,

$$\sigma_{rr} = -p \text{ at } r = R_1 \quad (5.8)$$

Nevertheless, pressure is replaced by an imposed displacement at inner surface.

$$\sigma_{rr}(r = R_1) = -p \Rightarrow u_r(R_1) = u \quad (5.9)$$

Outer surface

$$r = R_2 \quad \vec{n}^{(o)} = (1 \ 0 \ 0)^T \quad (5.10)$$

By definition,

$$\vec{t}^{(o)} = \boldsymbol{\sigma}^{(o)} \cdot \vec{n}^{(o)} = \begin{pmatrix} \sigma_{rr} & 0 & 0 \\ 0 & \sigma_{\theta\theta} & 0 \\ 0 & 0 & \sigma_{\phi\phi} \end{pmatrix} \Big|_{r=R_2} \times \begin{pmatrix} 1 \\ 0 \\ 0 \end{pmatrix} = \begin{pmatrix} -\sigma_{rr} \\ 0 \\ 0 \end{pmatrix} \Big|_{r=R_2} \quad (5.11)$$

And we know that,

$$\vec{t}^{(o)} = \begin{pmatrix} p \\ 0 \\ 0 \end{pmatrix} \quad \forall(\theta, \phi) \in [0, \pi] \times [0, 2\pi] \quad (5.12)$$

Remark that we consider "zero relative pressure" outside the sphere: this means an atmospheric pressure ($p_{rel} = p - p_{atm}$). So,

$$\sigma_{rr} = 0 \text{ at } r = R_2 \quad (5.13)$$

Summary

$$u_r(R_1) = u \quad (5.14)$$

$$\sigma_{rr}(r = R_2) = 0 \quad (5.15)$$

$$(5.16)$$

5.1.3 Equilibrium equation

Summary of fields of displacement, deformation and stress

$$\begin{cases} u_{\theta\theta} = u_{\phi\phi} = \sigma_{r\theta} = \sigma_{r\phi} = \sigma_{\phi\theta} = \varepsilon_{r\theta} = \varepsilon_{r\phi} = \varepsilon_{\phi\theta} = 0 \\ u_{rr} = f_1(r) \\ \sigma_{rr} = f_2(r), \sigma_{\theta\theta} = \sigma_{\phi\phi} = f_3(r) \\ \varepsilon_{rr} = f_4(r), \varepsilon_{\theta\theta} = \varepsilon_{\phi\phi} = f_5(r) \end{cases} \quad (5.17)$$

Simplification of quasi-static equilibrium equation along \vec{e}_r

$$\frac{d\sigma_{rr}}{dr} + \frac{2}{r}(\sigma_{rr} - \sigma_{\theta\theta}) = 0 \quad (5.18)$$

Because we neglect body forces here (quasi-static)

$$\rho_0 \bar{b}_r = 0 \quad (5.19)$$

5.1.4 Kinematic equations

$$\varepsilon_{rr} = \frac{du_r}{dr}, \varepsilon_{\theta\theta} = \varepsilon_{\phi\phi} = \frac{u_r}{r} \quad (5.20)$$

Because there is no shear stress, there is no shear strain, the material behavior is isotropic.

5.1.5 Constitutive equations

General expression for elasto-plasticity

$$\dot{\sigma}_{ij} = \mathbb{H}_{ijkl}(\dot{\varepsilon}_{ij} - \dot{\varepsilon}_{kl}^p) \quad (5.21)$$

With,

- \mathbb{H}_{ijkl} the fourth order Hooke's tensor
- $\dot{\varepsilon}_{kl}^p$ the plastic strain rate tensor

Simplification of Hooke's law in elasticity

$$E\varepsilon_{rr} = (\sigma_{rr} - 2\nu\sigma_{\theta\theta}), E\varepsilon_{\theta\theta} = ((1-\nu)\sigma_{\theta\theta} - \nu\sigma_{rr}) \quad (5.22)$$

We will now simplify notation because only diagonal terms remain,

$$\varepsilon_{rr} \rightarrow \varepsilon_r \quad \varepsilon_{\theta\theta} \rightarrow \varepsilon_\theta \quad \varepsilon_{\phi\phi} \rightarrow \varepsilon_\phi \quad \sigma_{rr} \rightarrow \sigma_r \quad \sigma_{\theta\theta} \rightarrow \sigma_\theta \quad \sigma_{\phi\phi} \rightarrow \sigma_\phi \quad u_{rr} \rightarrow u_r \quad (5.23)$$

5.1.6 Elastic solution $0 \leq u < u_y^0$

Substituting equations 5.20 in 5.22 and then in 5.18, we get a differential equation

$$\frac{d^2u_r}{dr^2} + \frac{2}{r} \frac{du_r}{dr} - \frac{2}{r^2} u_r = 0 \Rightarrow \frac{d}{dr} \left(\frac{1}{r^2} \frac{d}{dr} (r^2 u_r) \right) = 0 \quad (5.24)$$

And the solution,

$$\frac{1}{r^2} \frac{d}{dr} (r^2 u_r) = C \quad (5.25)$$

$$\frac{d}{dr} (r^2 u_r) = C r^2 \quad (5.26)$$

$$r^2 u_r = C \frac{r^3}{3} + C_2 \quad (5.27)$$

$$u_r = C_1 r + \frac{C_2}{r^2} \quad (5.28)$$

Substitution of equation 5.28 in 5.22 and 5.20, we obtain

$$\sigma_{rr} = E \left(\frac{C_1}{1 - 2\nu} - \frac{2C_2}{(1 + \nu)r^3} \right) \quad (5.29)$$

$$\sigma_{\theta\theta} = \sigma_{\phi\phi} = E \left(\frac{C_1}{1 - 2\nu} + \frac{C_2}{(1 + \nu)r^3} \right) \quad (5.30)$$

With C_1 and C_2 are constant terms obtained with boundary conditions,

$$u = C_1 R_1 + \frac{C_2}{R_1^2} \quad (5.31)$$

$$0 = E \left(\frac{C_1}{1 - 2\nu} - \frac{2C_2}{(1 + \nu)R_2^3} \right) \quad (5.32)$$

$$C_1 = u \frac{2R_1^2(1 - 2\nu)}{(1 + \nu)R_2^3 + 2R_1^3(1 - 2\nu)} \quad (5.33)$$

$$C_2 = u \frac{R_1^2 R_2^3 (1 + \nu)}{(1 + \nu)R_2^3 + 2R_1^3(1 - 2\nu)} \quad (5.34)$$

Stress field

$$\sigma_r(r) = \frac{2uER_1^2}{(1 + \nu)R_2^3 + 2R_1^3(1 - 2\nu)} \left(1 - \frac{R_2^3}{r^3} \right) \quad (5.35)$$

$$\sigma_\theta(r) = \sigma_\phi(r) = \frac{uER_1^2}{(1 + \nu)R_2^3 + 2R_1^3(1 - 2\nu)} \left(2 + \frac{R_2^3}{r^3} \right) \quad (5.36)$$

Strain field

$$\varepsilon_r(r) = \frac{2uER_1^2}{r((1 + \nu)R_2^3 + 2R_1^3(1 - 2\nu))} \left((1 - 2\nu) - \frac{R_2^3(1 + \nu)}{r^3} \right) \quad (5.37)$$

$$\varepsilon_\theta(r) = \varepsilon_\phi(r) = \frac{uER_1^2}{r((1 + \nu)R_2^3 + 2R_1^3(1 - 2\nu))} \left(2(1 - 2\nu) + \frac{R_2^3(1 + \nu)}{r^3} \right) \quad (5.38)$$

Displacement field

$$u_r(r) = \frac{uER_1^2}{((1 + \nu)R_2^3 + 2R_1^3(1 - 2\nu))} \left((1 - 2\nu) + \frac{R_2^3(1 + \nu)}{r^3} \right) \quad (5.39)$$

Yield displacement u_y^0 We can compute the initial yield displacement (u_y^0 such that $\bar{\sigma}_{VM} = \sigma_y^0$) using Von Mises criterion in 3D (for boundary condition $u_r(R_1) = u$),

$$100 = \sigma_y^0 = \bar{\sigma}_{VM} = \sigma_r(R_1) - \sigma_\theta(R_1) = \frac{3EC_2}{(1+\nu)R_1^3} = \frac{u_y^0 3ER_2^3}{R_1((1+\nu)R_2^3 + 2R_1^3(1-2\nu))} \Rightarrow u_y^0 = 0.0533 \text{ [mm]} \quad (5.40)$$

Note that Von Mises criterion is here equivalent to $\bar{\sigma}_{VM} = \sigma_{rr} - \sigma_{\theta\theta}$ because $\sigma_{\phi\phi} = \sigma_{\theta\theta}$. Remark that this initial yield pressure is the pressure from which material enters in plastic domain (yield pressure will be constant for purely plastic behavior, for elasto-plastic it will increase linearly).

Summary We have display the different fields on Fig. 77 and we see well that σ and ε are of the same form (respect the Hooke's law $\sigma = E\varepsilon$).

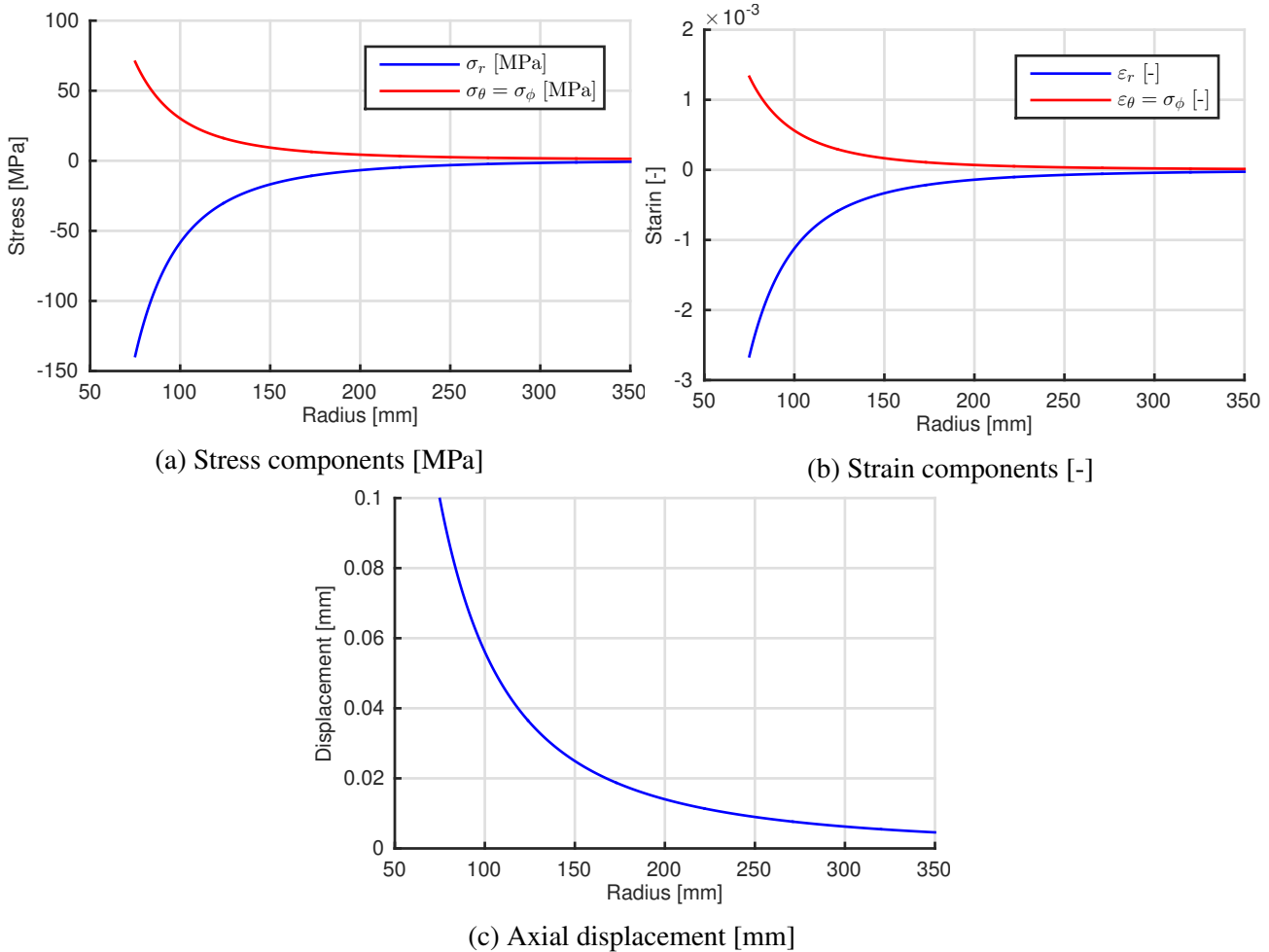


Figure 77 – Distribution of components r, θ, ϕ of tensors σ, ε and distribution of axial displacement along the sphere (from R_1 to R_2); this is done for a maximal displacement $u(R_1) = 0.1$ [mm] to be in elasticity ; $E = 70000$ [MPa], $\nu = 0.33$ [-], $R_1 = 75$ [mm], $R_2 = 350$ [mm]

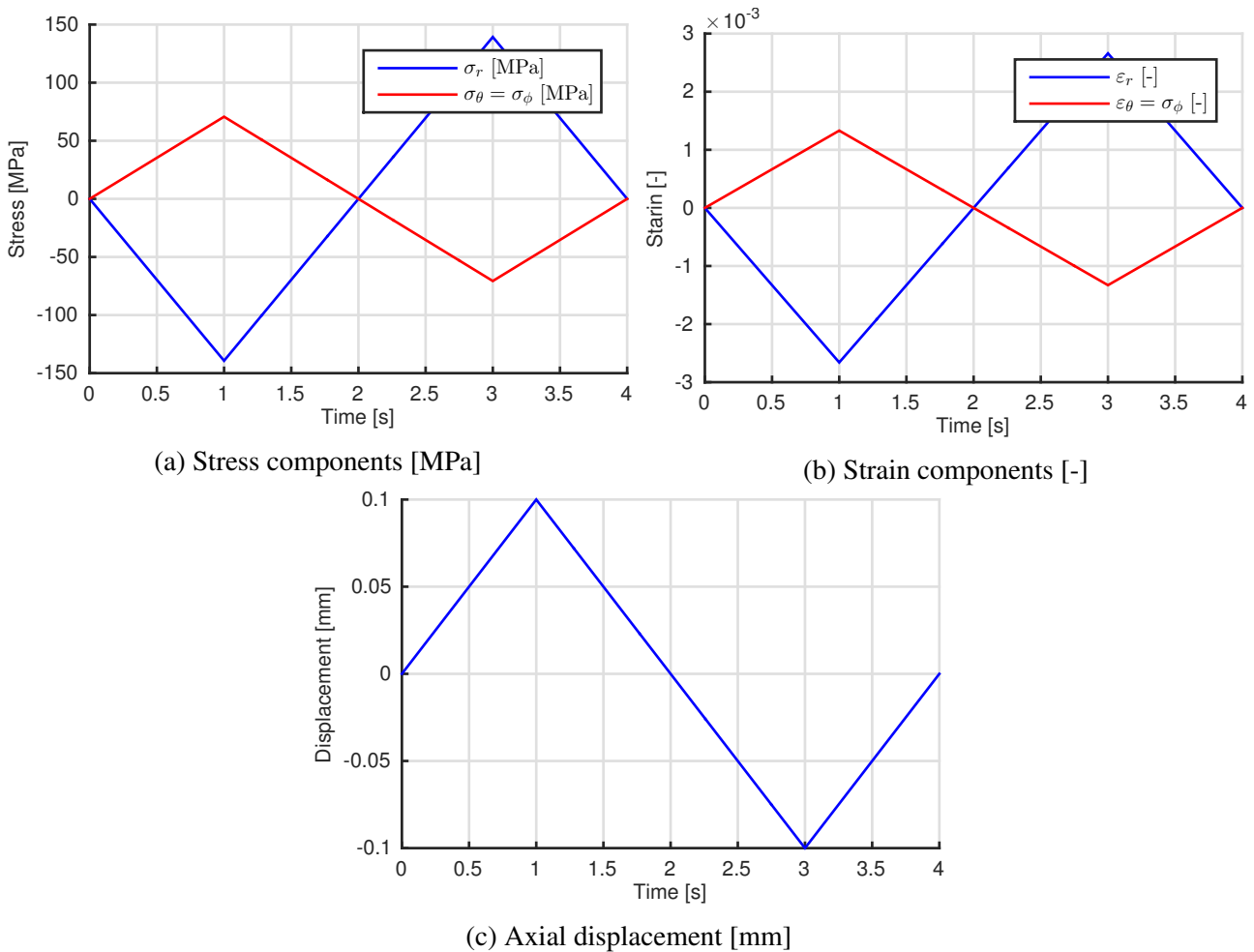


Figure 78 – Temporal variation of components r, θ, ϕ of tensors σ, ϵ and distribution of axial displacement for a sawtooth loading/unloading cycle (at inner surface R_1); this is done for a maximal displacement $u_{max} = 0.1$ [mm] (at $u_r(R_1)$) to be in elasticity ; $E = 70000$ [MPa], $\nu = 0.33$ [-], $R_1 = 75$ [mm], $R_2 = 350$ [mm]

5.1.7 Elasto-plastic solution $u > u_y^0$

We will now extrapolate results of previous section and estimate the behaviour for elasto-plasticity, when the pressure p exceeds the initial yield pressure p_y^0 (reasonings from [1]). In this case, a plastic zone appears for $R_1 < r < c$ and the zone $c < r < R_2$ remains elastic (Fig. 79).

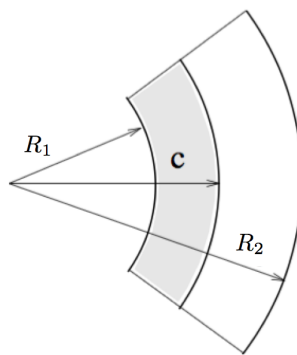


Figure 79 – Evolution of plastic and elastic zones from inner surface

For $r = c$, the radial stress is equal to the yield stress,

$$\sigma_y^0 = \frac{3u_y^0 E R_1^2 R_2^3}{c^3((1+\nu)R_2^3 + 2R_1^3(1-2\nu))} \sigma_y^0 \leftrightarrow u_y^0 = \frac{\sigma_y^0((1+\nu)R_2^3 + 2R_1^3(1-2\nu))c^3}{3R_1^2 R_2^3 E \sigma_y^0} \quad (5.41)$$

Then, replace u by u_y^0 into equation of $\sigma_r(r)$

$$\sigma_r(r) = \frac{2c^3}{3R_2^3} \left(1 - \frac{R_2^3}{r^3}\right) \sigma_y^0 \quad (5.42)$$

$$\sigma_r(c) = \frac{2}{3} \left(\frac{c^3}{R_2^3} - 1\right) \sigma_y^0 \quad (5.43)$$

$$(5.44)$$

Fields in the elastic zone are given by equations 5.38 to 5.39 where we replace R_1 by c and u by u_y^0 . To study the plastic zone, we must taking into account these equations (equilibrium and pasticity criterion),

$$\frac{d\sigma_r}{dr} + \frac{2}{r}(\sigma_r - \sigma_\theta) = 0 \quad (5.45)$$

$$\sigma_r - \sigma_\theta = \sigma_y^0 \quad (5.46)$$

So,

$$\frac{d\sigma_r}{dr} - \frac{2}{r}\sigma_y^0 = 0 \quad (5.47)$$

And we get the solution,

$$\sigma_r(r) = 2\sigma_y^0 \ln(r) + C_3 \quad (5.48)$$

Where C_3 comes from the continuity of σ_r at $r = c$,

$$2\sigma_y^0 \ln(c) + C_3 = \frac{2}{3} \left(\frac{c^3}{R_2^3} - 1\right) \sigma_y^0 \quad (5.49)$$

Thus,

$$\sigma_r^p(r) = -\frac{2}{3}\sigma_y^0 \left(1 + 3 \ln\left(\frac{c}{r}\right) - \frac{c^3}{R_2^3}\right) \quad (5.50)$$

$$\sigma_\theta^p(r) = \frac{2}{3}\sigma_y^0 \left(\frac{1}{2} - 3 \ln\left(\frac{c}{r}\right) + \frac{c^3}{R_2^3}\right) \quad (5.51)$$

$$(5.52)$$

Plastic does not produce volume variation so the volume variation is only due to elastic deformation,

$$\varepsilon_r + 2\varepsilon_\theta = \frac{1-2\nu}{E}(\sigma_r + 2\sigma_\theta) \quad (5.53)$$

So, the displacement can be computed,

$$\frac{du_r}{dr} + 2\frac{u_r}{r} = \frac{-2\sigma_y^0(1-2\nu)}{E} \left(3 \ln\left(\frac{c}{r}\right) - 3 \frac{c^3}{R_2^3}\right) \quad (5.54)$$

$$u_r(r) = \frac{C_4}{r^2} - \frac{2(1-2\nu)}{E} r \sigma_y^0 \left(\ln\left(\frac{c}{r}\right) + \frac{1}{3} \left(1 - \frac{c^3}{R_2^3}\right)\right) \quad (5.55)$$

C_4 is obtained thanks to continuity of u_r at $r = C$,

$$\frac{C_4}{c^2} - \frac{2(1-2\nu)}{E} c \sigma_y^0 \left(\frac{1}{3} \left(1 - \frac{c^3}{R_2^3} \right) \right) = C_1 c + \frac{C_2}{c^2} \quad (5.56)$$

Then, we get u_r , ε_r and ε_θ by replacing C_4 , C_1 and C_2 and taking u_y^0 as a function of σ_y^0 (equation 5.41),

$$u_r(r) = \frac{\sigma_y^0}{E} r \left((1-\nu) \frac{c^3}{r^3} - \frac{2}{3}(1-2\nu) \left(1 + 3 \ln \left(\frac{c}{r} \right) - \frac{c^3}{R_2^3} \right) \right) \quad (5.57)$$

$$\varepsilon_r^p(r) = \frac{2\sigma_y^0}{E} (1-\nu) \left(1 - \frac{c^3}{r^3} \right) \quad (5.58)$$

$$\varepsilon_\theta^p(r) = \varepsilon_\phi^p(r) = -\frac{\sigma_y^0}{E} (1-\nu) \left(1 - \frac{c^3}{r^3} \right) \quad (5.59)$$

The strain rate is (if we take c as loading parameter),

$$\dot{\varepsilon}_r^p = \frac{d\varepsilon_r^p}{dc} = -\frac{6\sigma_y^0}{E} (1-\nu) \frac{c^2}{r^3} < 0 \quad (5.60)$$

$$\dot{\varepsilon}_\theta^p = \dot{\varepsilon}_\phi^p = -\frac{1}{2} \dot{\varepsilon}_r^p \quad (5.61)$$

5.2 Influence of the loading speed

For this test we will study the influence of the loading speed on the results. The goal of this study is not to discuss the influence of the loading speed on the material but on the time integration schemes. The loading speed as not influence on the elasto-plastic models. Well on the elasto-plastic model but a full section is specially dedicated to it. We here study the influence of the loading speed and the time-step in the time-integration scheme.

In order to study the influence of the loading speed on the time integration scheme, we will change the time of loading. It is asked to keep the same maximum displacement. So the only way to make change the loading speed is to change the loading time. The loading time will be set between 0.006 second to 10 seconds. Note that the quasi-static loading is assumed. This means that all computed state are supposed to be at equilibrium. The non-balanced forces are under a tolerance factor. We keep the same time step of 0.006 second.

This study will drive us in order to find a good trade-off for the time step. As you can see on Figure 80, if the time step is to large with respect to the loading time, the phenomena will not be computed. This is the case for the loading time of 0.006 and 0.06 second.

On the figure 81 you can also observe that if the time step is too small with respect to the loading time, some peaks appears at the end of the elastic phases (even if we are in a no-hardening elasto-plastic model). This happens because the computer has computed the solution for a time where the first Gauss Point is in plasticity (equivalent VM stress equals to the yield stress) and the second not (lower than the yield stress). This values are computed at the GP and extrapolated to the nodes by the shape form functions. The extrapolation induced some errors like this.

This short study clearly shows that the choice of the time step is a trade-off. It must be small enough in order to represent the studied phenomena but there exists a limit, linked to the geometrical resolution of the mesh, under which the time step may not go. Otherwise, some errors linked to

the extrapolation appear. An other parameter may be taken into account. The numerical costs must be limited. The more refined is the model, the more data's it stores and computes. This means more calculation time, required free memory, etc. This is why we have taken a maximum time step of 0.006 second for a loading speed of 0.8mm/sec . This provides sufficiently good results, without inducing too much extrapolation errors and taking too much numerical costs.

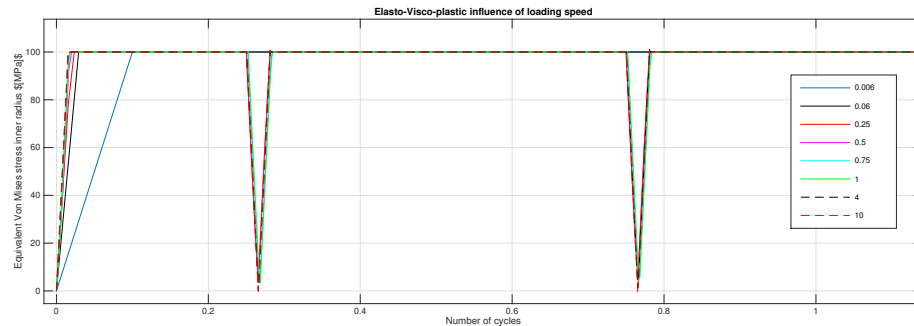


Figure 80 – Inlfuence of the loading speed with on the time integration scheme.

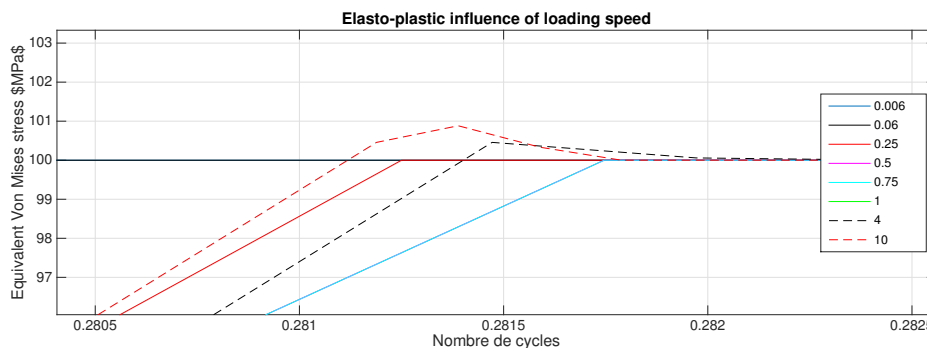


Figure 81 – Inlfuence of the loading speed with on the time integration scheme.

5.3 Influence of spatial discretisation

5.3.1 Introduction

As we use the finite elements method to solve our problem, it is obvious that an important parameter that should be taken into account is the dimensions of the elements.

But first, we should have chosen the number of elements we would use to get a compromise between CPU time and accuracy of the results but as we have a great limitation in term of nodes (maximum 500 nodes), we tried to always be as close as possible of the limit.

So, the only parameters we have actually studied are the number of radial divisions, the number of circumferential divisions and the distribution of radial distributions.

5.3.2 Number of radial divisions

Here, we will compare different number of radial divisions (Nr) using a constant number of circumferential divisions. If we look at the evolution of von Mises' equivalent stress at the inner surface for different choices of radial divisions when it enters in plasticity for no hardening model(Fig. 82), we can observe the presence of a peak whose amplitude is higher than the yield stress.

This observation is in total contradiction with the model considered and it seems very important to understand its origin. We can do that if we think about the way the results of P1 are computed. Indeed,

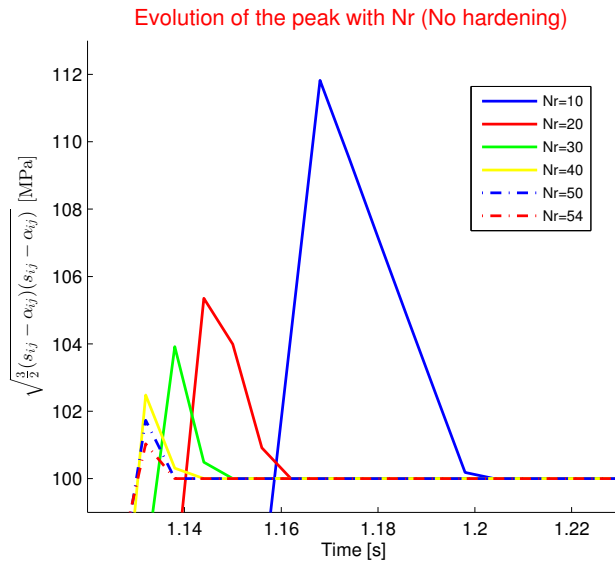


Figure 82 – Evolution of $\bar{\varsigma}_{VM}$ at the peak with different Nr.

we know that in each elements, the unknown are solved at the Gauss points and then extrapolated to get some values at the nodes using the shape functions. That's where the problem lies : when the first Gauss point enters in plasticity, its von Mises' equivalent stress is equal to the yield stress but it is not the case for the further Gauss points so that when the extrapolation is performed, the value is too high at P1. The diminution is due to the enter in plasticity of the other points so that there isn't anymore an introduced error by the extrapolation.

If we look at Fig. 82, we can see that indeed the more radial divisions there is, less is the amplitude of the peak and less is the duration of the peak, due to closer Gauss points.

We can also see on Fig. 83 that with 54 radial divisions the relative error is only about 1 %, which make this choice quite attractive.

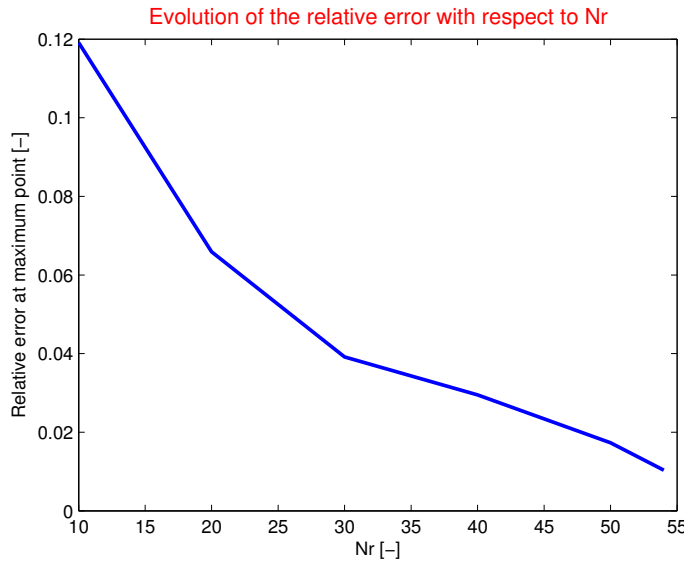


Figure 83 – Evolution of the realtive error on $\bar{\varsigma}_{VM}$ at the peak with different Nr.

5.3.3 Number of circumferential divisions

To study the effect of the number of circumferential divisions (No), we use a constant number of radial divisions. Because the variation of the stress field is higher in the radial direction, it seems logical that the impact on the amplitude of the peak is smaller than for radial divisions and we can observe it on Fig. 84. So, because of the precision that is already obtained with Nr=54, we will use the corresponding No so that we don't cross the limit and this value is 8. We could be tempted to increase more and more Nr but to keep an acceptable aspect ration, we didn't go any further. Finally, we will use those parameters for every mesh.

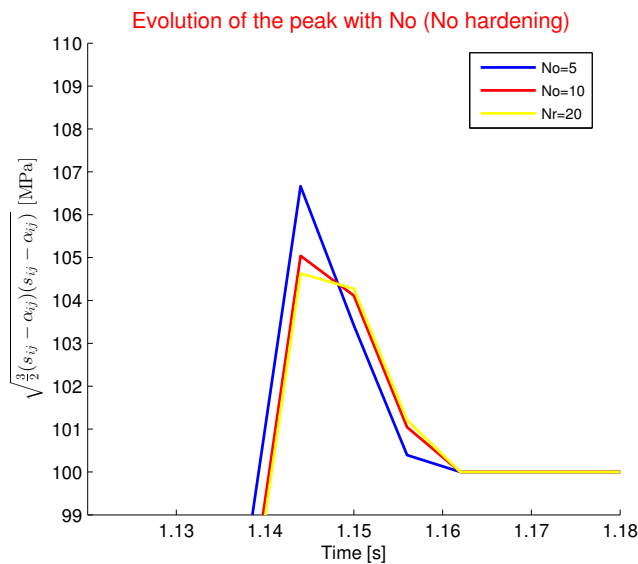


Figure 84 – Evolution of $\bar{\varsigma}_{VM}$ at the peak with different No.

5.3.4 Radial distribution of the elements

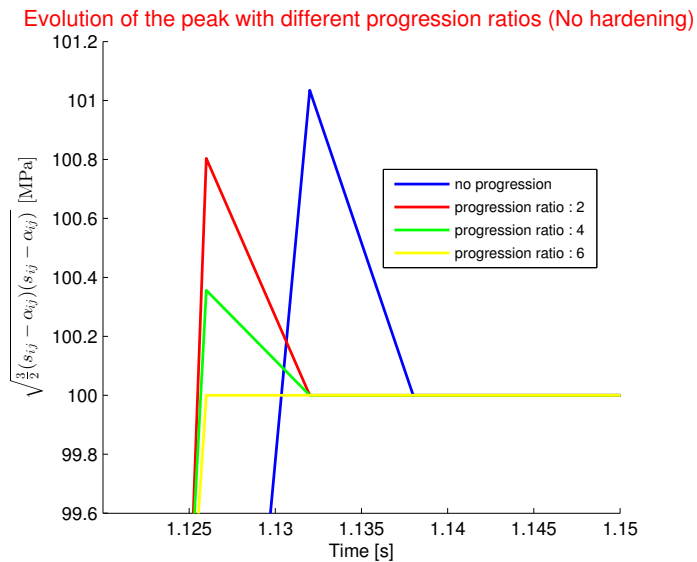


Figure 85 – Evolution of $\bar{\varsigma}_{VM}$ at the peak with different distribution ratios.

Another way to increase the accuracy of the results where the applied forces are the higher is to use a non-uniform mesh. To do that, we introduce the parameter dr, that is the ratio between the radial

dimension of the outer element and the radial dimension of the inner element. Between those two values, the dimension increases linearly so that we have smaller elements near the inner surface. If we look at the amplitude of the peak on Fig. 85 depending on dr , we can observe that the peak has disappeared for $dr=6$. Thus, we will use this value for our mesh.

We should also notice that even if we have used this mesh for most of our simulations, it wasn't always appropriate. Indeed, when we look at the evolution of a certain value depending on the position in the sphere, we should rather use a uniform mesh, and we did that, for instance, in the evolution of residual stresses.

Also, when we're looking at precise point inside the sphere that is not too close from P1, we rather used a quadratic distribution of the division density, with the highest density at the considered point. We used that particular mesh for the research of the critical radius.

A last important think to say is that even if we studied the influence of spatial discretisation with the no hardening model, the conclusions are still valid for all the elasto-plastic and visco-elastoplastic models, because the problem of the extrapolation from Gauss points is present in every model.

5.3.5 Comparison of stresses at outer surface

We have compared several meshes,

- Mesh 1: $N_r = 10, N_o = 10, d = 1$
- Mesh 2: $N_r = 22, N_o = 20, d = 1$
- Mesh 3: $N_r = 40, N_o = 10, d = \frac{R_2}{R_1}$
- Mesh 4: $N_r = 54, N_o = 8, d = \frac{R_2}{R_1}$

To study stresses (equivalent Von Mises $\bar{\sigma}^{VM}$, σ_{XX} and $\sigma_{YY} = \sigma_{ZZ}$ [MPa]) at outer surface for elasto-viscoplasticity with $\eta = 10^4$ [MPa.s] without hardening for 3 cycles in sawtooth with 1 [s] for each loading. Note that we saw that at outer surface, this is elasticity so we are waiting for linear evolutions of stresses.

Von Mises's equivalent stresses As attended, stresses are linear (Fig. 86). Moreover, meshes seem to converge, there are only negligible differences.

XX stresses Our 4 meshes change a lot in radial direction XX (from $N_r = 10$ to $N_r = 54$). Results vary between meshes but not much from mesh 3 and 4. In fact, at outer surface radial stresses are low (Fig. 87).

YY stresses All results (for different mesh) are almost superposed, there is only a negligible difference. In fact, our meshes were wider than thick and N_o does not change between our meshes. Stresses along YY (width direction) are thus similar on Fig. 88.

Von Mises's equivalent stresses at inner surface Remember the shape of equivalent Von Mises stresses at inner surface (elasto-viscoplasticity with $\eta = 10^4$ [MPa.s] without hardening): there is no instability (like the peak of elasto-plasticity) thanks to viscosity (smooth shape on Fig. 89). Von Mises's yield criterion is thus verified at each point whatever the mesh. We see nevertheless on Fig. 89 that mesh 4 is the best because results do not change much between mesh 3 and 4. We will more study the influence of temporal discretisation on elasto-viscoplasticity in the next section.

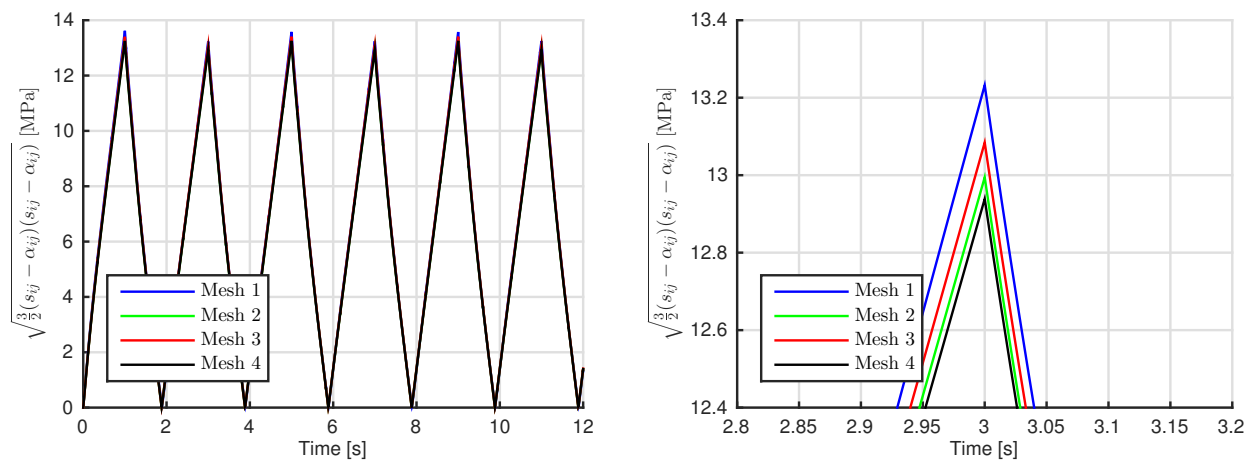


Figure 86 – Influence of the mesh on the equivalent Von Mises stress [MPa] at outer surface for elasto-viscoplasticity with $\eta = 10^4$ [MPa.s] without hardening for 3 cycles in sawtooth with 1 [s] loading

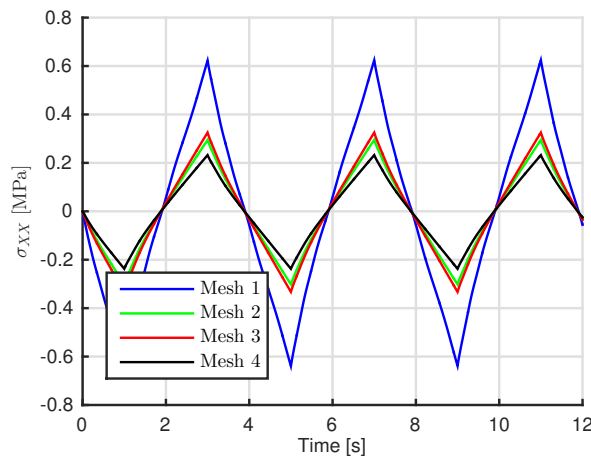


Figure 87 – Influence of the mesh on the XX stress [MPa] at outer surface for elasto-viscoplasticity with $\eta = 10^4$ [MPa.s] without hardening for 3 cycles in sawtooth with 1 [s] for each loading

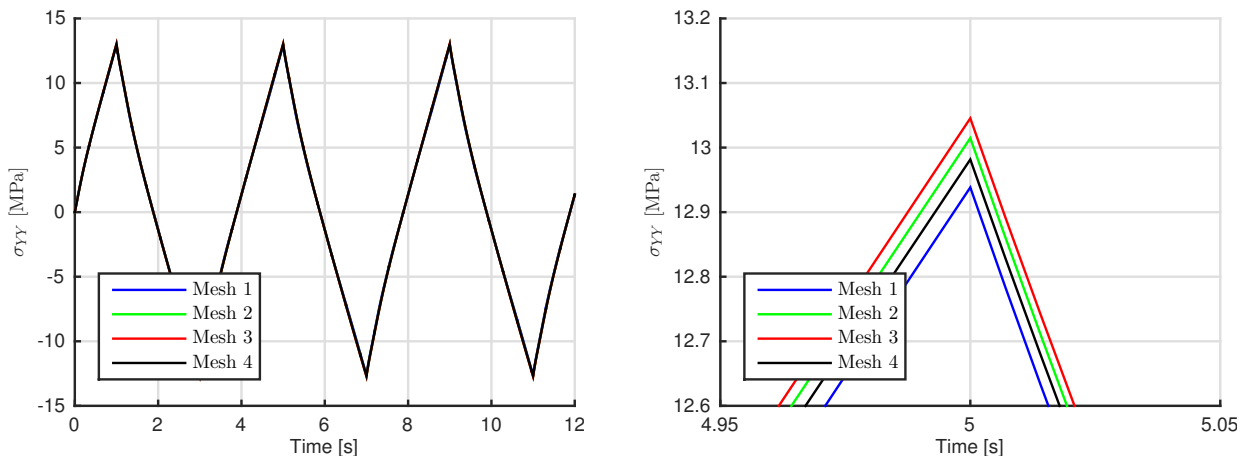


Figure 88 – Influence of the mesh on the YY stress [MPa] at outer surface for elasto-viscoplasticity with $\eta = 10^4$ [MPa.s] without hardening for 3 cycles in sawtooth with 1 [s] for each loading

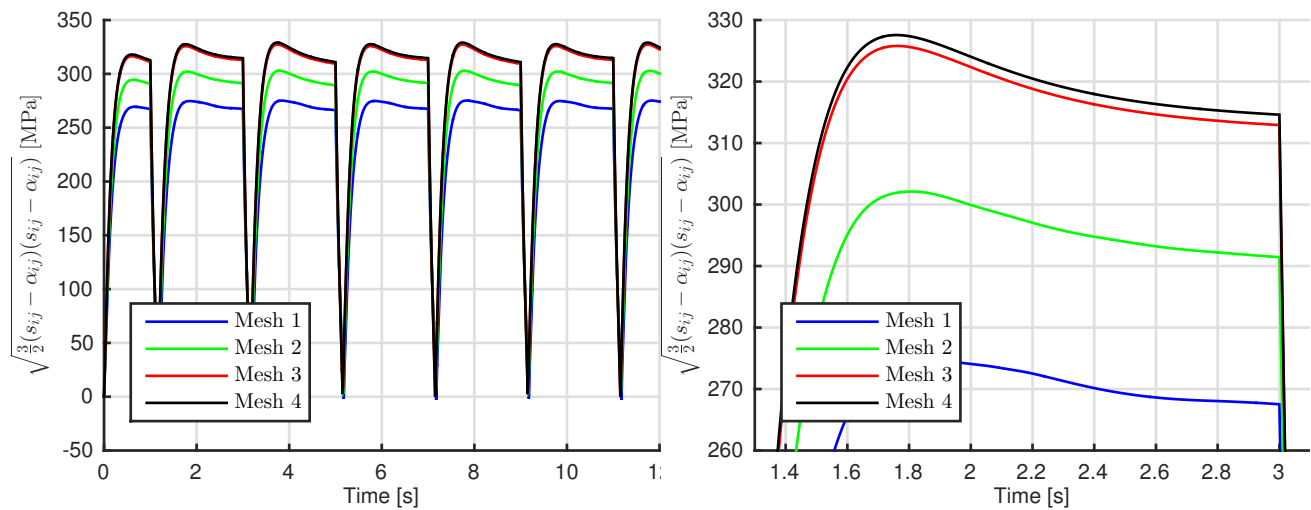


Figure 89 – Influence of the mesh on the equivalent Von Mises stress [MPa] at inner surface for elasto-viscoplasticity with $\eta = 10^4$ [MPa.s] without hardening for 3 cycles in sawtooth with 1 [s] for each loading

5.4 Influence of temporal discretisation

5.4.1 Introduction

The time step is a key parameter in a numerical study. It is obvious that a large time step will give worse results than a small one. Nevertheless, it is again a compromise between sufficient precision and real CPU time. In fact, time discretisation is associated to spatial discretisation. If you will know the influence of one type of discretisation, it is obvious that you must keep one constant. Here, we will keep the mesh used in the project, with $N_r = 54$, $N_o = 8$, $d = \frac{R_2}{R_1}$ (with d is the progression used to have a progressive mesh distribution). This is the best case to study the influence of time discretization, the thinner mesh. Note that analysis of time step is obviously the same that the loading speed: we can study the influence of one by keeping the other constant (if we change the time step and the loading speed by the same value, we will not see any difference on results). To represent the most the reality, we need to have a small modification of the displacement (no big gaps) and a method to do that is to use a reasonable time step. We will also analyse this influence for several behaviors:

- elasto-plastic with no-hardening
- elasto-plastic with linear isotropic hardening
- elasto-viscoplasticity with $\eta = 10^4$ [MPa.s] with mixed hardening case (most general case)

We will also study differences of real CPU time [s].

5.4.2 General discretisation and discretisation of **Metafor**

General case For an loading/unloading cycle in sawtooth such as the one of this project needs explanation for time step. Indeed, we have seen during theoretical lectures that some points are *mandatory* to represent well the problem. Even if the time step is too large and precision is not sufficient, we *must* have calculation and points on extrema of the imposed displacement u . Indeed, if you choose a time step which is not a divisor of the time of loading, you cannot represent change of direction of displacement at u_{max} as we can see some "jumps" on Fig. 90 (for $\Delta t = 2/3$ [s] in red). We must then choose Δt which are divisor of loading time 1 [s]. After that, we must choose in these time steps which one is the best compromise between precision and computation time. This is thus a question of compromise, use a small time step but respecting the physic of the problem.

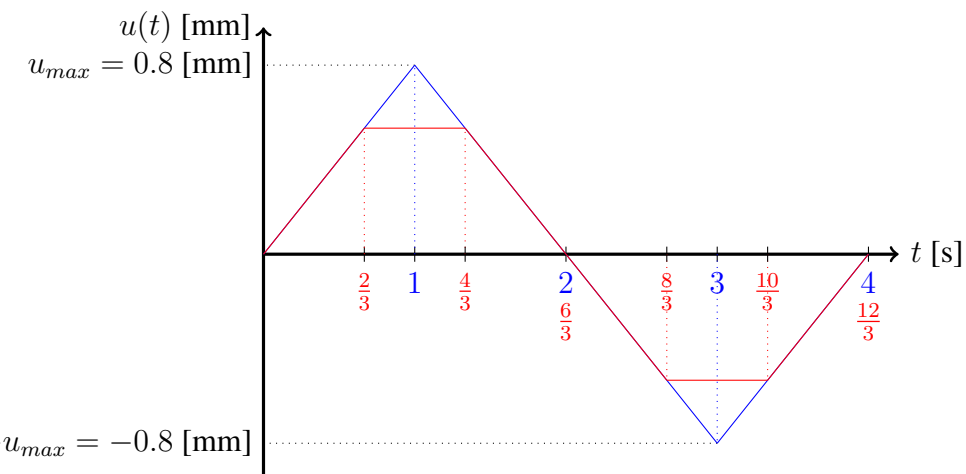


Figure 90 – Influence of time step Δt [s] on the consideration of displacement u

Case of Metafor In fact, Metafor does not use a *simple* time step but an *adaptive* one and "jumps" do not occur. We need to choose 2 parameters associated to the time step in Metafor:

- Δt_{max} (Deltatmax): maximum time step tolerated [s]
- Δt_{init} (Deltatinit): initial time step use (for first iteration)

Practically, we have chosen $\Delta t_{max} = \Delta t_{init}$ for our computations. The computation is based on a Newton-Raphson scheme and this method needs a convergence to continue the computation. Metafor will divide the maximum time step while convergence is not reached. This convergence can takes 2 forms

- tolerance ε on the convergence: for an equation that must be verified like $f = a$, this leads to $f - a < \varepsilon$
- lower bound of time step of Metafor: if the software does not converge after several division of Δt_{max} and the current time step is below this lower bound (usually 10^{-10} [s]), the software stops the computation. This kind of condition is needed, if not, there can be an infinite loop if convergence can not be reached (it is often stops by the epsilon machine of the computer $\varepsilon \approx 10^{-18}$).

If the convergence is reached, Metafor can continue the computation and restarts with a time step Δt_{max} . We see thus that the problem of "jumps" of u_{max} are removed with this kind of *adaptive* time step.

5.4.3 Elasto-plasticity without hardening

We see on Fig. 91 that thiner time step gives more precise solution as attended. After the first loading, an elastic part begins and stresses change their sign so passes by 0. If the time step is thiner, equivalent stresses will increase and reach the yield stress of 100 [MPa] faster (left decay if Δt decreases, see the right figure of Fig. 91). We see also that if the time step is smaller, peak appear on the region of transition between fast increase of the stress and its constant value of 100 [MPa]: this is a "cusp" (singularity) due to extrapolation on Gauss points. If a point is in plasticity and the other next in elasticity, the gap will be important and a sufficiently small time step will put this in evidence. Note that this kind of peak does not represent the reality and is due to instability. If the time step is larger, this peak is ignored and passed without loss much precision. Decays of the first jump between time steps seems to decrease with time. Note that because of *adpative* time step, we have a value for $\Delta t = 0.5$ [s] on $t = 1.13$, the software had to make more iterations at this point and reduce the time step to converge. Finally, we used a time step of $\Delta t = 0.007$ [s] in order to have a very low peak and a good precision.

5.4.4 Elasto-plasticity with linear isotropic hardening

We see on Fig. that larger time step need more iterations to converge (see *adaptive* time step in Newton-Raphson). In fact, elasto-plastic model are physically rate-independent but numerically, we see that the time step has an influence on values of equivalent stress. After the first loading, using a time step of 0.5 [s] ignores totally the decrease towards 0 (elastic part) and passes over.

For 0.1 and 0.05 [s], results are again wrong. For 0.01 [s], we does not see any difference and the path remains the same. Note that these differences decrease with the time. Indeed, we see that curves of all time steps are superposed after the fourth jump. In fact, extrema (begin and end of jump, corresponding on elastic and plastic parts) were in the beginning not in phase with extrema of displacement. Nevertheless, as time increases, these extrema becomes in phase thanks to hardening.

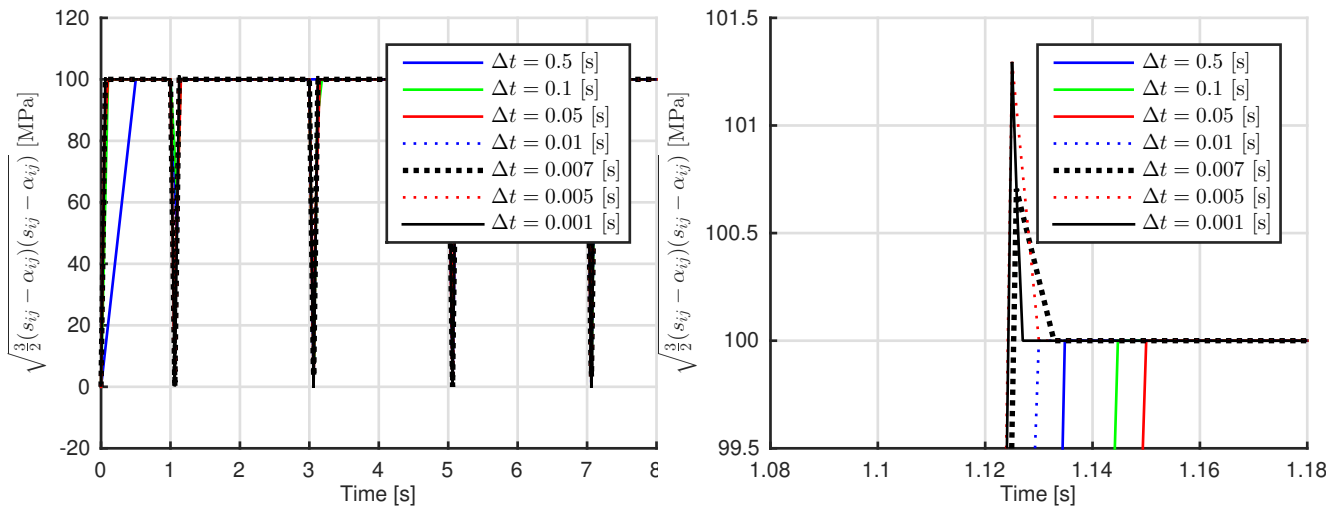


Figure 91 – Influence of the time step [s] on the equivalent Von Mises stress [MPa] at inner surface for elasto-plasticity without hardening for 2 cycles in sawtooth with 1 [s] for each loading

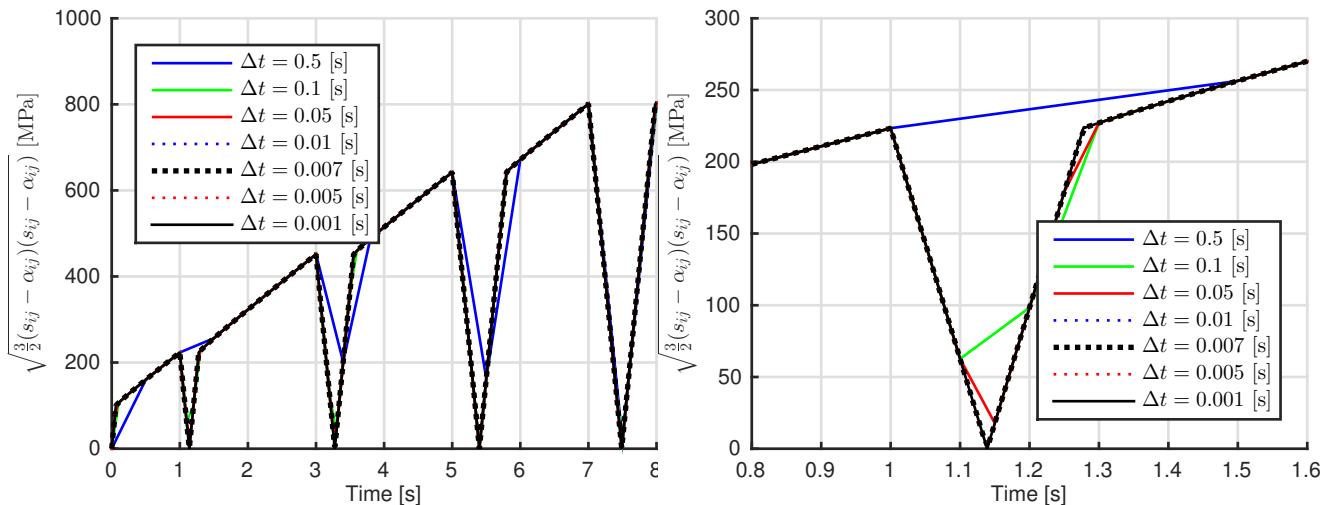


Figure 92 – Influence of the time step [s] on the equivalent Von Mises stress [MPa] at inner surface for elasto-plasticity with linear isotropic hardening for 2 cycles in sawtooth with 1 [s] for each loading

Time steps chosen which are able to represent well the displacement can also represent equivalent stresses (superposition of all time steps). There is no reason to change the time step here, the precision and stability remain the same, so we keep $\Delta t = 0.007$ [s].

5.4.5 Elasto-viscoplasticity with mixed hardening and $\eta = 10^4$ [MPa.s]

This behavior thanks into account other phenomenon: a physically rate dependent behavior. Equivalent stresses are dependent of the loading speed also in reality, no only numerically. Once again, we see on Fig. 93 that there are huge difference between $\Delta t = 0.5$ [s] and other time step for the first jump but these differences decrease with time and are no more visible at the fourth jump (extrema of stresses occur at the same time as extrema of displacement but this is due to the elasto-viscoplastic behavior which reduce the plastic part when the time increases. This is not a general remark because $\Delta t = 0.5$ [s] tends to fit well with other time steps. We keep the same loading speed as elasto-plastic models and also the same time step $\Delta t = 0.007$ [s] because of once again a good compromise between precision, stability and real CPU time. Note that this real CPU time is shown as a function of the time step in table 3 and we see that this is a linear dependence (as smaller time step needs a larger computation time approximately proportionally). Von Mises's yield criterion seems to

be satisfied at every material point in the elasto-viscoplastic zone (in any case at inner surface).

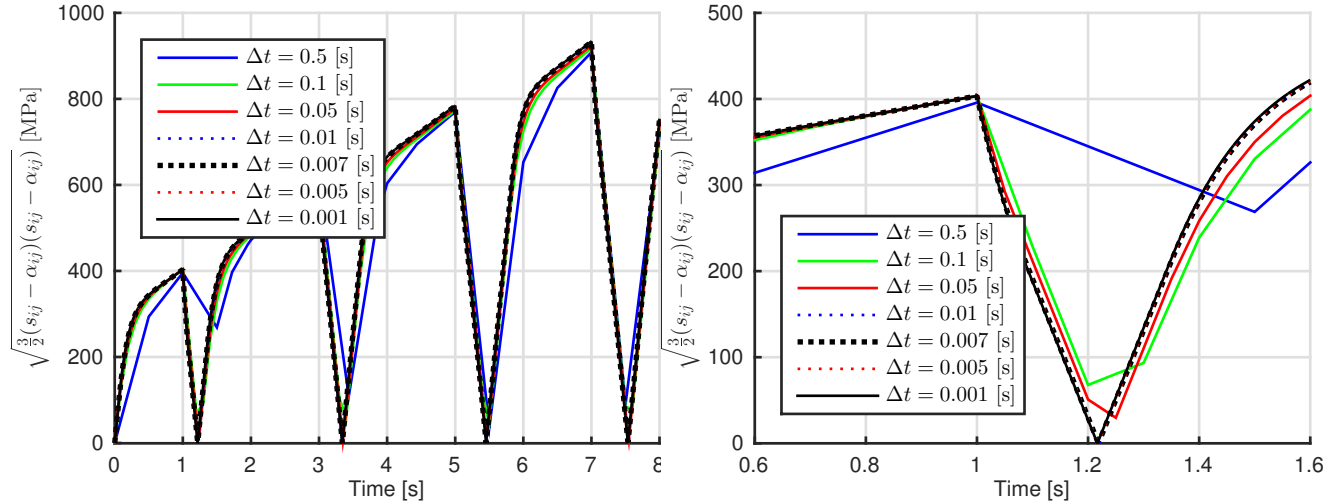


Figure 93 – Influence of the time step [s] on the equivalent Von Mises stress [MPa] at inner surface for elasto-viscoplasticity with linear isotropic hardening for 2 cycles in sawtooth with 1 [s] for each loading

Time step Δt [s]	Real CPU time [s]
0.5	3.21
0.1	4.78
0.05	7.41
0.01	24
0.005	40.79
0.001	149.46

Table 3 – Evolution of real CPU time [s] with the time step Δt [s] for Fig. 93

5.5 Remarks on radial return algorithm

It is suggested in the tips of the project instruction to compare the final value (in time) of the reaction pressure $p(t)$ and the equivalent plastic strain $\bar{\varepsilon}^p(t)$ for several meshes and time steps in the case of elasto-plasticity in mixed linear hardening for one loading/unloading cycle or several. We will compare these final values and explain from what it can come (links with numerical integration methods).

Remember the shape of $\bar{\varepsilon}(t)$ for an elasto-psatic behavior with mixed hardening on Fig. 94 for 3 cycles. The final value increases if the mesh is refined (Fig. 94 and table 4). Nevertheless, we see that there is almost no difference when we take different time steps (Fig. 94 and table 5). We will explain that according to the radial return algorithm.

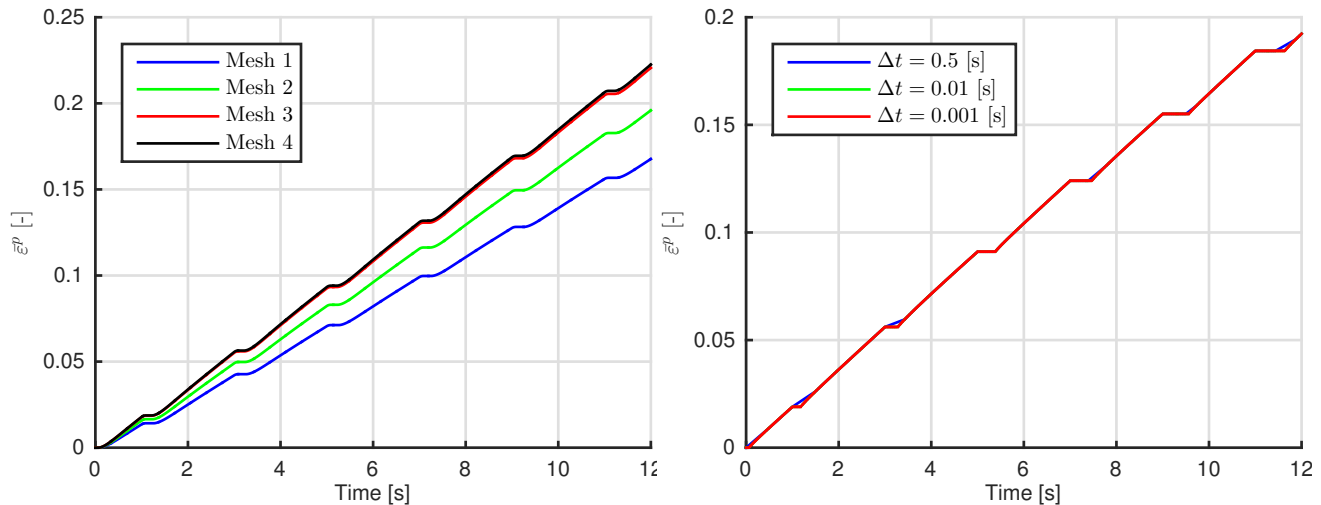


Figure 94 – Influence of the mesh and the time step [s] on the equivalent plastic strain [-] at inner surface for elasto-plasticity with linear mixed hardening for 3 cycles in sawtooth with 1 [s] for each loading

We see clearly in table 4 that obviously $\bar{\varepsilon}(t)_{final}$ increases as the number of cycles increase because of plasticity and accumulation of residual strain. Nevertheless, the most interesting is that these values for a same number of cycle increase if the mesh is refined.

	Number of cycles		
	1	3	5
Mesh 1 $N_r = 10, N_o = 10, d = 1$	0.0633	0.1458	0.2553
Mesh 2 $N_r = 22, N_o = 20, d = 1$	0.0630	0.1697	0.2538
Mesh 3 $N_r = 40, N_o = 10, d = \frac{R_2}{R_1}$	0.0709	0.1907	0.2850
Mesh 4 $N_r = 54, N_o = 8, d = \frac{R_2}{R_1}$	0.0715	0.1923	0.2875

Table 4 – Final value of $\bar{\varepsilon}(t)$ [-] depending on the mesh and the number of cycle, $\Delta t = 0.01$ [s], at inner surface for elasto-plasticity with linear mixed hardening for cycles in sawtooth with 1 [s] for each loading

Remember that in chapter 6 of [3], we saw different methods for numerical time integration of constitutive equations. The general scheme is a return mapping algorithm with elastic predictor and

	Number of cycles		
	1	3	5
$\Delta t = 0.1$	0.0715	0.1923	0.2875
$\Delta t = 0.01$	0.0715	0.1923	0.2875
$\Delta t = 0.001$	0.0715	0.1923	0.2875

Table 5 – Final value of $\bar{\varepsilon}(t)$ [-] depending on the time step Δt [s] and the number of cycle, mesh: $N_r = 54$, $N_o = 8$, $d = \frac{R_2}{R_1}$, at inner surface for elasto-plasticity with linear mixed hardening for cycles in sawtooth with 1 [s] for each loading

plastic corrector. Different methods can be chosen for the normal discretisation ($\mathbf{N} = \mathbf{N}(t)$), discretised by,

$$\mathbf{N}_\theta = (1 - \theta)\mathbf{N}_0 + \theta\mathbf{N}_1 \quad (5.62)$$

Where,

- θ is "user chosen"
- \mathbf{N}_0 is the normal at yielding point
- \mathbf{N}_1 is the normal at elastic predictor

For the radial return algorithm, we suppose that $\theta = 1$ so that the current normal is in the same direction as the one of elastic predictor (Fig. 95). Once again, if the size of the mesh is greater (coarse mesh) and if one Gauss point is in plasticity and the other one in elasticity, the gap (and extrapolation) will give worst results and errors will accumulate because we assume that the normal at elastic predictor is the true/right normal. Influence of time step is almost not visible because values are well extrapolated (same mesh). Moreover, the elastic predictor does not change during successive time steps. Thus, these time steps have almost no influence on values (obviously, if the time step is too large, some values are not computed and only linear extrapolation will be done, but extreme values of these linear extrapolation are the same than those of other time steps).

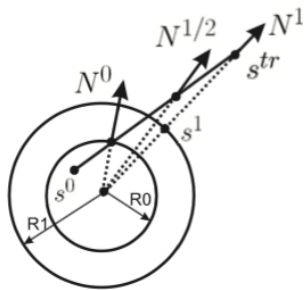


Figure 95 – Illustration of return mapping algorithm with different values of θ

Then, we need to describe how to compute the reaction pressure. A method to get the reaction pressure $p(t)$ is to use the reaction force R computed with `Metafor` at curves C1 and C3. By doing an equilibrium on the quarter of the sphere:

$$P = \sqrt{P_1^2 + P_2^2} \quad (5.63)$$

$$P_1 = P_2 = P_0 \text{ (symmetry)} \quad (5.64)$$

$$P = \sqrt{2}P_0 \quad (5.65)$$

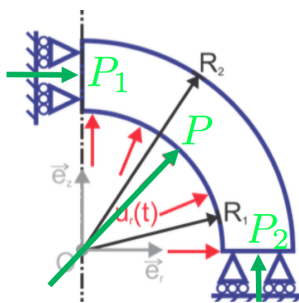


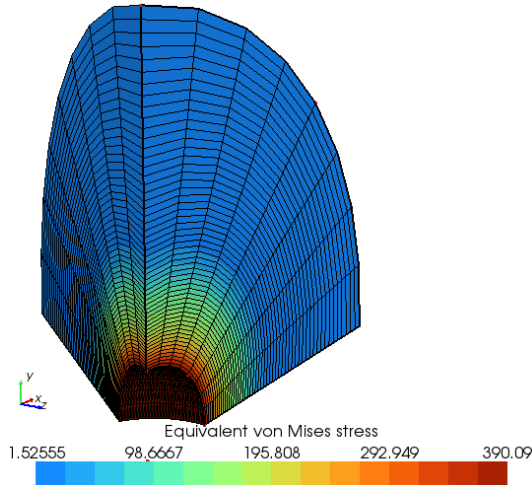
Figure 96 – Equilibrium of reactions in the sphere

By definition of the pressure,

$$p(t) = \frac{P(t)}{A} \quad (5.66)$$

With A the area of the inner surface. Note that in **Metafor**, the computation is done in an angle ϕ of one radian (Fig. 97). So, we have from the area of a sphere $4\pi r^2$, for a half sphere of 1 radian,

$$A = \frac{4\pi R_1^2}{2 \cdot 2\pi} = R_1^2 \Rightarrow p(t) = \frac{\sqrt{2}P_0}{R_1^2} \quad (5.67)$$

Figure 97 – 3D view of the sphere computed in **Metafor**, equivalent Von Mises stresses [MPa]

Unfortunately, this method does not give the exact solution, certainly due to the complex orientation of axis in **Metafor** which does not represent Fig. 96.

As another approximation, we can take p as $-\sigma_{XX}$. In fact, it represents well the radial pressure present in the sphere but at a *node*. In fact, a nodal value is an extrapolation and because of numerical jumps for extrapolations at Gauss points, values obtained are not perfectly exact. We must keep that in mind while analysis of results. Nevertheless, we are sure of the orientation.

Results are shown on Fig. 98 and tables 6 and 7. We observe same behavior as those of $\bar{\varepsilon}^p(t)$ and conclusions are the same for radial return algorithm. Difference for different time steps are more visible because of the order of magnitude of $-\sigma_{XX}(t)$, greater than the one for $\bar{\varepsilon}^p(t)$.

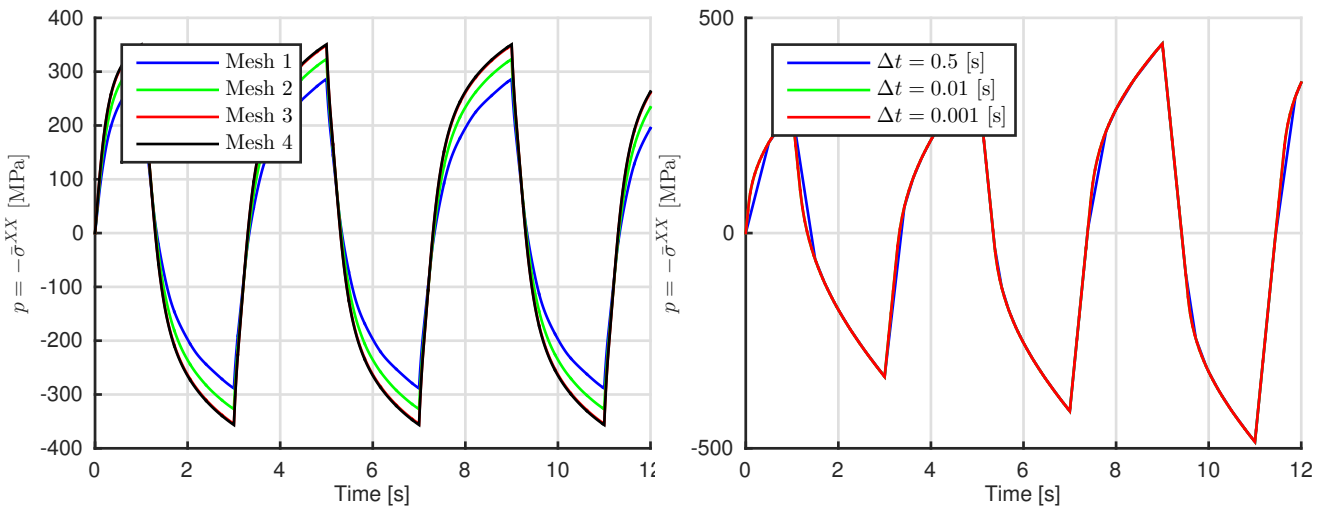


Figure 98 – Influence of the mesh and the time step [s] on the reaction pressure [MPa] at inner surface for elasto-plasticity with linear mixed hardening for 3 cycles in sawtooth with 1 [s] for each loading

	Number of cycles		
	1	3	5
Mesh 1 $N_r = 10, N_o = 10, d = 1$	194.2805	259.9145	382.8735
Mesh 2 $N_r = 22, N_o = 20, d = 1$	193.2832	308.3827	380.3827
Mesh 3 $N_r = 40, N_o = 10, d = \frac{R_2}{R_1}$	214.6904	346.6923	431.6435
Mesh 4 $N_r = 54, N_o = 8, d = \frac{R_2}{R_1}$	216.1775	349.5262	435.5428

Table 6 – Final value of $p(t) = -\bar{\sigma}_{XX}(t)$ [MPa] depending on the mesh and the number of cycle, $\Delta t = 0.01$ [s], at inner surface for elasto-plasticity with linear mixed hardening for cycles in sawtooth with 1 [s] for each loading

	Number of cycles		
	1	3	5
$\Delta t = 0.1$	216.1778	349.5103	435.5427
$\Delta t = 0.01$	216.1775	349.5262	435.5428
$\Delta t = 0.001$	216.1782	349.5286	435.5446

Table 7 – Final value of $p(t) = -\bar{\sigma}_{XX}(t)$ [MPa] depending on the time step Δt [s] and the number of cycle, mesh: $N_r = 54, N_o = 8, d = \frac{R_2}{R_1}$, at inner surface for elasto-plasticity with linear mixed hardening for cycles in sawtooth with 1 [s] for each loading

5.6 Validation of the numerical simulation based on the TPE

The numerical simulation are based on a finite element model. In order to make it possible, we need to transform the strong form of the budget equations, valid at all point of the structure with an infinite number of DOF in a weak form. The strong form equation is the local form here below. See equation 5.71.

$$\frac{\partial \sigma_{ij}}{\partial x_j} + \rho \bar{b}_i = \rho \ddot{x}_i \quad (5.68)$$

$$\varepsilon_{ij} = \frac{1}{2} \left(\frac{\partial u_i}{\partial x_j} + \frac{\partial u_j}{\partial x_i} \right) \quad (5.69)$$

$$\sigma_{ij} = H_{ijkl} \varepsilon_{kl} \quad (5.70)$$

$$\dot{\sigma}_{ij} = M_{ijkl} D_{kl} \quad (5.71)$$

Those equations are successively the momentum equilibrium, displacement deformation relation in small strain. Constitutive law in elasticity and elasto-plasticity. They must be satisfied at each point in order to solve the strong form. It is possible to express all the equation in function of the displacements.

To solve this problem we may integrate on the whole volume see eqn. 5.72 to get the weak form.

$$\int_V \delta u_i \left[\frac{\partial \sigma_{ij}}{\partial x_j} + \rho(\bar{b}_i - \ddot{x}_i) \right] dV - \int_S \delta u_i (\sigma_{ij} n_j - \bar{t}_i) dS = 0 \quad (5.72)$$

We may transform in order to get the equation below eqn 5.73.

$$\int_V \rho \delta u_i \ddot{x}_i dV + \int_V \sigma_{ij} \frac{\partial \delta u_i}{\partial x_j} dV = \int_V \rho \delta u_i \bar{b}_i dV + \int_S \delta u_i \bar{t}_i dS \quad (5.73)$$

Where the first term is the inertial term, second work done by the internal forces and the right-hand side term the work done by the external forces. This is valid for all model. If we work on a quasi-static model, the first term is neglected. If we want to work with the TPE, we need the hyperelastic assumption. This is out of our project statement : we want to study the elasto-plastic behaviour. Note that in elasticity, ans quasi-static behaviour, the internal and external work take the same value at the end of the loading-unloading cycle.

6 Conclusion

During this project we tried to compare the influence of each assumption on the material behaviour. In the case of a thick walled hollow sphere plastically deformed by a driven displacement of the inner radius.

In order to study the most accurate data's possible we first began with the study of the influence of the numerical parameters. The first step was to find a mesh that provides good results. Because of the shape of the structure to study, a progressive mesh was necessary. Because the gradient of the stress and strain as to be zero in the circumferential direction, we can lower the number of element in the circumferential direction. After a short study of the influence of the number of element in this direction we concluded that more than 8 elements on a quart circle was unnecessary. Then we studied the influence of the number of elements in the radial direction. We were surprised that we got the most accurate results (less jump in the graph of the equivalent Von Mises stress at the inner radius) when the number of radial elements was maximum (54 because of our limitation of number of nodes) and not when we tried to have a good aspect ratio of all the elements. Once the mesh was chosen, we had to determine the best time step. Once again, we have compared different curves of the equivalent Von Mises stress at the inner radius and have chosen for the one that provided the less jumb (and the lower jumb) on the graph. This time step must be sufficiently low in order to "capture" all the phenomena's we wanted to study but not to small in order to safe computational costs. We chosen for a time step of 0.007 sec when the loading rate was of 0.8mm/sec.

In the first part of the project, we studied basic elasto-plastic hardening model, such as the no hardening model, the isotropic linear hardening, the kinematic linear hardening and the mixed linear hardening. In the analysis of relevant variables, we highlighted some common points between those models as well as some great differences. In particular, in the mixed linear hardening, we clearly identified the convergence effect of the linear isotropic hardening as well as the consequence of the Bauschinger's effect of the kinematic part on it. We also realized that even if we had to distinct zones, with one that is submitted to hardening and the other one isn't, those zones influenced each other and couldn't treated independently. Also, we saw that even if we chose appropriate discretisation parameters, the numerical errors are inherent to this discretisation, and that it should always be taken into account in our interpretation of the results.

During the second part of the project we had to study the influence of a non-linear hardening on the important parameters already studied in the first part. Especially when the kinematic hardening was non linear. When the evolution of the backstress tensor was driven by the Armstrong Frederick's evolution law. At first, we had to study the influence of the dynamic recovery parameter. We saw that this parameter was very important in the relative weight of the non linear effects on the general behaviour. We also have enlightened on the non linear effects of the non linear kinematic hardening. Even id the yield stress doesn't evolves, if the yield surface moves and the loading is cyclic, we see that the beginning of each hardening phase has stronger plastic effect than the end : this happens if the backstress tensor is in the opposite direction than the deviatoric stress tensor. After this we have studied the evolution of the parameters in case of mixed hardening. Firstly when the isotropic hardening was linear then when it was non linear. For all the assumptions we tried to express the plastic modulus and we have explained the effect of the corresponding terms coming from the behaviour assumption. We saw that when the isotropic hardening was non linear, the plastic effect were less strong when the equivalent plastic strain was high. This reflects a kind of saturation effect coming from the non linear isotropic.

During the third part, we have see the influence of the viscosity parameter in elasto-viscoplastic behavior with Perzyna's model. We did this for linear isotropic and mixed hardening, firstly for

a sawtooth cycle. We have seen that the viscosity introduce a time decay due to friction (viscosity). Moreover, we deduced limit case, corresponding to elasto-plasticity for $\eta = 0$ and elasticity for $\eta + \infty$. We compared with mixed hardening, which only introduced backstress. During our study, we analysed effect of viscosity on equivalent stresses, backstresses, pressure and strain. We saw also effect of relaxation when imposing of constant displacement during sawtooth cycle: the material reacts as a decreasing exponential and tends to an asymptotic value slower when viscosity increases (braking of plastic flow) and we have compared numerical and analytical values, conclusions were thus the same. We computed asymptotic values of equivalent stress, backstress and yield stress. We analysed stress components in elastic and plastic zones for a relaxation (keeping a constant displacement for a long time). We were able to compare different behaviors/hardening for hydrostatic pressure but the general shape was more difficult to extrapolate. Finally, an analyse gave that the maximum signum distance increases with loading speed as well as with viscosity.

By the way, we want to enlighten that a time integration scheme is necessary for the elasto-plastic models. We may not use the TPE to verify our results because the TPE uses the assumption of a hyperelastic material. What is precisely not the case if there are plastic deformations.

References

- [1] http://mms2.ensmp.fr/emms_paris/plasticite3D/exercices/eSpherePress.pdf
- [2] Duchene, Laurent, *MECA0012-6: Mécanique du solide*, University of Liege, 2014
- [3] Jean-Philippe Ponthot, *Advanced solid mechanics*, University of Liege, 2015
- [4] <http://mathworld.wolfram.com/SphericalCoordinates.html>
- [5] Erik Quaeghebeur, *SYST002 : Modélisation et analyse des systèmes*, University of Liege, 2014

A Example of file .py to modify parameters of dictionary

We used the Metafor Launcher to execute in one time several different computations (with different properties or values).

```
#-*- coding: latin-1;-*-

from wrap import *
import math
import sphere as m
_metafor = None # Empty Metafor Analysis

def getMetafor(_parameter={}):
    global _metafor

    if _metafor == None:
        from sphere import getMetafor
        parameters = { 'PropertyToChange' : "Property", 'ValueToChan
: Value}
        _metafor = m.getMetafor(parameters)
    return _metafor
```

B Values exported from Metafor

Equivalent Von Mises stress [MPa]	$\bar{\sigma}^{VM}$	IF_CRITERION
Current yield stress [MPa]	σ_y	IF_STATIC_YIELD
Hydrostatic pressure [MPa]	p	IF_P
Stress tensor Cartesian components [MPa]	$\sigma_{XX\dots}$	IF_SIG_XX...
Equivalent back stress [MPa]	$\bar{\alpha}$	IF_ALP_J2
Equivalent plastic strain [-]	$\bar{\varepsilon}^p$	IF_EPL
Plastic energy dissipated [mJ]		THERMODYN_EN_DIS